

Aus der Zentrum für Medizinische Forschung
der Medizinischen Fakultät Mannheim
Direktor: Prof. Dr. med. Norbert Gretz
(Aufgelöst zum 16.04.2020)

Development of dyes/tracers for analysis of renal functions

Inauguraldissertation
zur Erlangung des akademischen Grades
Doctor scientiarum humanarum (Dr. sc. Hum.)
der
Medizinischen Fakultät Mannheim
der Ruprecht-Karls-Universität
zu
Heidelberg

vorgelegt von
Srishti Vajpayee

aus
Faridabad, India

2023

Dekan: Prof. Dr. med. Sergij Goerd
Referent: Prof. Dr. med. Norbert Gretz

***This Ph.D. thesis is dedicated to my parents
for their endless support.***

Table of Contents

Abbreviations	3
1. Introduction	5
1.1 Renal diseases	6
1.2 Current statistics	7
1.3 Diagnosis of renal diseases	7
1.3.1 Endogenous markers and their shortcomings	8
1.3.2 Exogenous markers and their shortcomings	9
1.3.3 Fluorescent markers for the assessment of kidney function ...	10
1.3.4 Near infrared dyes/tracers in kidney functional analysis	12
1.4 Markers for kidney functional assessment	12
1.4.1 Marker for glomerular filtration.....	13
1.4.2 Markers for secretion	15
1.4.3 Markers for reabsorption	16
1.4.4 Markers for vascular imaging	18
1.5 Aims of the project	19
2. Material and Methods.....	20
2.1 Instruments and special materials.....	20
2.2 Fluorescent markers and their characterisation	21
2.3 Optical property characterisation.....	21
2.4 Degree of labelling measurement	22
2.5 Photostability assays.....	22
2.6 Calibration curves	23
2.7 Plasma protein binding assays	23
2.8 Luminescent cell viability assays.....	24
2.9 <i>In vitro</i> cellular uptake studies.....	24
2.9.1 Uptake assays for secretion markers	24
2.9.2 Uptake assays for reabsorption markers.....	25
2.10 Transcutaneous device.....	25
2.11 MSOT imaging	26
2.12 Tissue clearance and fluorescent microscopy.....	26
3. Results.....	27
3.1 Markers for secretion	27

3.1.1	Introduction and work strategy	27
3.1.2	Physicochemical and optical properties	32
3.1.3	Calibration curves and dosage	32
3.1.4	PPB assays	35
3.1.5	Cell viability assays	36
3.1.6	<i>In vitro</i> uptake assays	37
3.2	Markers for reabsorption	38
3.2.1	Introduction and work strategy	38
3.2.2	Physicochemical and optical properties	41
3.2.3	Calibration curves and dosage	41
3.2.4	PPB assays	42
3.2.5	Cell viability assays	43
3.2.6	<i>In vitro</i> uptake assays	43
3.3	Markers for vascular imaging	45
3.3.1	Introduction and work strategy	45
3.3.2	Physicochemical and optical properties	55
3.3.3	Photostability studies	56
3.3.4	DOL calculation	57
3.3.5	Fluorescent microscopy using the kidney imaging markers ...	57
4.	Discussion	59
4.1	GFR marker	59
4.2	Secretion markers	60
4.3	Reabsorption markers	64
4.4	Markers for vascular imaging	67
4.5	Conclusion	70
5.	Summary	71
6.	References	73
7.	Appendix	81
8.	Curriculum Vitae and Publications	106
9.	Acknowledgements	109

Abbreviations

⁵¹ Cr-EDTA	Chromium-51-ethylene diamine tetracetic acid
^{99m} Tc-DTPA	Technetium-99m-diethylenetriaminepentaacetic acid
AcCl	Acetyl chloride
BCRP	Breast cancer resistance protein
CiPTEC	Conditionally immortalized proximal tubular epithelial cells
CT	Computed tomography
D ₂ O	Deuterium oxide
DMSO	Dimethyl sulfoxide
DOL	Degree of labelling
FDA	Food and drug administration
FITC	Fluorescein isothiocyanate
GAG	Glycosaminoglycan
GFR	Glomerular filtration rate
HPCD	Hydroxypropyl-cyclodextrin
HPLC	High performance liquid chromatography
ICG	Indocyanine green
LC-MS	Liquid chromatography - tandem mass
LED	Light-emitting diode
MeSO ₃ H	Methane sulfonic acid
MRI	Magnetic resonance imaging
MSOT	Multispectral optoacoustic tomography
MWCO	Molecular weight cut-off
NHS	<i>N</i> -Hydroxysuccinimide
NIR	Near infrared
NMR	Nuclear magnetic resonance
OAT	Organic anion transporter
OCT	Organic cation transporter
PAH	Para-aminohippuric acid
PBS	Phosphate buffered saline
PEI	Poly (ethylenimine)
PPB	Plasma protein binding
TLC	Thin layer chromatography
UV-Vis	Ultraviolet-visible
WGA	Wheat germ agglutinin

1. Introduction

Nephrons are the kidney's primary functional unit consisting of glomeruli and tubules. They govern urine formation by three key physiological processes: *glomerular filtration*, *tubular reabsorption*, and *tubular secretion* [1]. While glomeruli are responsible for filtration, secretion and reabsorption takes place in the tubules [2] (Figure 1).

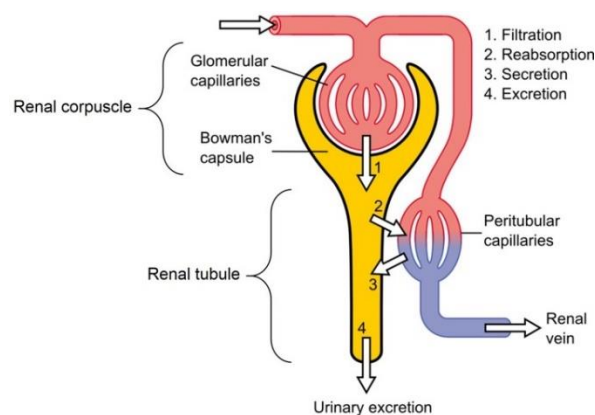


Figure 1: Schematic diagram of urine formation carried out by the nephrons [3]

Glomerular filtration involves filtration of plasma across the fenestrated endothelial membrane of the glomeruli capillaries into the tubules. This process eliminates high molecular weight proteins, and other smaller molecules that are bound to plasma proteins, while most salts and organic molecules are freely filtered across this membrane [2]. Once inside, the glomerular filtrate passes sequentially through different regions of the renal tubules: the *proximal convoluted tubule*, the *loop of Henle*, the *distal convoluted tubule*, and the *collecting duct* [2]. During this passage, molecules can be reabsorbed by the transporters present in the tubular cells and transferred back into the blood plasma (for example water, glucose, amino acids, and ions). This process is called *tubular reabsorption* and can occur via passive (osmosis or diffusion) or active transport. In contrast to glomerular filtration, tubular reabsorption is a very selective process and is necessary for regulating the excretion of specific substances [2].

Apart from filtration and reabsorption, few molecules, such as xenobiotics, are secreted directly from the blood vessels into the renal tubules. This process

primarily takes place in the proximal tubules. *Tubular secretion* is an active transport, which is majorly carried out by the *organic anion transporters (OATs)* and the *organic cation transporters (OCTs)*, depending on the overall charge of the molecule that needs to be secreted [4]. Other than these, there are few minor transporters belonging to the *solute carrier (SLC)* superfamily and the remaining belonging to the *ATP-binding cassette* of tubular transporter proteins [4].

These three processes together determine the amount of a substance excreted through urine. When mathematically expressed,

$$\text{Urinary excretion} = \text{Glomerular filtration} - \text{Tubular reabsorption} + \text{Tubular secretion} \text{ [3]}$$

1.1 Renal diseases

Being such a complex system, kidneys can be affected in many ways, thereby compromising their healthy functioning. Kidney diseases are broadly categorised into two groups: *acute kidney diseases (AKDs)*, and *chronic kidney diseases (CKDs)*. AKDs are spontaneous and may result in a complete or an almost complete decline of kidney function. CKDs however develop slowly over a period, thereby causing problems in early detection. This often results in unrecoverable damages, which could also involve complete loss of renal function, and/or proteinuria [5].

AKDs can be caused due to various factors: *prerenal*, due to low blood flow towards kidney; *intrarenal*, affecting blood vessels, glomeruli, or tubules; or *postrenal*, such as obstruction in urine outflow due to kidney stones. If it goes untreated in time, the patient can have complete loss of kidney function [5]. CKDs present a more complicated case. CKDs can be caused from several reasons, such as metabolic disorders (e.g., diabetes mellitus, obesity), hypertension, immunological disorders, infections, nephrotoxins such as heavy metals and xenobiotics, vascular disorders and many more [5]. Due to a progressive loss of functional nephrons, often they go undetected at an early stage. There are several stages of CKDs depending on the severity of the disease. The most common way of characterising these stages in clinics is through the measurement of the glomerular filtration rate. The National Kidney Foundation has proposed the following criteria to identify the CKD stage within patients [6, 7]:

Stage	Estimated GFR (eGFR) mL/min per 1.73 m ²
1	≥90
2	60 to 89
3	30 to 59
4	15 to 29
5	<15

Table 1: Stages of CKDs defined by the National Kidney Foundation [6]

1.2 Current statistics

Kidney problems affect 10% of the global population, causing millions of deaths each year. Only 10% of the affected population has access to the required health facilities. The middle-economy and developing nations are more severely hit because of the high cost of treatment for the end-stage CKD patients. In 2005, 35 million out of 58 million deaths world-wide were due to CKDs [8, 9].

The major problem comes with the stage 5 CKD patients, when the only option available is renal replacement therapies (RRTs), i.e., kidney transplantation or dialysis. RRTs are very expensive. Kidney transplantation is also limited by the availability of organ donors. Dialysis is an effective and the most popular option, but it greatly reduces quality of life for the patients [8, 9].

Moreover, kidney diseases are often accompanied by other diseases, such as iron deficiency, inflammation, and collection of toxins within blood and urine [10]. CKD patients often develop cardiovascular diseases (CVDs). Low glomerular filtration rate (GFR) can also lead to left-ventricular dystrophy in many patients. Apart from these, the electrolyte imbalance in the body can cause inflammation and dyslipidaemia [7, 11-14].

1.3 Diagnosis of renal diseases

It is necessary to diagnose and treat kidney diseases at an early stage, while the damage is still recoverable/preventable. There are already various biomarkers and clinical diagnostic techniques to detect them. The most common includes the assessment of GFR and urine analysis. These tests may use markers present

within the body (endogenous markers) or ingested/injected into the body (exogenous markers).

1.3.1 Endogenous markers and their shortcomings

A GFR marker should have certain characteristics: it should neither be secreted nor be reabsorbed by tubular cells, and it should be freely and completely filtered by the glomeruli (no extrarenal source of elimination) [15]. *Creatinine* is the most used endogenous marker for GFR analysis. However, it differs from one person to another based on an individual's muscle mass. Also small amounts of creatinine are secreted by the tubular cells. Moreover, people with muscular dystrophy, high/low protein intake, amputations, or elderly may show erroneous results [15-16].

Blood urea nitrogen (BUN) is a waste product of protein metabolism. The serum urea is cleared via the kidney (approximately 85%) and the gastrointestinal tract (15%). Its level within blood increases when the kidney is not functioning properly. However, problems such as age-related issues, high/low dietary intake of proteins, gastrointestinal bleeding, dehydration, or liver diseases can cause fluctuations in BUN levels [15, 17].

Cystatin C is a 13.3 kDa protein that is filtered freely by the glomeruli. Within the proximal tubules, it is taken up by the cells and broken down into amino acids, which are then reabsorbed into the blood. This allows it to maintain a constant rate within the body serum. During kidney dysfunction, the level of cystatin C is elevated, and this allows it to be used as a diagnostic marker. Nevertheless, the serum concentration of cystatin C can be affected by the prevalence of cancer, thyroid disease, administration of corticosteroids, and sometimes even smoking [15, 17-19].

Other than GFR, the level of *urine albumin* is also used as an indicator for kidney diseases. Albuminuria can indicate glomerular dysfunction or problems in tubular reabsorption. However, albuminuria can occur due to other reasons too, such as, fever and exercising [15]. Due to these limitations with the endogenous markers, the focus has shifted to finding exogenous compounds that could help overcome the challenges posed by the endogenous markers.

1.3.2 Exogenous markers and their shortcomings

Inulin, though poorly water-soluble, is regarded to be the gold standard for GFR measurement. It is a linear polysaccharide made up of fructose subunits and matches all the criteria needed for the GFR marker. It is a natural polymer, derived from dahlia roots and Jerusalem artichokes, and is roughly 5.2 kDa in size. It is chemically inert and is filtered freely and completely by the kidneys without being metabolised. To measure inulin, a constant concentration is maintained in the plasma using constant infusions [20]. Continuous blood and urine samples are drawn out after a steady state is achieved, which is often assisted by catheterization of the bladder, to ensure complete and timed urine collection. Later with the help of the known values for urine flow rate and concentration of inulin in plasma and urine, GFR can be assessed [17]. This procedure makes the measurement of inulin tedious and invasive. Also extraction of inulin from plants and purification is laborious and expensive [17, 20].

Sinistrin is a β -D-fructan version of inulin with branching at C6 position. It behaves like inulin when injected in the body: chemically inert, almost negligible plasma protein binding, completely filtered by the glomeruli, and neither secreted nor reabsorbed by the tubular cells [21-22]. It offers an added advantage over inulin by being water-soluble due to its branched structure. Inulin must be heated up till 80°C to completely dissolve [22]. Nevertheless, sinistrin faces the same challenges as inulin by being an invasive, tedious, and expensive way for diagnosis.

As an improvement to the steady-state markers such as inulin and sinistrin, *radioactive tracers* have been popularised as GFR markers. They require single bolus injection (usually intravenous), with time-to-time blood sampling, which is less invasive, and faster as compared to inulin measurement. They are assessed based on their plasma half-lives, which allows to get rid of urine-dependency for analysis [23]. Two of the most widely used radiotracers in clinics are $^{51}\text{Cr-EDTA}$ and $^{99\text{m}}\text{Tc-DTPA}$. While $^{51}\text{Cr-EDTA}$ undergoes renal reabsorption [24-26], $^{99\text{m}}\text{Tc-DTPA}$ shows dissociation within the body when injected [25]. Also $^{99\text{m}}\text{Tc-DTPA}$ shows overestimation of GFR by 3.5mL/min [27-29]. Apart from these shortcomings, $^{51}\text{Cr-EDTA}$ and $^{99\text{m}}\text{Tc-DTPA}$ suffer the indispensable requirements of licencing, storage, handling, and disposal of radioactive material, which makes their usage meticulous and limited.

To overcome the disadvantages faced by radiotracers, non-radioactive chemical tracers have been studied, such as *iohexol* and *iothalamate*, in combination with X-ray detection [30]. However, *iohexol* shows roughly 1.5% plasma protein binding, and approximately 5% extra-renal clearance [31-33]. Also *iothalamate* is partially secreted by the kidney's tubular cells. Most importantly, both these markers require costly detection equipment [27].

1.3.3 Fluorescent markers for the assessment of kidney function

To overcome the shortcomings of the aforementioned kidney markers, significant progress has been made in the field of fluorescent tracers/markers.

Lanthanide chelates have long been used for GFR estimation but suffer low quantum yields. Research has been done to increase the fluorescence of lanthanide metal complexes by introducing molecular 'antennae' via intermolecular fluorescence resonance energy transfer (FRET). Nevertheless, addition of the 'antennae' leads to excretion of a part of these complexes via tubular secretion, in addition to glomerular filtration [34-35].

Another approach to modify already-existing markers involves making them more hydrophilic and anionic to promote their renal excretion via filtration. *Pyrazine* is a heterocyclic aromatic compound, which is modified in many ways to yield photostable fluorescent compounds that can be used as GFR markers. MB-102 is a very recent example of one such modified-pyrazine dyes as a GFR marker. It has already been demonstrated to be safe and efficient from its first in-human trial and is now under the phase 2 trial [36].

Polyethylene glycol (PEG) derivatives of the pyrazine dyes have been studied for their kidney-mediated clearance. PEG chains with molecular weight less than 6 kDa are freely filtered by the glomeruli with no tubular reabsorption [37-38]. Nevertheless, the low yields and high cost of production for large-scale synthesis associated with the pegylated pyrazines makes them less favourable as a diagnostic tool.

Apart from modifying and improving the already-known dyes for their biological activity and optical characteristics, research in this field has also focused on labelling well-known GFR markers with dyes with favourable photochemical

properties. For example, a *fluorescein isothiocyanate-conjugate of inulin (FITC-inulin)* (Figure 2) allows GFR assessment using very small quantities of the marker. Single-bolus injection followed by the study of elimination kinetics in the blood over a period of time, provides a urine-free and a highly reproducible detection method. However, the need to heat and dialyse FITC-inulin prior to its biological usage still makes this marker unsuitable [38-40]. As an improvement, *FITC-sinistrin* (Figure 2) is used. It is a one-step synthesis and produces a marker that is soluble even at room temperature. Nevertheless, continuous drawing of blood to study elimination kinetics can often be stressful for the patients [38-40].

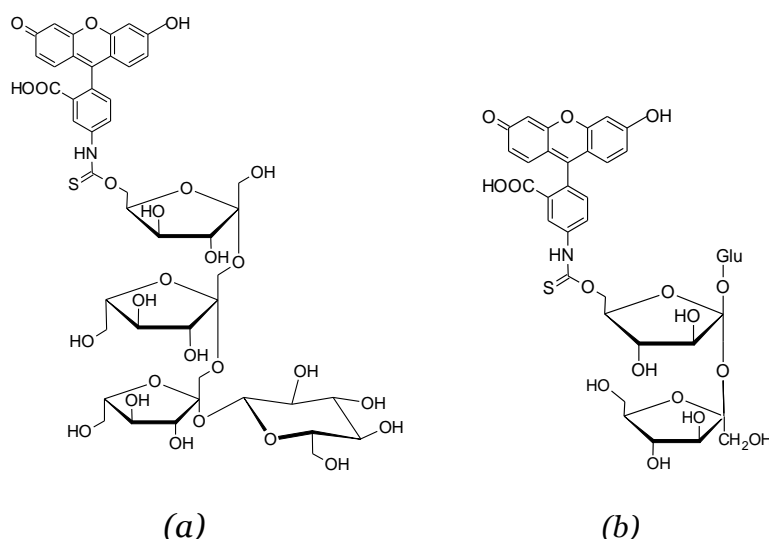


Figure 2: Chemical structures of (a) FITC-Inulin and (b) FITC-Sinistrin

Therefore, to eliminate the use of traditionally invasive and cumbersome methods for renal assessment, transcutaneous detection techniques have been developed. These devices have been tested with the various fluorescent markers, especially FITC-sinistrin, and can record fluorescent emission of the dyes and generate an elimination-kinetics curve based on the data collected over a period of time [41].

As cheaper and readily available alternatives to inulin and sinistrin, recently *cyclodextrins* have been investigated as GFR markers [38, 42-43]. These are cyclic amylose-derived oligomers composed of multiple glucose units linked via α -1-4 bond. Based on the number of repeating units, they can be classified as α -, β -, γ -cyclodextrins. Out of all the variants of cyclodextrins, *2-hydroxypropyl-cyclodextrins (HPCDs)* are of utmost interest due to their hydrophilicity, low PPB, higher stability, and FDA approval. They have already been studied for their

biological activity as a GFR marker in conjugation with fluorescent dyes such as FITC, fluorescein and XITC [38, 42].

Even though, the switch from urine/blood sampling to transcutaneous measurement has been a major leap in the field of kidney diagnostics, the use of dyes with their electromagnetic spectrum in the visible region (majorly blue and green) sets back the advantages of the non-invasive detection techniques due to their poor tissue penetration and low signal-to-noise ratio. Hence, this creates a need to move towards the longer wavelengths, particularly in the *near infrared (NIR) region* (650-900 nm) [45] for the development of kidney markers.

1.3.4 Near infrared dyes/tracers in kidney functional analysis

The use of fluorescent GFR markers has been revolutionising and offers great advantages over the previously used techniques. But the current clinically approved fluorescent markers lie mainly in the visible region of the electromagnetic spectrum. Moreover, these fluorescent markers still use invasive and expensive detection/measurement techniques, such as blood analysis, urine analysis and MRI.

Recent research in this field has seen increasing focus on developing dyes in the NIR region, such as *indocyanine green (ICG)* and *IRDye800CW* [38]. It further allows deeper tissue penetration and a better assessment [38, 44]. For example, cyanine 7 dyes have been studied in conjugation with cyclodextrins as a non-toxic way for assessing the GFR in NIR range [43-44]. There has been another study that used *Cy7.5 dye* to label *carboxymethyl inulin (CMI)* to measure the GFR [45].

In conclusion, NIR markers for GFR analysis have been proved beneficial. Nevertheless, it is important to develop methods for kidney diagnosis that include the evaluation of the other two functions of the kidneys, namely reabsorption and secretion, with the help of a non-invasive technique, such as transcutaneous measurement, to diagnose function-specific and location-specific abnormalities at an early stage.

1.4 Markers for kidney functional assessment

As stressed before, tubular secretion and reabsorption play as much a role in healthy functioning of the kidney as does filtration. Therefore, this project focuses

on synthesising novel dyes/tracers not only for measuring GFR, but also for evaluating secretion and reabsorption. Since the goal would be to measure all the three kidney functions simultaneously, the absorbance and emission wavelength for each marker is designed specifically different from each other to avoid spectral overlap.

These dyes are designed such that they are compatible with the transcutaneous device developed at Mannheim Medical Centre, Heidelberg University. The detection can be done in parallel with multiple LEDs, or successively. Moreover, the renal clearance of some of these markers are studied extensively using MSOT at iThera Medical, Germany and University of Liverpool, England.

1.4.1 Marker for glomerular filtration

An ideal GFR marker is cleared solely by the kidneys, where it is completely filtered by the glomeruli, and is neither secreted nor reabsorbed by the tubular cells. This ensures its clearance through the urine.

ABZWCY-H β CD (*Figure 3*) has been studied as a GFR marker and is proven efficient in doing so. It is filtered by glomeruli with minimal reabsorption or secretion by the tubular cells [44, 46]. It consists of a zwitterionic cyanine 7 dye, conjugated to 2-hydroxypropyl- β -cyclodextrin (HP β CD). Since anionic and cationic compounds may interact with the plasma proteins or can be secreted or reabsorbed within the proximal tubules of the nephrons, a zwitterionic charge on a cyanine 7 dye secures unhindered renal clearance with more than 97% urine recovery. Besides, the carrier H β CD, is a non-toxic hydrophilic oligosaccharide, which shows very low PPB (\sim 3.7%) and guarantees kidney-mediated clearance of the compound [44, 46].

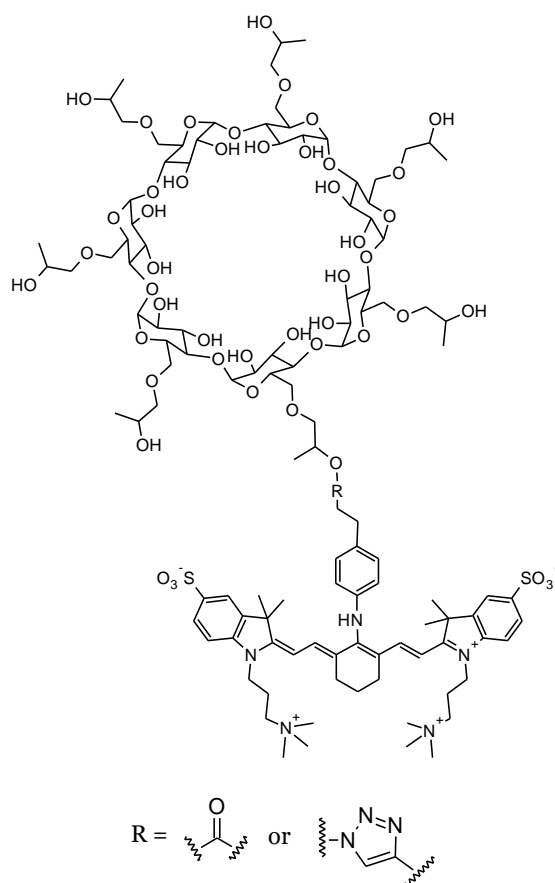


Figure 3: ABZWCY-H β CD [44, 46]

Also, ABZWCY-H β CD is stable and non-toxic, as demonstrated by *in vitro* and *in vivo* studies. ABZWCY dye is a NIR dye (Figure 4) with a large Stokes shift of 84 nm. This provides a better signal-to-noise ratio and allows deeper tissue penetration [44, 46].

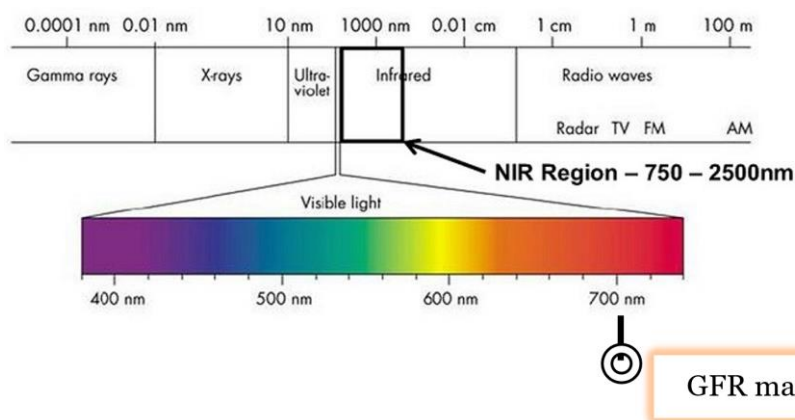


Figure 4: Representation of the GFR marker on the electromagnetic spectrum

The initial biological studies performed on ABZWYC-H β CD indicated scope for this compound as a GFR marker [44, 46]. The current investigation tests this marker's compatibility with the new transcutaneous device developed at University of Heidelberg, in combination with the other two markers that are developed for reabsorption and secretion. Furthermore, ABZWYC-H β CD's clearance is validated through live animal imaging using MSOT imaging at iThera Medical.

1.4.2 Markers for secretion

Tubular secretion in kidneys is a very important physiological process that helps the body to get rid of the waste and toxic compounds, including various drugs. Damage to these cells can lead not only to kidney impairment but affects other organs as well. Hence, it is important to develop markers that can diagnose compromised secretion in the kidneys [47].

For developing secretory markers, analogues of known OAT substrates are chosen in this project. PAH has already been reported to be secreted by the OATs in the tubular cells, but it is not fluorescent (*Figure 5*) [48]. Besides PAH, fluorescein is another known substrate for the OATs [47]. However, fluorescein has a pH dependent fluorescence, where it is highly fluorescent in alkaline pH but lowering the pH reduces its fluorescence intensity [49].

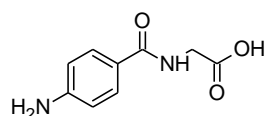


Figure 5: p-Aminohippuric acid

Therefore, to overcome the disadvantages of the known OAT substrates, various analogues are developed and analysed in this project. For example, rhodamine-derivatives are structurally analogous to fluorescein, but they do not have a pH dependency for their fluorescence. Hence, these markers will provide an added advantage for their biological application. The secretion markers will also be designed in the visible range, with discrete wavelengths from the reabsorption and the GFR markers. This is to ensure simultaneous transcutaneous measurement of different markers using the transcutaneous device.

These markers are tested for their chemical and biological characteristics, as described under *Materials and methods* and *Results*.

1.4.3 Markers for reabsorption

Apart from filtration and secretion, reabsorption is a very important kidney function. This in turn helps in maintaining the osmotic balance and optimum physiological conditions within the body.

A large variety of biomolecules, including glucose, amino acids, and peptides, along with xenobiotics, water and ions are reabsorbed by the tubular cells. Therefore, it is equally important to evaluate the kidney tubular reabsorption, as GFR, for a healthy kidney [50]. An ideal reabsorption marker should be completely filtered by the glomeruli and then reabsorbed entirely by the tubular cells.

Glucose is the metabolic fuel of a human body. It is needed for the functioning of each cell, and subsequently each organ and the organ system. Glucose requirements are not only met through diet, but also through body's endogenous production through glycogenolysis and gluconeogenesis. The proximal tubules in the kidneys are one of the sites for gluconeogenesis. For a molecule so crucial, it is important to always maintain its level in the blood flow. Kidney is the key organ involved in glucose homeostasis. Plasma glucose is unbound to proteins or other macromolecules, and hence gets freely filtered by the glomeruli. It is then through reabsorption in the proximal tubules that all the glucose gets retained in the body. This reabsorption is mainly mediated by GLUT1 and GLUT2 transporter proteins. A healthy kidney reabsorbs almost all the glucose reaching the tubules [51]. As a result, glucose suits both the requirements for a reabsorption marker and is chosen as a candidate molecule to be labelled with a dye.

In the design of the fluorescent glucose, two different aspects come under consideration:

1. The extent of uptake for each marker by the GLUT transporter proteins when there are one, two or three molecules of glucose in proximity. This can be achieved by conjugating a dye molecule with varying numbers of glucose molecules (*Figure 6*).

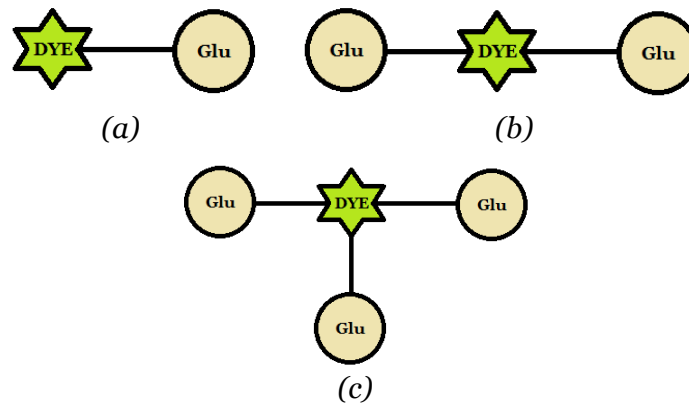


Figure 6: Dye conjugated with (a) one glucose (b) two glucose and (c) three glucose molecules

2. The extent of uptake for each marker by the GLUT transporter proteins when the glucose is labelled with the dye at its carbon 1 and carbon 2 position (Figure 7). *Hergenrother et. al.* has demonstrated that fluorescent glucose shows better uptake when labelled with a dye at C1-position, in comparison to when labelled at C2-position [52].

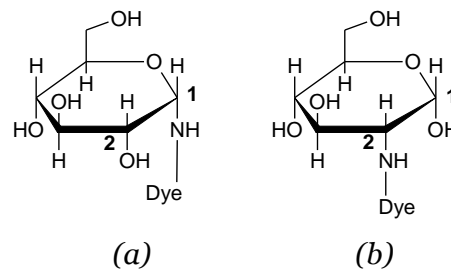


Figure 7: Glucose tagged to dye at (a) C1 and (b) C2 carbon position

The reabsorption markers will be developed in the NIR range electromagnetic spectrum in the using cyanine 7 dyes (Figure 8). This distinguishes them from the spectra of GFR and secretion markers.

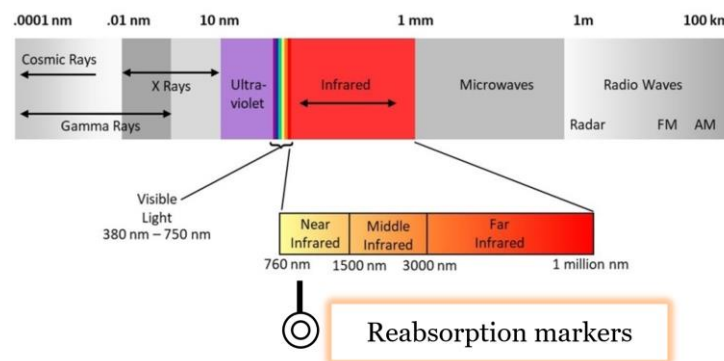


Figure 8: Representation of the reabsorption markers on the electromagnetic spectrum

1.4.4 Markers for vascular imaging

All cells in a body are supplied with a constant flow of blood to provide nutrients, oxygen and to eliminate the waste generated within these cells. Therefore, changes in the body's vascularisation, which in turn leads to an imbalanced blood flow to the cells, could have adverse effects on the organ functioning. Kidneys are affected in a similar way. Therefore, in addition to the functional analysis, it is useful to study the histology of the kidneys to get a better grasp at disease progression.

Previously, Gretz *et al.* reported one such fluorescent marker by conjugating a cationic cyanine dye (MHI148) to polyethyleneimine (PEI), which proved very useful (*Figure 9*). They also reported an ethyl-cinnamate based clearing protocol, which provides a faster, safer, and effective way for tissue clearing [53].

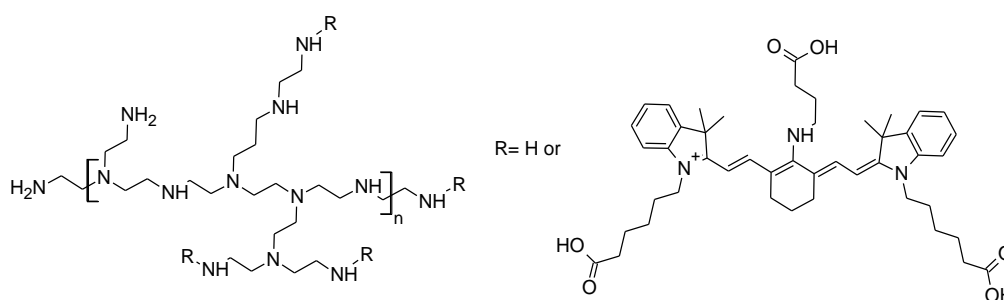


Figure 9: MHI-148-PEI [53]

It was reported by Gretz *et al* that a fluorescent marker with a hydrodynamic diameter (HD) larger than 6 nm, and the molecular weight more than 50 kDa will not get filtered through the vascular fenestrations. Moreover, PEI, is a highly cationic polymer that allows strong electrostatic interactions with the negatively charged GAGs [53]. MHI148-PEI showed good results, with the possibility of visualising the bigger blood vessels and the glomeruli [53]. Nevertheless, PEI has been reported to be toxic for biological systems and can create problems with the Regulatory Affairs [54]. Further, the cyanine dye used in the study (MHI148) has certain drawbacks that will be discussed in detail under *Results*.

The current research explores the development and use of newly synthesised fluorescent markers for staining kidney vasculature, which aim to overcome the disadvantages of MHI-148-PEI.

1.5 Aims of the project

The primary goals for this project include:

- ❖ development/optimisation of fluorescent markers that are:
 - filtered by glomeruli.
 - excreted by tubular secretion.
 - reabsorbed by tubules.

and are compatible with the transcutaneous device for parallel/successive measurement, as well as the multispectral optoacoustic tomography (MSOT) imaging.

- ❖ develop NIR dyes compatible for use with whole animal perfusion-fixation protocols to facilitate imaging of intact 'cleared' organs ex vivo.

The next section outlines the materials and methods used for achieving the above-mentioned goals.

2. Material and Methods

2.1 Instruments and special materials

Instruments/Product	Model/Manufacturers
Analytical balance	Sartorius CP225D, France
Confocal microscope	Leica TCS SP8, Leica Microsystem, Germany
Deuterium chloride solution	Aldrich, Italy
Dialysis bags	Pur-A-Lyzer™ Mega Dialysis Kit (MWCO 3500), Aldrich, Italy
	Slide-A-Lyzer™ Dialysis Flask, 2K MWCO, 250mL, ThermoFisher Scientific, United States
Dowex 50 W X 8-200 ion-exchange resin	Aldrich, Italy
Fluorescence spectrophotometer	Cary Eclipse, Varian, United States
Freeze dryer	StepBio Labryo – 85, Italy
HPLC	1260 Infinity II LC System, Agilent Technologies, United States
HPLC column	Poroshell 120 EC-C18, 4 µm, 4,6 x 150 mm, Agilent Technologies, United States
Hydrogen gas cylinder	Messer™ CANgas, 99.999 %, Aldrich, Italy
LightSheet microscope	Leica TCS SP8 DLS, Leica Microsystem, Germany
MALDI-Tof mass spectrometer	XEVOG2-Xs Q-Tof, Waters™, United States
Microcentrifuge tubes	Eppendorf® Safe-Lock CAPP Expell Secure, Germany
Microvolume UV-Vis spectrophotometer	NanoPhotometer®, Implen, Italy
Milli-Q water	Elix 5 and Milli-Q Gradient A10, Millipore SAS, France
	Elix 10 and Milli-Q Advantage A10, Millipore SAS, France
MSOT	MSOT inVision, iThera Medical, Germany
NIR confocal microscope	Stellaris SP8, Leica Microsystem, Germany
NMR solvents	Euriso-top®, France
NMR spectral analyses	MercuryPlus 400 MHz, Varian and MercuryPlus 600 MHz,

	Varian, United States
pH-Meter	Mettler Toledo SevenCompact™ Duo, Italy
pH-Meter electrode	Mettler Toledo InLab® Science Pro-ISM, Italy
Plasma protein binding assay kit	Fast Micro Equilibrium Dialyzer (25 to 1,500 µl Sample Volume), Harvard Bioscience, Inc., United States
Pre-packed silica gel and C18 columns	Interchim®, France
Rotary evaporator	Heidolph, Schwabach, Germany
Silica gel	Aldrich, technical grade, pore size 60 Å, 200-425 mesh particle size, Italy
Silica gel plates	Polygram® Sil G/UV254, Macherey-Nagel, Germany
Solvents and chemical reagents	Aldrich, Italy
Ultrasonic Bath	Sonica 2200, Soltec, Spain
UV-Vis spectrophotometer	Cary 100 Bio, Varian, United States

Table 2: List of instruments and special materials

2.2 Fluorescent markers and their characterisation

The fluorescent markers and their precursors, for assessing kidney functions and imaging the vasculature, were designed according to the requirements as discussed in detail in the *Results* section. Their synthesis and purification methods are further described in detail in the *Appendix*. The characterization of each compound included TLC, analytical HPLC and ¹H-NMR. In the case of fluorescent compounds, UV-Vis and fluorescence spectrophotometry were carried out, along with the calculation of ϵ (molar absorption coefficient, M⁻¹cm⁻¹). For all the compounds that have been reported for the first time in literature, ¹³C-NMR and LC-MS spectrometry was also carried out.

2.3 Optical property characterisation

All aqueous solutions were prepared using Milli-Q water. All solvents were supplied by Aldrich, Italy and used as received. Stock solutions of all the compounds were prepared in dark and were prepared fresh right before the experiments. All the spectroscopic measurements were conducted in Milli-Q

water for the hydrophilic compounds and in methanol for the hydrophobic compounds. UV-Vis and fluorescence spectra were acquired using the UV-Vis spectrophotometer and the fluorescence spectrophotometer respectively (*Table 2*). All measurements were conducted at 25 °C. Extinction coefficients were calculated using the Lambert-Beer law (*Equation 1*) [55].

$$A = \epsilon cl$$

(*Equation 1*) [55]

where,

A = Absorbance

ϵ = Molar absorption coefficient ($M^{-1}cm^{-1}$)

c = Molar concentration (M)

l = optical path length (cm)

2.4 Degree of labelling measurement (DOL)

The DOL for all the fluorescent water-soluble chitosan markers were calculated using the spectroscopy method and the Lambert-Beer law [55]. In this study, the DOL is the average number of dye molecules coupled to WS Chitosan. It is calculated based on *Equation 2*.

$$DOL = m1/m2$$

(*Equation 2*)

where,

m1 is the moles of dye, calculated based on the *Equation 1*, where the value of **A** is measured using the UV-Vis spectrophotometer, value of **l** is known for the used spectrophotometer and the value of **ϵ** is known from the literature and is specific to the dye under examination.

m2 is the moles of dye-WS Chitosan. The moles were calculated based on the weight of compound used for their UV measurements, assuming that the contribution of the dye to the molecular weight of the conjugate is negligible.

2.5 Photostability assays

These studies were carried out in collaboration with the Department of Biopharmanet-TEC, University of Parma. Measurement of absorption and fluorescence were obtained using a Cary 4000 UV-Vis spectrophotometer (Agilent) and an FS5 (Edinburgh Instruments) spectrofluorometer (FLUORACLE

software). The analyses were performed in phosphate buffered saline (PBS) at pH 7.4 at 20 °C.

Spectrophotometer parameters:

Data interval	1 nm
Scan rate	300 nm/min

Spectrofluorometer parameters:

Bandwidth	2 nm
Dwell time	0.3 s

Serial dilutions of WS Chitosan and PEI conjugated dyes were made in PBS and absorption spectra were generated. The concentration with the absorption maxima between 0.01 and 0.1 was chosen for the stability studies. Mean absorption and emission spectra (3 replicates) were collected before (time 0) and after 170 minutes of continuous illumination. The corresponding percentage loss of fluorescence was recorded for each marker.

2.6 Calibration curves

The calibration curves were performed on a series of known concentrations of free dyes and conjugates. Dye stock solution 0.01 Mm were prepared using Milli-Q water for all the markers. The dilutions were carried out differently for different markers. The curves are presented under *Results*. In case of the reabsorption markers, since they are all Cyanine 7–based dyes, the dilutions tested were kept the same for all four markers. The markers were diluted to a concentration ranging from 10 Mm to 0.1 Mm. The calibration curves for Cy7 – monoGlucose C1, Cy7 – monoGlucose C2, Cy7 – diGlucose C2 and Cy7 – triGlucose C2 were generated using the fluorescence readout from the spectrophotometer. For secretion markers, different types of dyes were used. Therefore, the concentrations tested for each marker, and the corresponding calibration curves were different.

2.7 Plasma protein binding assays

Ms. Yinuo Xie at University of Heidelberg performed the PPB assays using the Fast Micro Equilibrium Dialyzer (25 to 1500 mL sample volume), provided by

Harvard Bioscience, Inc (*Figure 10*) according to the protocol described in Huang J *et al* [44] and calculated the PPB for each marker using the formula derived from the Lambert-Beer law [55]:

$$\%PPB = \frac{[A(\text{Plasma})-A(\text{Plasma ctrl})] - [(A(\text{PBS})-A(\text{PBS ctrl}))]}{[A(\text{Plasma})-A(\text{Plasma ctrl})] + [(A(\text{PBS})-A(\text{PBS ctrl}))]} * 100\%$$

(Equation 3)

where *A* is the absorption value recorded using UV-Vis spectrophotometer.

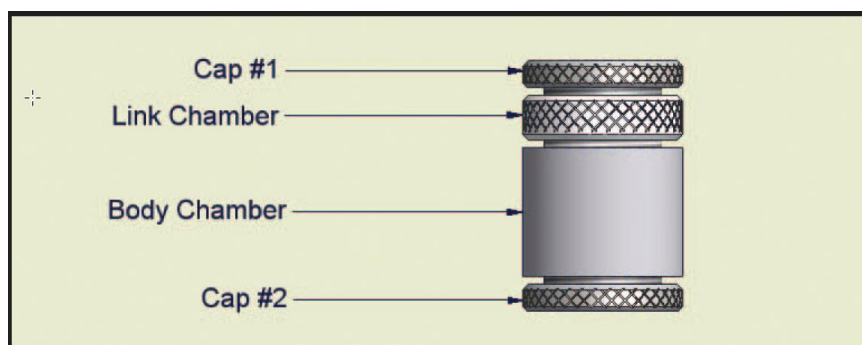


Figure 10: Fast Micro Equilibrium Dialyzer provided by Harvard Bioscience, Inc.

2.8 Luminescent cell viability assays

Ms. Yinuo Xie at University of Heidelberg performed the cell viability assays using the protocol provided with CellTiter-Glo® 2.0 reagent based luminescent cell viability assays. The cell viability is determined by the quantification of the cell's metabolic activity in terms of ATP production. CiPTEC expressing organic anion transporters 1 (CiPTEC-OAT1) were used for studying the secretory markers, while human renal proximal tubular epithelial cells (HK-2) were used for the reabsorption markers. Concentrations used for each marker were based on their calibration curve studies.

2.9 *In vitro* cellular uptake studies

2.9.1 Uptake assays for secretion markers

Mr. João Ferreira Faria at Utrecht University performed the cellular uptake assays for all the secretion markers. ciPTEC-OAT1 were cultured as described by Nieskens *et al* [56]. Uptake assays were performed using the protocol reported in Mihaila, S.M. *et al* [57]. Fluorescein (1 μM) was used as a positive control.

To confirm the activity of OAT1, probenecid (500 μ M) was simultaneously incubated with fluorescein or the secretion markers. The uptake of the selected dyes was assessed by looking into the functional activity of OAT1 transporter, and the efflux pumps BCRP and intracellular fluorescence was detected using the GloMax[®] Discover microplate reader at excitation wavelength and emission wavelength specific to the marker under study.

2.9.2 Uptake assays for reabsorption markers

Mr. João Ferreira Faria at Utrecht University performed the uptake assays for all the reabsorption markers. Human renal proximal tubular epithelial cells were cultured according to the manufacturer's instructions (HK-2; ATCC[®], CRL-2190[™]). Uptake assays were performed using the protocol reported in Mihaila, S.M. *et al* [57]. Intracellular fluorescence was detected using the GloMax[®] Discover microplate reader at excitation wavelength and emission wavelength specific to the marker under study. Data were corrected for the background and normalized to untreated cells.

2.10 Transcutaneous device

A new transcutaneous device was developed by Mr. Mohammed Mohiuddin Yusuf at the University of Heidelberg in collaboration with Bundesministerium für Bildung und Forschung (BMBF) project, *OxiFlexIT* (Grant number: 13GW0330).

The newly developed device consists of a single photodiode along with eight LEDs placed at different positions as shown in *Figure 11(a)*. Each LED housing has a combination of three LEDs of different wavelengths: red (650 nm), near-infrared (950 nm) and green (525 nm). The distance between any two adjacent LED combination is 1 cm, so is the distance between the photodiode and any of the adjacent LED combination. The three wavelengths correspond to the measurement of the three kidney functions being analysed. The device is connected to the computer for power via a USB-C cable. Another USB-C connection from the device into the computer is responsible for the data transfer.

The fixation of the device onto the skin is facilitated by a double-sided adhesive patch as shown in *Figure 11(b)*. The device is first stuck on one side of this patch after which the other adhesive side is carefully placed on the skin. The use of this

patch avoids variability in the fixation of the device on the skin surface and helps to reduce movement artifacts. Since there are precise cut-outs for LEDs and photodiode on the patch, this also provides insulation from ambient light.

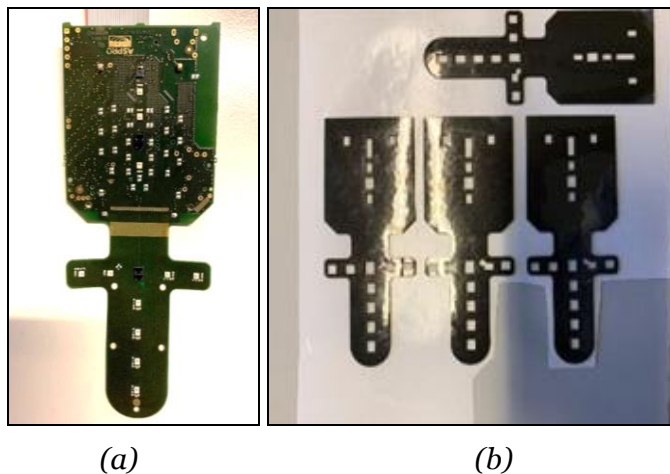


Figure 11: (a) New device; (b) double-sided adhesive patches

2.11 MSOT imaging

Mr. James Littlewood at iThera Medical, Germany carried out the MSOT studies on the GFR marker in mice using a protocol described in his Ph.D. thesis [58].

The image reconstruction was done using viewMSOT 4.0 (iThera, Germany) with 4.0 back projection algorithm and a field of view of 25 mm.

2.12 Tissue clearing and fluorescent microscopy

Ms. Tiziana Picascia at University of Heidelberg performed the tissue clearing and perfusion according to the protocol reported by Huang, J., Brenna, C., Khan, A.M. *et al* [53]. They have developed a pressure- and volume-controlled retrograde perfusion protocol, which allows the use of all parts of an animal (*Figure 12*).

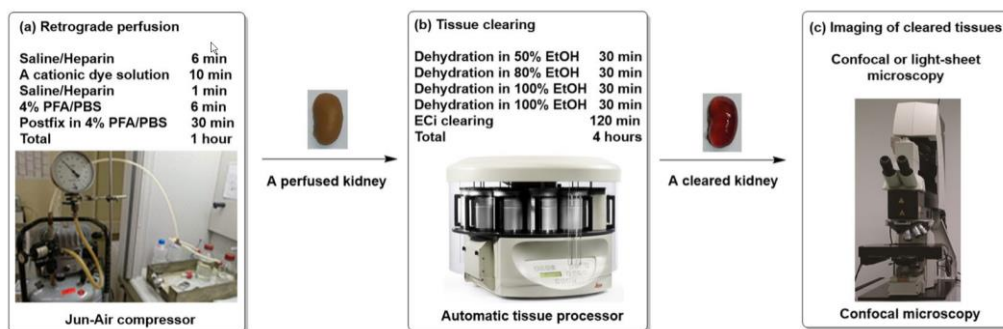


Figure 12: Image and protocol adapted from Huang, J., Brenna, C., Khan, A.M. *et al* [53]

3. Results

3.1 Markers for secretion

3.1.1 Introduction and work strategy

As discussed in *section 1.4.2*, secretion markers were designed to mimic the activity of known OAT substrates, such as PAH and fluorescein [47-48]. These markers are designed in the visible range, with discrete wavelengths well separated from the reabsorption and the GFR markers (*Figure 13*). This is to ensure the possibility of a simultaneous transcutaneous measurement of different markers.

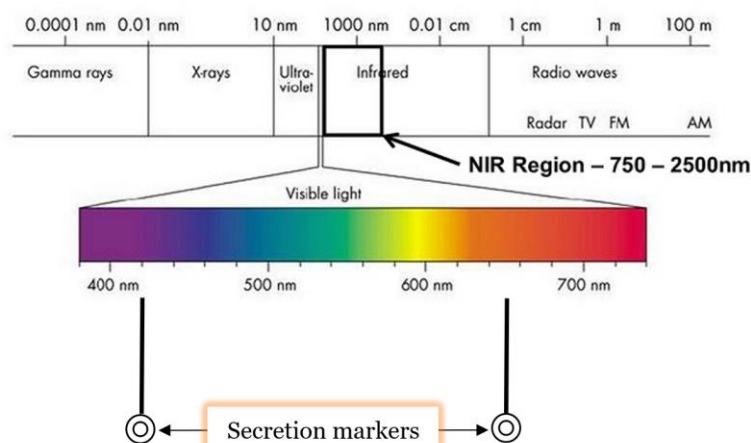


Figure 13: Representation of the secretion markers on the electromagnetic spectrum

To mimic PAH's biological activity, it was important for the markers to have a molecular weight less than 600 Da, the presence of a carboxyl group, and an overall negative/neutral charge [48]. Therefore, three markers fulfilling these criteria were chosen as the initial candidates for the secretion markers (*Figure 14*).

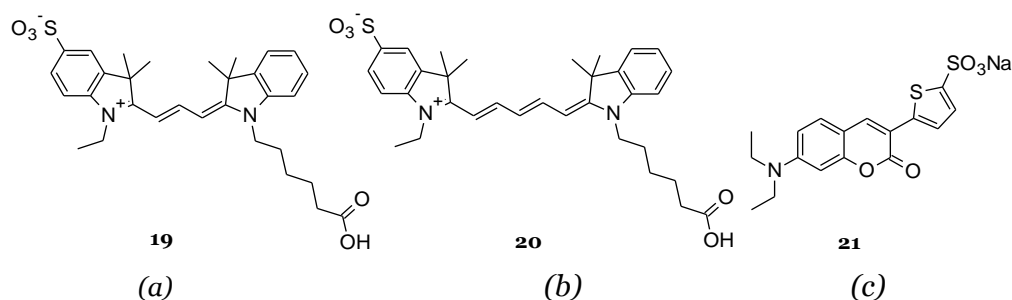


Figure 14: Chemical structures of the first three secretion markers: (a) Cy550Z - 01 (19), (b) Cy645Z - 01 (20) and (c) CUM450 LSS - 01 (21)

Even though these markers suited all the characteristics needed for a secretion marker (Table 3), they presented solubility issues. Being hydrophobic, they were neither fully soluble in water, nor in aqueous solution containing 10% DMSO. For a biological experiment, 10% DMSO solution is the maximum limit since beyond this percentage it can be toxic to cells. Also it has been shown that hydrophobic compounds have a high affinity for the OAT1 and thereby have very low transportation rate. Therefore, these markers act as OAT1 blockers [59].

Secretion markers	λ_{ab} (nm)	λ_{em} (nm)	ϵ ($M^{-1} cm^{-1}$)	M.w. (Da)	Net charge
Cy550Z - 01	546	560	150,000	550.71	0
Cy645Z - 01	643	660	250,000	576.75	0
CUM450 LSS - 01	457	515	37,000	401	-1

Table 3: Chemical and spectrophotometric characteristics of the first-generation secretion markers

As a result, the biological tests performed on these markers were non-reproducible and non-deductive and were taken out of consideration.

To overcome the challenges from the initial secretion markers, a new set of markers were designed, which were highly hydrophilic due to the presence of multiple negatively charged functional groups (Figure 15).

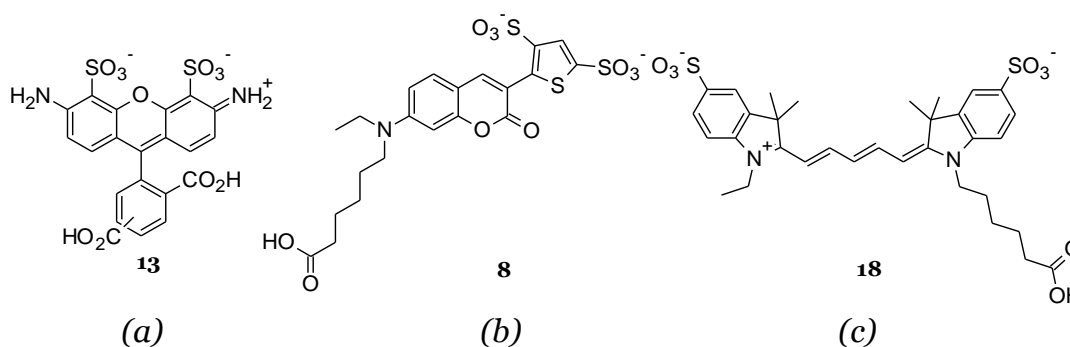


Figure 15: Chemical structures of the new secretion markers: (a) STAR FLUOR 488 Acid (13), (b) STAR FLUOR 405L Acid (8) and (c) Cy645A-Acid-01 (18)

Like the previous dyes, these markers also have a free carboxylic group, an overall negative/neutral charge and molecular weight around 600 Da. Also the absorption and emission spectra for these dyes are in the visible range, thereby being discrete from that of the reabsorption and GFR markers (Table 4).

Secretion markers	λ_{ab} (nm)	λ_{em} (nm)	ϵ ($M^{-1} cm^{-1}$)	M.w. (Da)	Net charge
STAR FLUOR 488 Acid	488	520	73,000	552.26	-2
STAR FLUOR 405L Acid	412	507	26,000-27,000	543.58	-2
Cy645A-Acid-01	648	667	250,000	694.90	-1

Table 4: Chemical and spectrophotometric characteristics of the new secretion markers

These dyes are completely soluble in water, and hence are a better fit for the biological experiments. Additionally, rhodamine **13** mimics fluorescein in its structure, which is a known substrate for OATs in the renal tubules [47]. Unlike fluorescein, compound **13**'s fluorescence is pH independent. Also coumarin **8** provides an additional advantage of a large Stokes shift (80 nm). A small Stokes shift leads to crosstalk between the light of the excitation source and the emission of the dye, which can in turn lead to low signal-to noise ratio. Also this crosstalk can cause back-scattering from the biological specimen, resulting in self-quenching [60]. In addition, secretion markers **13** and **8** at higher concentrations, show very low quenching, thereby giving a heightened fluorescence. Cyanine 5 (**18**) (Figure 15) on the other hand moves further towards the NIR and hence provides a better signal-to-noise ratio, with a higher molar extinction coefficient as compared to compounds **13** and **8**.

Additionally, a third generation of secretion markers was developed. As shown in Figure 16, rhodamine **12** and coumarin **9** are a less anionic version of rhodamine **13** and coumarin **8**.

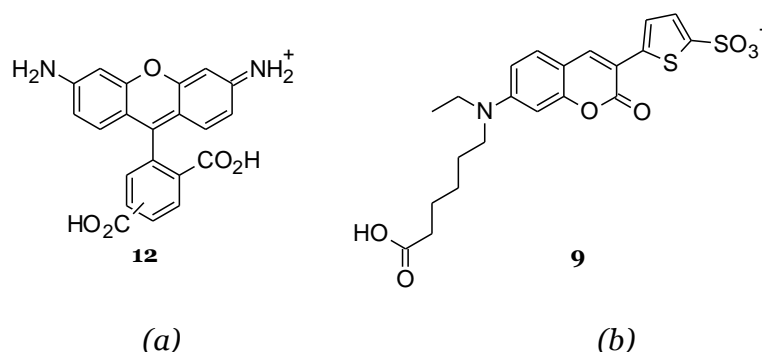


Figure 16: Chemical structures of the less anionic versions of the new secretion markers: (a) Rhodamine 110 (**12**) and (b) 500 LSS Acid – monoSO₃ (**9**)

This was done to mimic the overall chemical structures of the known secretion markers i.e., PAH and fluorescein. Rhodamine **12** does not have any sulfonate

group present, and mimics fluorescein's chemical structure more than rhodamine **13** (Figure 16 (a)). Also, PAH does not contain a sulfonate group, which gives it an overall neutral charge. Even if coumarin **9** has still one sulfonate group present, as it is needed for solubility in water, it resembles PAH's chemical properties better than coumarin **8** (Figure 16 (b)) by having a -1 net charge, as opposed to -2 of coumarin **8**.

Secretion markers	λ_{ab} (nm)	λ_{em} (nm)	ϵ ($M^{-1} cm^{-1}$)	M.w. (Da)	Net charge
Rhodamine 110	488	520	80,000	426.4	0
500 LSS Acid – monoSO ₃	444	518	44,000	464.52	-1

Table 5: Chemical and spectrophotometric characteristics of Rhodamine 110 (**12**) and 500 LSS Acid – monoSO₃ (**9**)

The synthesis of coumarin derivatives (**8** and **9**) involves consecutive amine-alkylations of 3-aminophenol **1**, followed by its formylation using Vilsmeier reagent. The salicylaldehyde derivative **5** is then hydrolysed to give a carboxylic acid **6**, and subsequently condensed with 2-(thiophen-2-yl) acetonitrile to give a coumarin **7**. This fluorescent solid, depending on the amount of sulfur trioxide dimethyl-formamide complex used, can yield a mono-sulfonated **9** or a di-sulfonated coumarin derivative **8** (Figure 17).

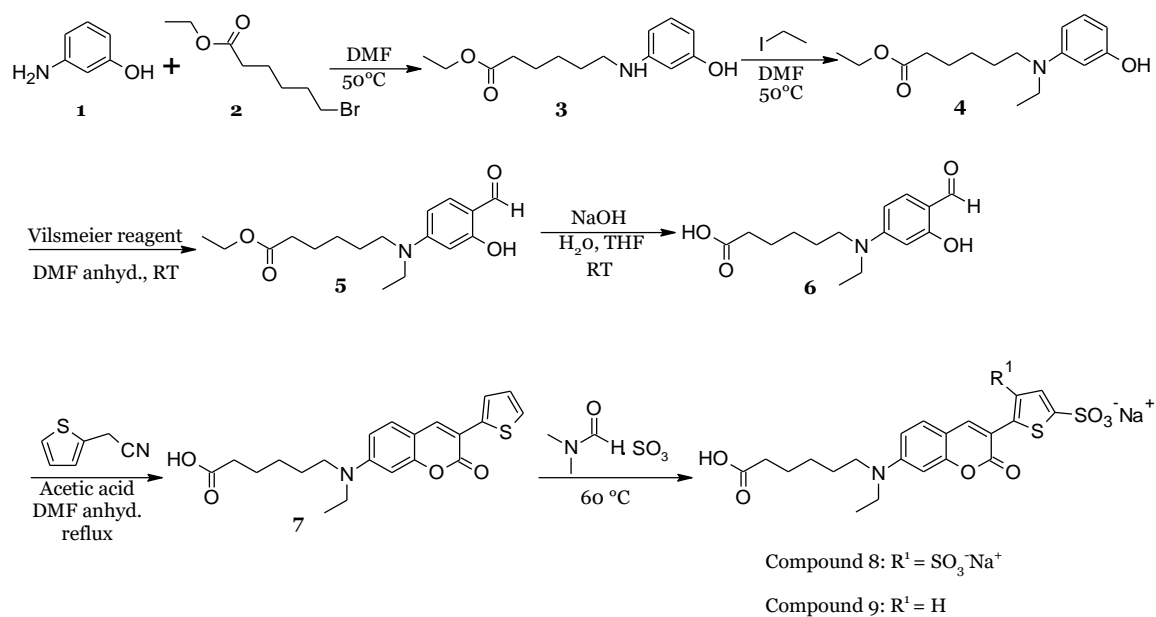


Figure 17: Reaction scheme for synthesising coumarin **8** and **9**

The synthesis of Rhodamine 110 (**12**) was carried out according to the procedure reported in CN105669634A, which involves a condensation reaction between 2 equivalents of ethyl (3-hydroxyphenyl) carbamate **11** and 1 equivalent of phthalic anhydride **10** in the presence of Friedel-Crafts reagents to give the product as an isomeric mixture **12** [61]. This can further be sulfonated using fuming sulfuric acid 30% to yield STAR FLUOR 488 Acid **13** (Figure 18).

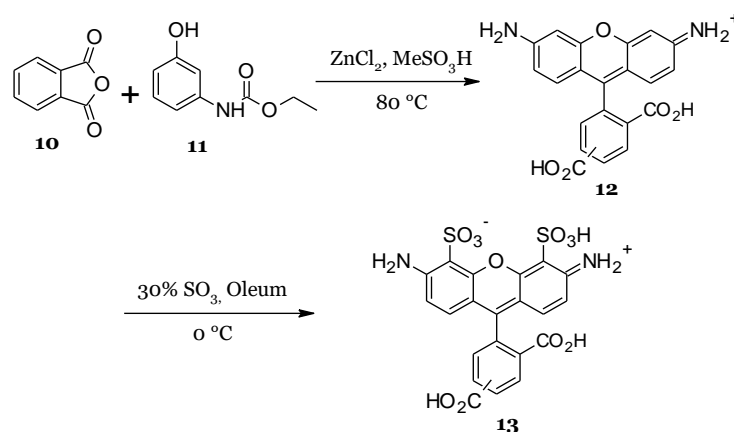


Figure 18: Reaction scheme for synthesising Rhodamine-derivatives

For the synthesis of Cy645A-Acid-01 (**18**), the general procedure for an asymmetric cyanine 5 dye was followed. The first step was the condensation reaction between the zwitterionic iodolium derivative **14** and malondialdehyde derivative **15** under acidic conditions to yield an acetylated intermediate **16**. This activated intermediate is further subjected to condensation with the *N*-carboxypentyl indolium **17** in the presence of potassium acetate to yield a crude product, that is further purified to obtain a blue, fluorescent cyanine 5 (**18**) in pure form (Figure 19).

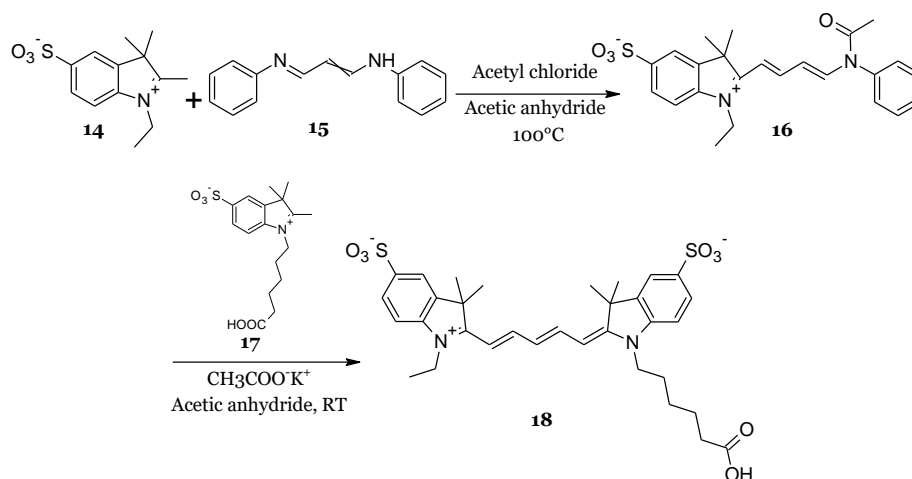
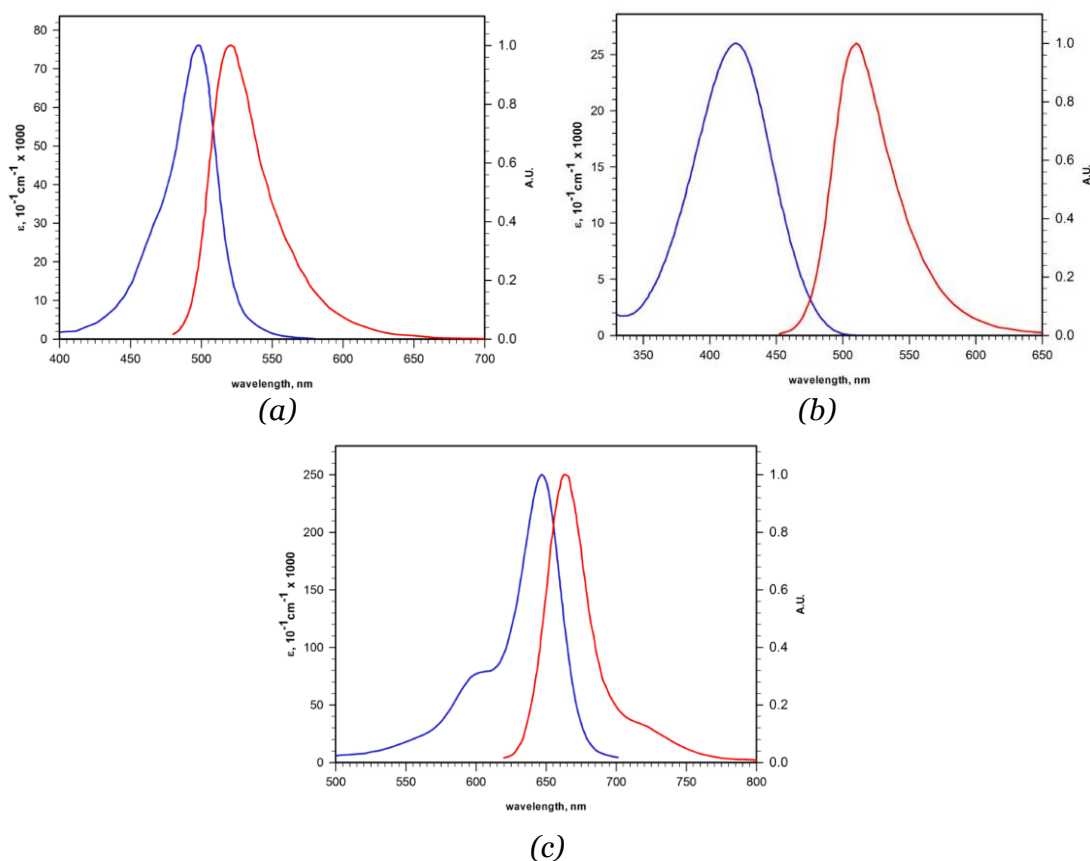


Figure 19: Reaction scheme for synthesising Cy645A-Acid-01 (**18**)

Synthesis, purification, and characterisation of the secretion markers is discussed in detail in the *Appendix*. Synthesis is not reported for Cy550Z – 01 (**19**), Cy645Z – 01 (**20**) and CUM450 LSS – 01 (**21**) as they were provided by Cyanagen for direct use in the project.

3.1.2 Physicochemical and optical properties

The secretion markers have been designed in the visible region of the electromagnetic spectrum to be distinguished from the filtration and the reabsorption markers to allow simultaneous examination of kidney functions (*Figure 20*).



*Figure 20 : Electromagnetic spectra of the secretion markers: (a) Rhodamine 110 (**12**) and STAR FLUOR 488 Acid **13**, (b) STAR FLUOR 405L Acid **8** and 500 LSS Acid – monoSO3 (**9**), and (c) Cy645A – Acid – 01 (**18**)*

3.1.3 Calibration curves and dosage

Due to the hydrophobicity problems encountered with secretion markers **19**, **20** and **21** (*Figure 14*), these markers were later removed from the library.

Therefore, the calibration curves were not generated for these markers. For rhodamines **13** (Figure 15) and **12** (Figure 16), the stock solution was diluted to a concentration ranging from 10 μM to 0.0005 μM . A single calibration curve for these two dyes was generated (Figure 21).

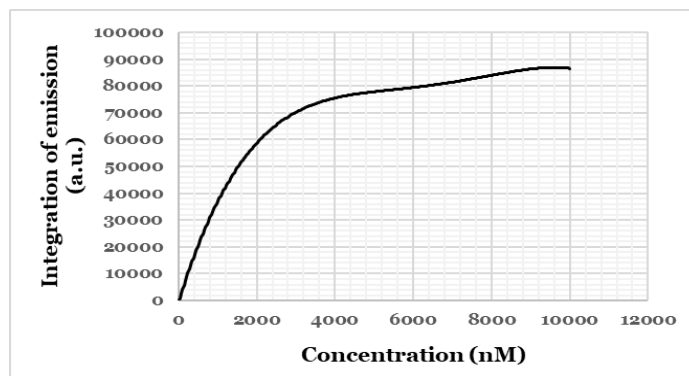


Figure 21: Calibration curve for rhodamines **13** and **12**

These dyes differ by the presence/absence of two sulfonate groups (Figure 22). This affects their overall optical properties slightly only at high concentrations, where rhodamine **13** shows less quenching when compared to **12**. Nevertheless, the difference in the calibration curves at very high concentrations is not relevant for this project, as the *in vivo* tests will be conducted at much lower concentrations (0.1–4 μM).

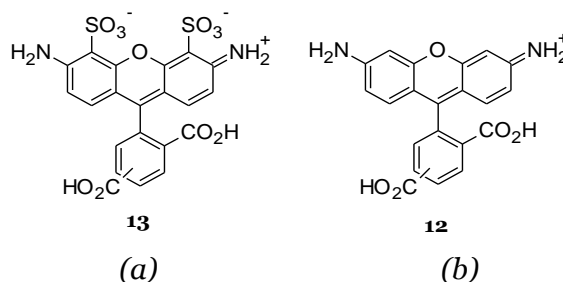


Figure 22: Chemical structures of the rhodamine-derived secretion markers, where **12** (b) differs from **13** (a) only by the absence of the two sulfonate groups

Like the rhodamine-derivatives **12** and **13**, a single calibration curve was generated for coumarins **8** (Figure 15) and **9** (Figure 16) with dilutions of the stock solution to concentrations ranging from 10 μM to 0.0005 μM (Figure 23).

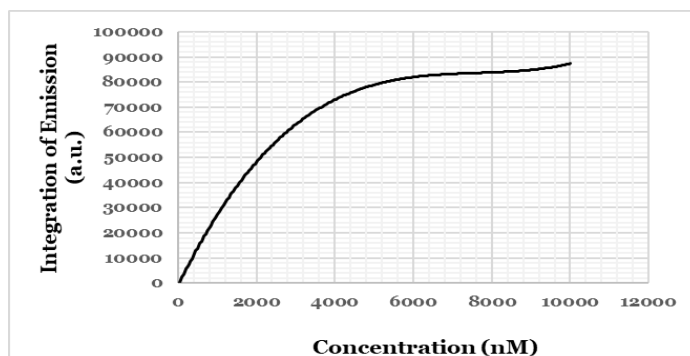


Figure 23: Calibration curve for coumarins **8** and **9**

Coumarins **8** and **9** also only differ by the presence/absence of one sulfonate group (Figure 24). However, coumarin **9** has a leftward shift in its emission spectra by 10 nm with respect to coumarin **8**. Even though, the difference in the presence/absence of sulfonate moieties influence quenching within these dyes, nevertheless that occurs at higher concentrations, which were not used in the current project.

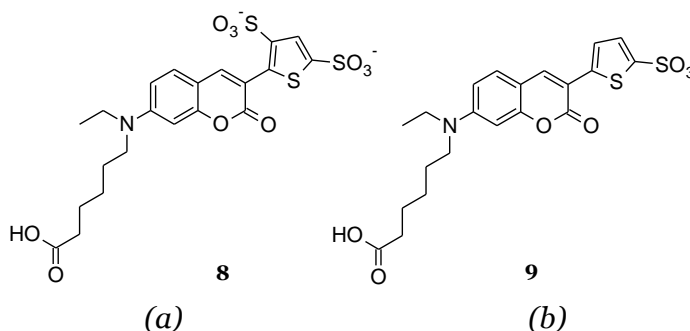


Figure 24: Coumarin **8** (a) differs from **9** (b) by the absence of a sulfonate group

Compound **18** (Figure 15(c)), unlike the rhodamine and coumarin derivatives depicted above, shows quenching after 3 μM concentration (Figure 25). The dye was diluted to concentrations ranging from 10 μM to 0.005 μM .

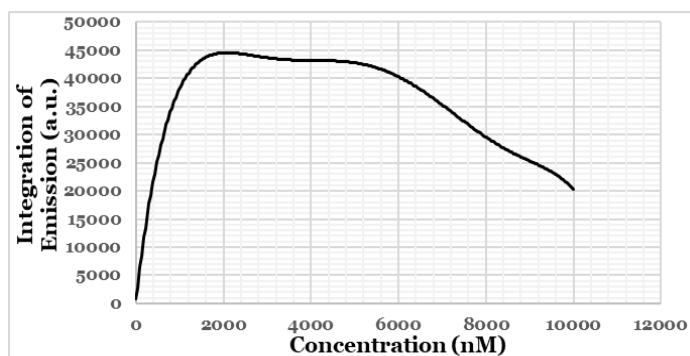


Figure 25: Calibration curve for Cy645A - Acid - 01 (**18**)

For cytotoxicity and cellular uptake evaluation of all the secretion markers, different points on the calibration curves were considered to study their activity at different concentrations. However, for *in vivo* applications, it is better if the concentration lies in the plateau region of the graph. This is because, within the plateau region, small differences in the concentration do not cause large variations in the fluorescence readout. This is especially important for *in vivo* applications, as small concentration variations might arise due to handling error, such as, solubilisation of the dye at an exact concentration, drawing up the dye solution in a syringe, injecting it in the animal/human subject etc. Therefore, based on the calibration curves, it is recommended to use a dosage concentration of more than 2 μM for rhodamine-derivatives (**12** and **13**) and 500 LSS Acid-derivates (**8** and **9**). While for Cy645A-Acid-01 (**18**), it is recommended to use a concentration between 1.5-5 μM .

3.1.4 PPB assays

Plasma protein binding is involved in determining pharmacokinetics, pharmacodynamics and biodistribution of a molecule or a pharmacophore. Therefore, it becomes necessary to study this characteristic for drugs and markers to predict their biological activities. Mostly, lipophilic dyes are associated with higher plasma protein binding and hepatic clearance, whereas hydrophilic dyes present shorter plasma half-life due to low PPB, and renal clearance [62-63]. Therefore, to predict the plasma half-life of the secretion markers, and their metabolic pathway *in vivo*, Ms. Yinuo Xie performed the PPB assays using the protocol mentioned in section 2.7 (Figure 26).

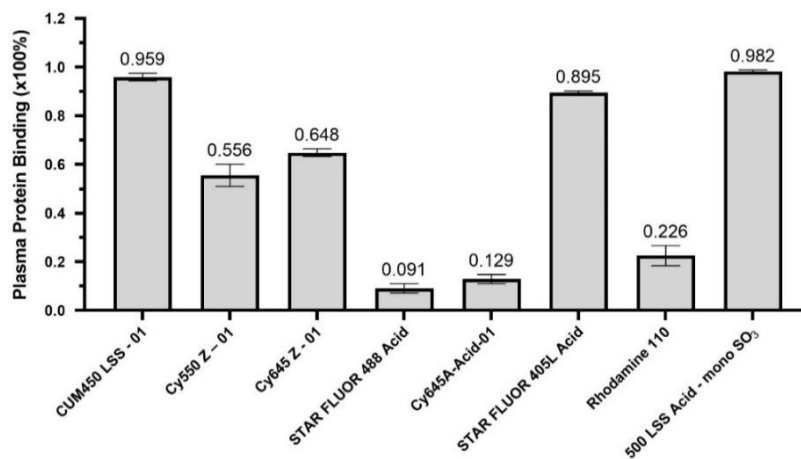


Figure 26: PPB assays performed by Ms. Yinuo Xie at the University of Heidelberg [64]

Different markers showed varying PPB, which is based on their chemical structures and affinity towards the plasma proteins. All the experiments were performed in triplicates.

3.1.5 Cell viability assays

The cell viability assays were performed for all the markers at different concentrations, as suggested by the calibration curves. All the five secretion markers from the second and the third generation were not toxic at concentrations below 10 μM , which is the recommended dose for the *in vivo* experiments (Figure 27). Hence, they are all safe for use in animal experiments.

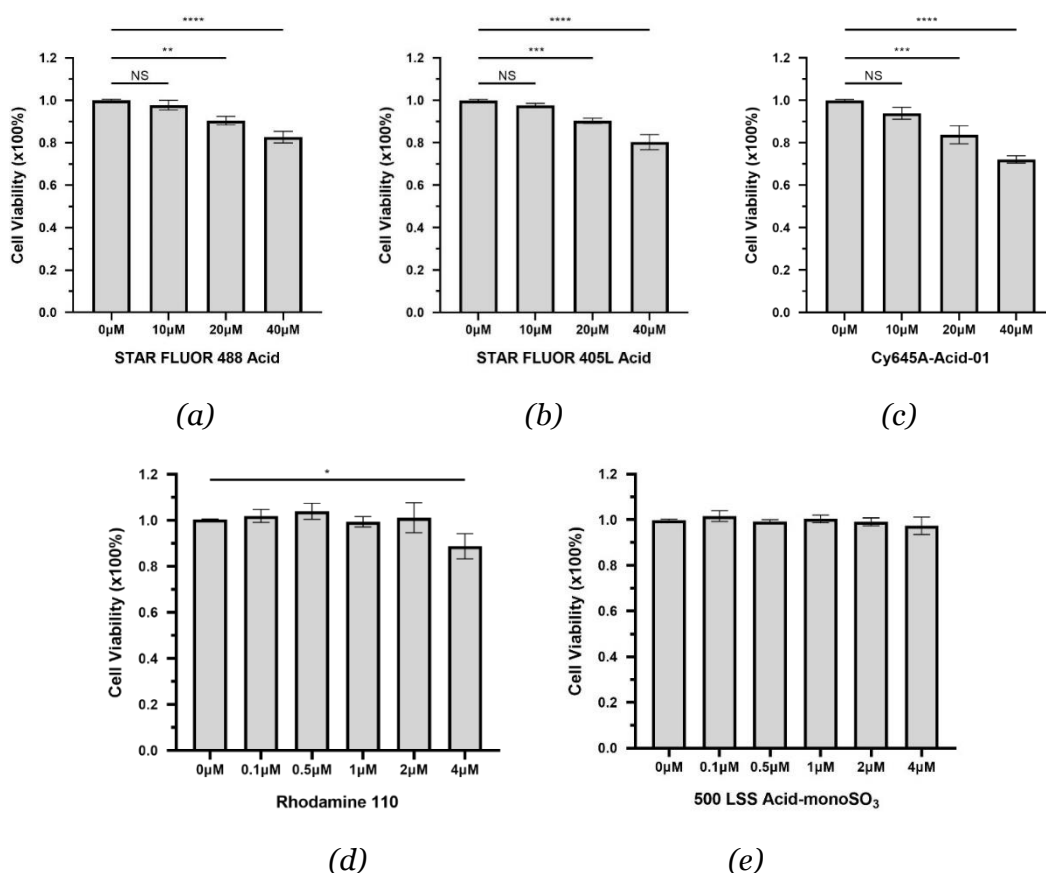


Figure 27: Cell viability assays performed by Ms. Yinuo Xie at the University of Heidelberg on *ciPTEC-OAT1* cell line when incubated with the secretion markers for 3 hr. The secretion markers consisted of (a) STAR FLUOR 488 Acid **13** (b) STAR FLUOR 405L Acid **8** (c) Cy645A-Acid-01 (**18**) (d) Rhodamine 110 (**12**) and (e) 500 LSS Acid-monoSO₃ (**9**) [64]

NS: no significant difference, * $p < 0.05$, ** $p < 0.01$, *** $p < 0.005$, **** $p < 0.0001$

3.1.6 *In vitro* uptake assays

In vitro uptake assays were carried out on the secretion markers at 1, 2 and 4 μM concentrations, as suggested by the calibration curves shown in the previous section. The biological activity of these markers was compared to a known OAT1 substrate, fluorescein, which acted as a positive control. Probenecid was used to block the uptake of the secretion markers by OAT1 into the cells, while the efflux pump blockers were used to inhibit the excretion of these markers out of the cells [56]. Figure 28 shows the results obtained for the various markers.

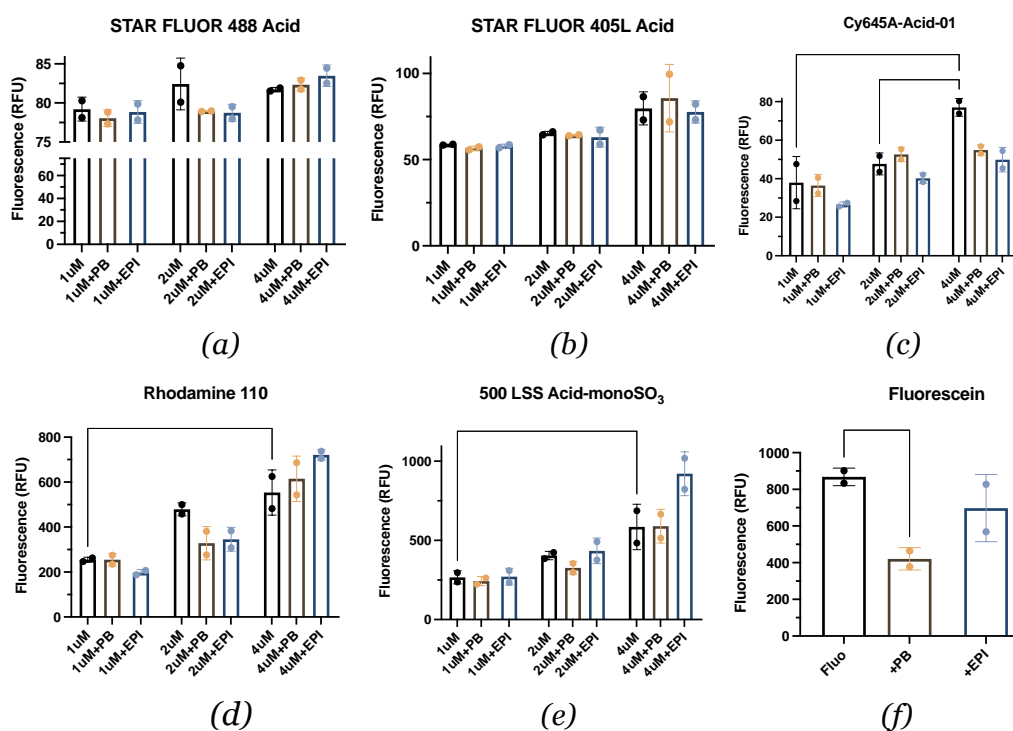


Figure 28: Comparison of uptake profiles of the different secretion markers on ciPTECs as performed by Mr. João Ferreira Faria at Utrecht University. The secretion markers consisted of (a) STAR FLUOR 488 Acid **13**, (b) STAR FLUOR 405L Acid **8**, (c) Cy645A-Acid-01 (**18**), (d) Rhodamine 110 (**12**), (e) 500 LSS Acid-monoSO₃ (**9**), and (f) fluorescein. Data are shown as mean \pm SD of three replicates from one or two independent experiments. * $p < 0.01$, ** $p < 0.01$, *** $p < 0.005$ and **** $p < 0.0001$ using one-way or two-way ANOVA analysis followed by Tukey's multiple comparison test.

3.2 Markers for reabsorption

3.2.1 Introduction and work strategy

As mentioned in *section 1.4.3*, the parent dye used for the reabsorption markers is a cyanine 7 in the NIR range, which was modified to have different side chains and functional groups. This was done to allow a varying number of glucose molecules to be conjugated to the dye.

For the cyanine dyes conjugated to glucose at C1 position, it was necessary to synthesise the starting material 1-aminoglucose **22** to have it conjugated to the dye at C1 position (*Figure 29*). β -anomeric azide **20** was obtained from α -bromo compound **19**, which was then reduces to 1-amino derivative **21** [65]. The deacetylation of the sugar was done using hydroxyl anion exchanged resin in the presence of methanol [66]. Once the reaction scheme was optimised and 1-aminoglucose **22** was obtained in good yields (*Figure 29*), it was conjugated to the cyanine 7 dye.

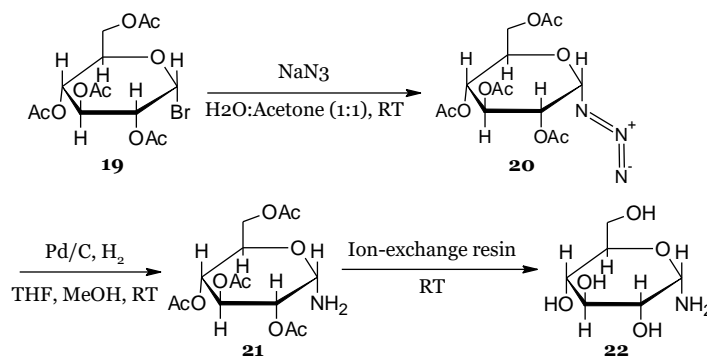


Figure 29: Reaction scheme for synthesising 1-aminoglucose 22

The reaction scheme for synthesising the cyanine 7 dyes used as reabsorption markers has been shown in *Figure 30*. The first step was the condensation reaction between the iodolium derivative (**25** or **30**) and Vilsmeier-Haack reagent **26** in the presence of sodium acetate. The choice of iodolium derivative depended upon the reabsorption marker under consideration. Since the labelling of glucose was carried out through amide bond linkage between the amine present on glucose and the terminal carboxylic acid group present on the dye, *N*-alkyl sulfonate moiety **25** was used for single-glucose derivatives. This was followed by nucleophilic substitution of *meso*-chloro **27** by phenolate (compound

28 in *Appendix*) for the single-glucose derivatives. In case of two and three glucose-containing reabsorption markers, hexanoic acid chains **30** were used, which provide two sites for glucose conjugation after condensation with the Vilsmeier-Haack reagent **31**. For the reabsorption marker containing two glucoses conjugated to a single dye, compound **31** was substituted with *p*-phenolsulfonate (compound **32** in *Appendix*), while for the three-glucose derivative phloretic acid (compound **34** in *Appendix*) was used. Phloretic acid provides the cyanine 7 dye **35** with an additional site for glucose conjugation.

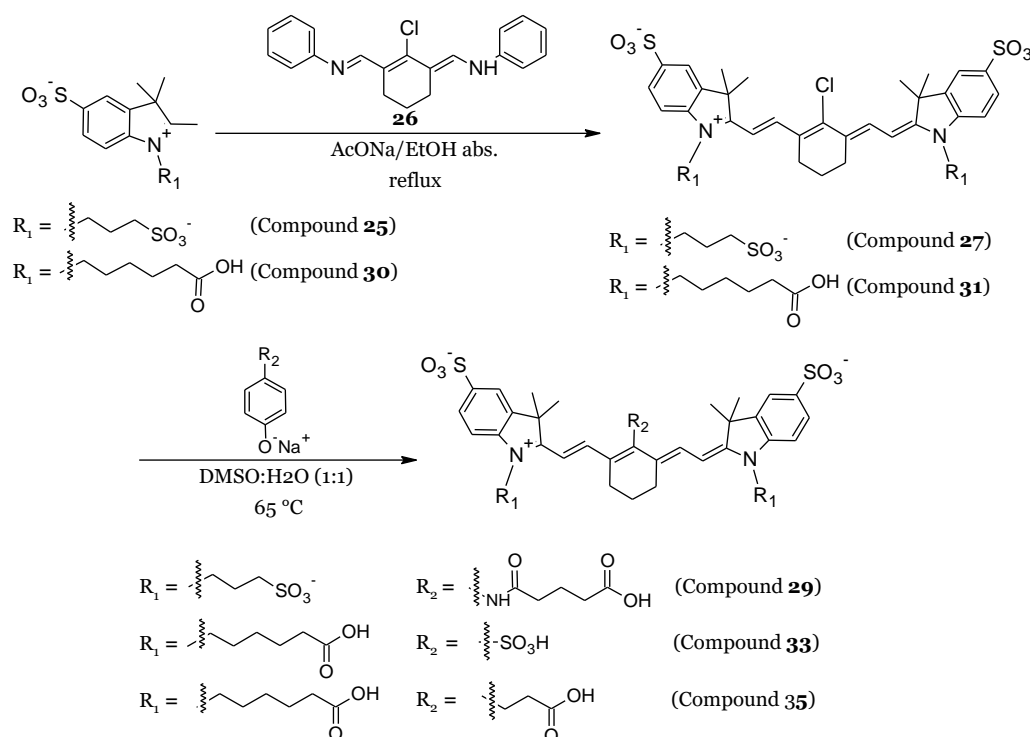


Figure 30: Reaction scheme for synthesising the cyanine 7 dyes used for glucose conjugation

Once the dyes were synthesised, they were conjugated to varying number of glucose molecules and at varying carbon positions on glucose to yield final markers (Figure 31). The terminal carboxylic acid for these markers paved way for the *in-situ* formation of NHS-ester, which could easily react with the amine at carbon 1 or carbon 2 of glucosamine and obtain respective conjugates. Some problems were observed during purification of these conjugates, as the polarity of the final compound and glucosamine are very similar. Various purification techniques and solvents/buffers were tested to finally optimise the purification of

these compounds over reverse phase C18 column in methanol and water. Synthesis, purification, and characterisation of all four reabsorption markers is discussed in detail in the *Appendix*.

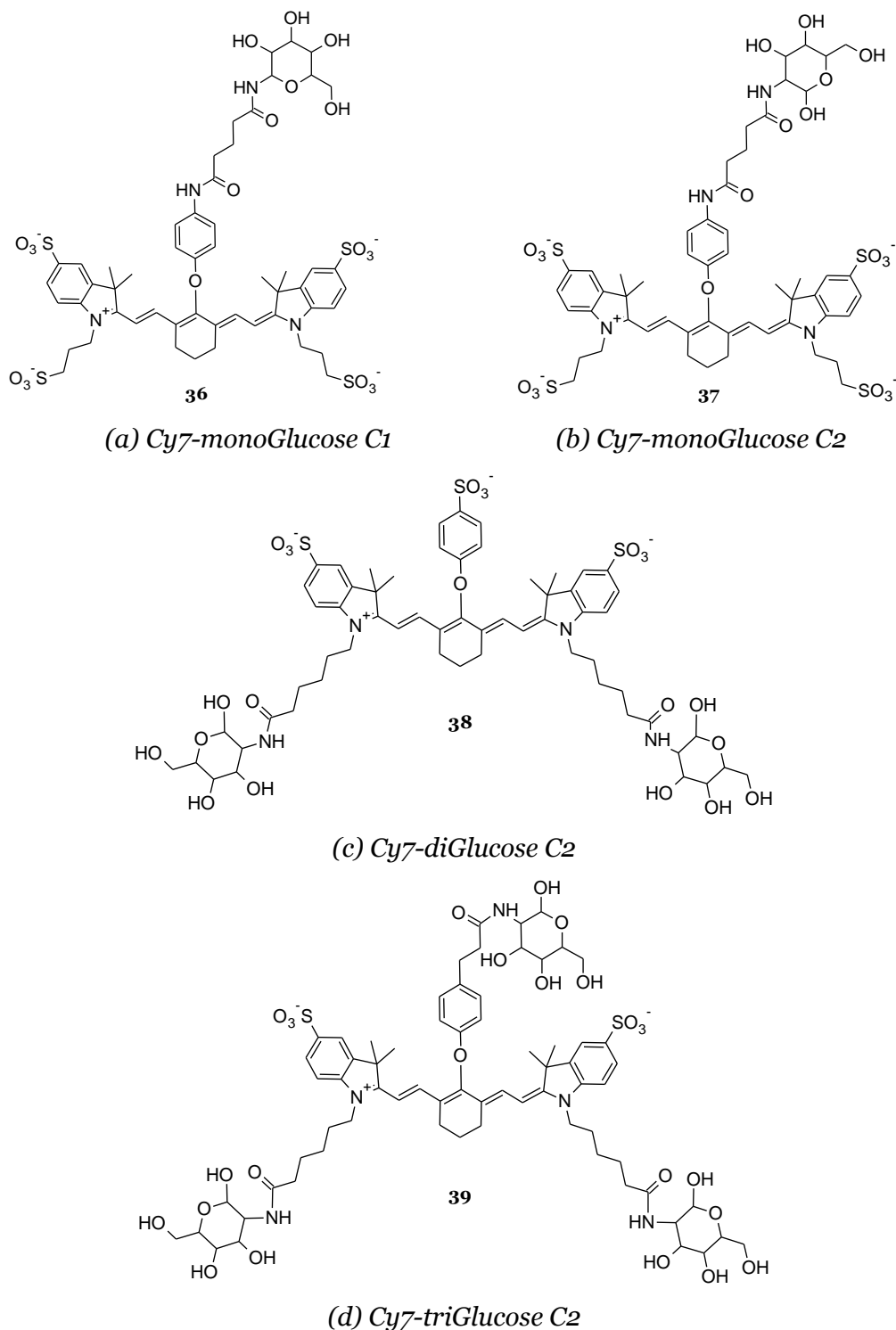


Figure 31: Modified cyanine 7 dyes conjugated to (a) 1 glucose molecule at C1 position **36**; (b) 1 glucose molecule at C2 position **37**; (c) 2 glucose molecules at C2 position **38**; and (d) 3 glucose molecules at C2 position **39**

3.2.2 Physicochemical and optical properties

The absorption and emission spectrum of the reabsorption markers are depicted in *Figure 32*. Because the reabsorption markers bear the same parent cyanine dye, their absorption-emission profiles are the identical. These dyes have an absorption peak at 770 nm. When excited at this wavelength, these dyes emit between 805 and 810 nm (depending on the concentration) and have a small Stokes shift of 30-40 nm (*Figure 32*).

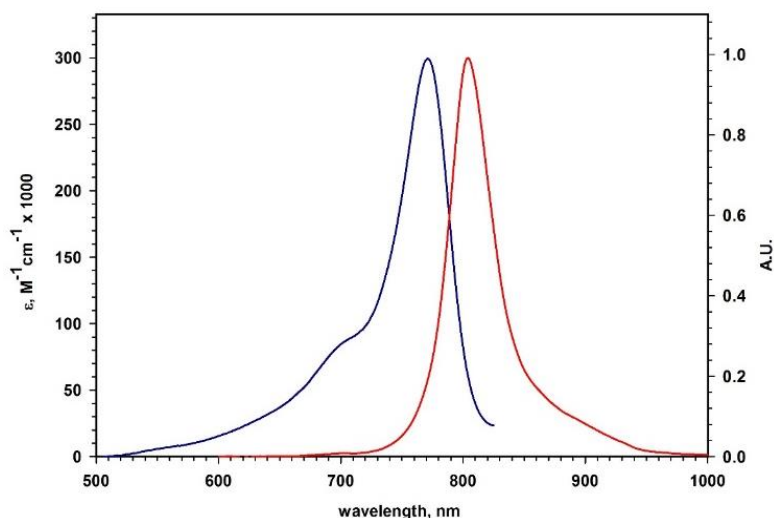


Figure 32: Electromagnetic spectrum of the reabsorption markers

Conjugation of these dyes to glucose molecules via amide bonds does not have any effect on the spectra. Further, their extinction coefficient remains unchanged upon conjugation. The extinction coefficient of these dyes was calculated using the Lambert-Beer law [55] and was found to be 270,000 M⁻¹cm⁻¹.

3.2.3 Calibration curves and dosage

Cyanine 7 dyes used for the reabsorption markers have a typical calibration curve for their fluorescence, characterized by an initial log phase, followed by a plateau region, and then a decrease in the fluorescence. This is because, at higher concentrations, these dyes show quenching due to aggregation phenomena and hence results in a decrease of fluorescence intensity [67]. For these markers, the maximum fluorescence is observed in the concentration range of 3 μM to 3.5 μM (*Figure 33*).

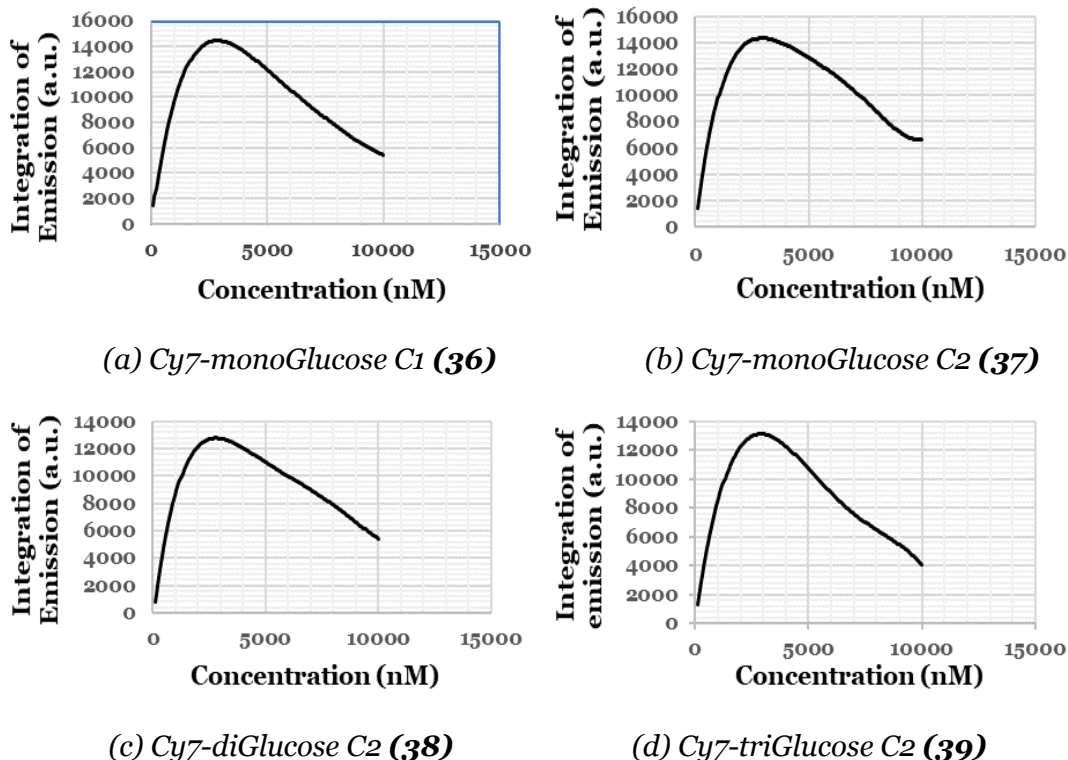


Figure 33: Calibration curves generated for the reabsorption markers

For *in vitro* studies, three different concentrations were chosen (1, 2 and 4 μM), to evaluate concentration-dependent uptake of these markers by the transporter proteins. As explained before, for *in vivo* applications, it is always better to inject a dye with its concentration in the plateau region. Therefore, according to the calibration curves done on the reabsorption markers, the proposed dosage range is 2-5 μM .

Nevertheless, these calibration curves must be repeated for their final application in the animal and human studies, since after being reabsorbed by the tubular proteins, the plasma concentration of these markers may vary.

3.2.4 PPB assays

The PPB assays were performed by Ms. Yinuo Xie at University of Heidelberg using the protocol mentioned in *section 2.7*. All experiments were performed in triplicate. The data are shown as mean \pm standard deviation (*Figure 34*). PPB of each of the markers in [%] was determined by averaging three independent measurements [64].

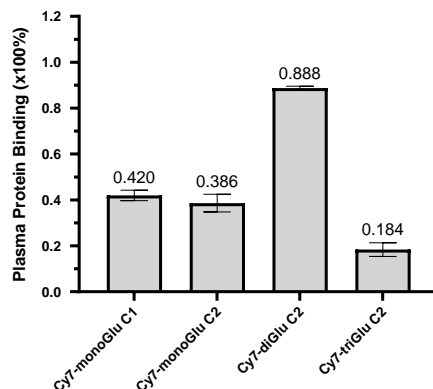


Figure 34: Plasma protein binding for reabsorption markers, as received from University of Heidelberg [64]

3.2.5 Cell viability assays

The cell viability assays for the reabsorption markers were evaluated by Ms. Yinuo Xie at University of Heidelberg using Luminescent Cell Viability Assay in HK-2 human proximal tubular cells. The results in Figure 35 show the viability of the cells treated with different concentration of different markers. Cell viability at different concentrations of markers was compared with the control group (0 μM) using One-way ANOVA. Cell viability of each of the markers in [%] was determined by averaging three independent measurements [64].

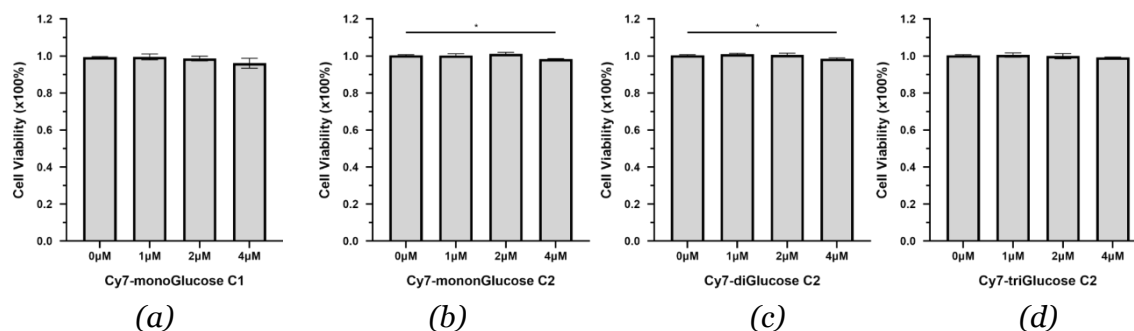


Figure 35: Cell viability assays performed on HK-2 human proximal tubular with reabsorption markers (a) Cy7-monoGlucose C1 (**36**), (b) Cy7-monoGlucose C2 (**37**), (c) Cy7-diGlucose C2 (**38**), and (d) Cy7-triGlucose C2 (**39**) for 3 hr [64].

NS: no significant difference, * $p < 0.05$

3.2.6 In vitro uptake assays

The uptake assay for the reabsorption markers was performed in HK-2 cells due to their known expression of glucose transporters [68]. 1, 2 and 4 μM concentrations were tested for each marker, as suggested by the calibration

curves. The results obtained from the *in vitro* studies (Figure 36) will be discussed under *Discussion*.

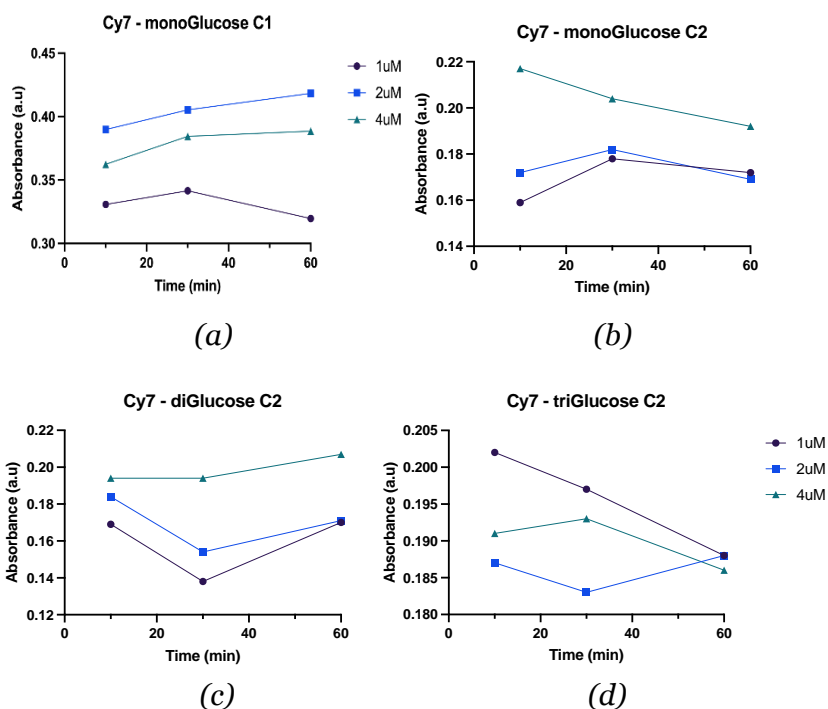


Figure 36: Comparison of uptake profiles of three reabsorption markers on human kidney-2 (HK-2) cells as performed by Mr. João Ferreira Faria at Utrecht University. Uptake profile was tested by incubating HK-2 cells with (a) Cy7-monoGlucose C1 (**36**), (b) Cy7-monoGlucose C2 (**37**), (c) Cy7-diGlucose C2 (**38**), or (d) Cy7-triGlucose C2 (**39**) over the course of 60 mins in HBSS at 37°C. Data are shown as mean of three replicates from one independent experiment

3.3 Markers for vascular imaging

3.3.1 Introduction and work strategy

The design of markers for vascular imaging is based on the idea that a fluorescent marker with a positive charge, and a size larger than the fenestrations will not be able to cross the endothelial membrane and hence will stain the glomerular capillaries. As previously discussed in *section 1.4.4*, Gretz *et al.* developed MHI148-PEI based on these criteria, but it had several disadvantages [53]. At physiological pH, the carboxylic acids of the dye and the amines of PEI are charged. These groups can therefore interact electrostatically instead of forming covalent bonds. This was proven through a set of experiments, where PEI and MHI-148 were mixed in water and dialysed for 36 hours. Even after multiple cycles of dialysis, PEI was still stained by the free dye, suggesting electrostatic interaction between the two molecules. This mixture of covalent bonds and electrostatic interactions may lead to batch-to-batch variation of the DOL, thereby creating reproducibility issues. Also PEI has been reported to be toxic in biological systems [54].

To overcome the problem related to MHI148, a cyanine 7 dye with only one carboxylic acid was designed, SV620C – 01 (**40**) (*Figure 37*). Cyanine 7 dye **40** has only one reactive moiety present and can conjugate with the polymer more specifically and with higher reproducibility. This leads to more specific covalent binding between PEI and the dye, allowing better control of the DOL and lowering the amount of fluorescent marker needed for staining the vessels.

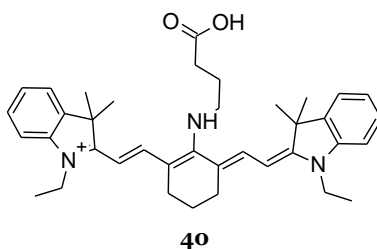


Figure 37: SV620C – 01 (40)

The large Stokes shift of MHI-148 and compound **40** is advantageous, as it gets rid of the interference from the overlapping absorption-emission spectra, as seen in dyes with shorter Stokes shift [69]. Furthermore, when excited at 645 nm, these dyes have their emission in the near infrared region, which gives them deeper

tissue penetration (*Figure 38*). This makes their biological examination easier, with a better signal-to-noise ratio. However, both these dyes have an intrinsic instability, which has been discussed later in this section.

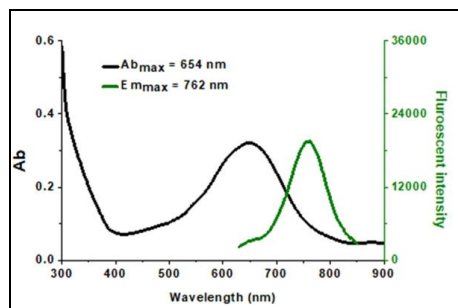


Figure 38: Spectrum of MHI-148 and SV-620C-01 (40) with $\epsilon = 90,000 M^{-1} cm^{-1}$ [53, 69]

One aspect emerging from the biological studies with SV620-01-PEI (compound **73**, *Appendix*) is that these cationic dyes conjugated to PEI are limited to staining the bigger blood vessels and give troubles in imaging the micro vessels. Therefore, in collaboration with Ms. Tiziana Picascia at the University of Heidelberg, dual staining of the vessels was tried with WGA conjugated to a dye, *STAR FLUOR 645* (dye commercialised by Cyanagen, spectra shown in *Figure 39*) and SV620C-01-PEI **73**.

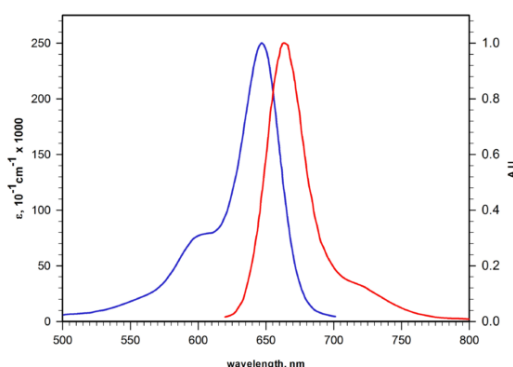


Figure 39: Spectrum of STAR FLUOR 645 with the value of $\epsilon = 250,000 M^{-1} cm^{-1}$. λ_{abs} of the dye is at 648 nm and λ_{em} is at 667 nm.

WGA has already been reported to bind effectively to the endothelial glycocalyx [70]. It has an affinity towards *N*-acetyl-glucosamine and sialic acid present in the glycocalyx that helps in staining the glomerular membrane. *STAR FLUOR 645* was chosen for dual staining in combination with SV620C-01-PEI **73** because both the dyes can be excited using a single laser, while their emission wavelengths remain discrete. This allows easy and rapid imaging of the vessels.

Nevertheless, both the cyanine 7 dyes, MHI148 and SV620C-01 (**40**), have an aliphatic amine chain at the *meso*-position. This aliphatic amine chain has a lone pair of electrons on the nitrogen that can delocalise into the electron-deficient carbon atom and form an iminium cation. This renders a non-emissive dye with a peak at 465 nm. This peak is always present for MHI148-PEI and SV620C-01-PEI (compound **73**, Appendix), and its absorbance intensity increases with time.

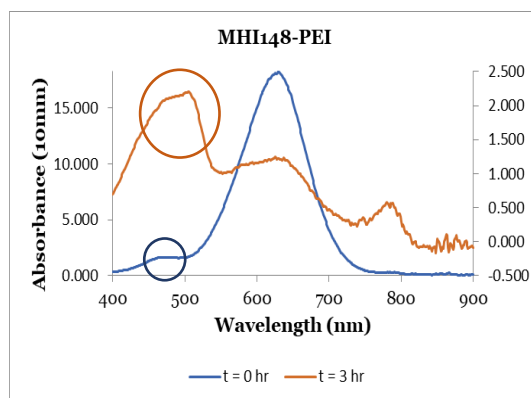


Figure 40: Absorption spectra of MHI-148-PEI with a peak at 465 nm coming from the partially degraded dye at $t = 0$ hr (in blue) and at the end of 3 hr (in orange) of continuous illumination

The poor stability of MHI-148 and SV620C-01 **40** in aqueous solution is also hypothesised to be caused by photoinduced decomposition, where the reactive singlet oxygen species incorporates within the dye (**41**) to form a stable iminium intermediate **41**, which leads to the breakdown of the dye into its non-fluorescent counterparts, **42** and **43** (Figure 41) [71].

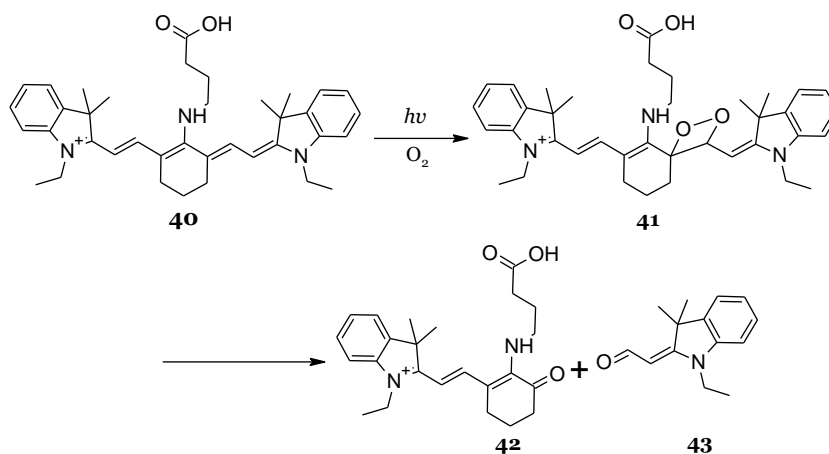


Figure 41: Reaction scheme explaining poor photostability of **40** in aqueous medium due to the incorporation of the reactive singlet oxygen species within the dye (**41**), leading to degradation of the dye into non-fluorescent compounds (**42** and **43**) [71]

Therefore, with slight modifications within the chemical structure, SV770C – 01 (**44**) [71] and SV770C – 02 (**45**) were synthesised (Figure 42).

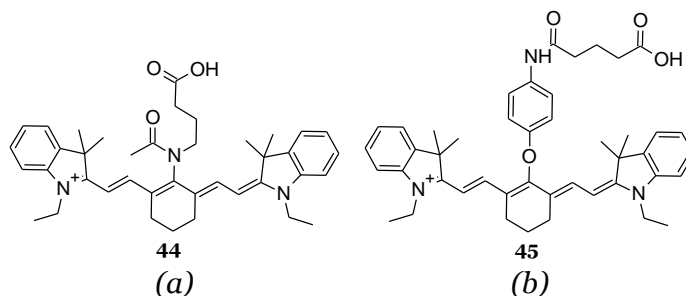


Figure 42: (a) SV770C - 01 (**44**) [71] and (b) SV770C - 02 (**45**)

These NIR dyes have a small Stokes shift (30-40 nm) but are much more stable than any of the previously used dyes (Figure 43).

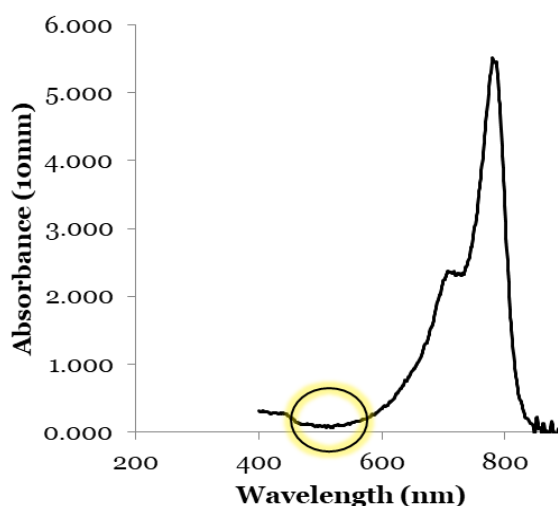


Figure 43: Peak at 465 nm from a partially degraded dye is not seen in case of the NIR cyanine 7 dyes SV770C – 01 (**44**) [71] and SV770C – 02 (**45**)

While SV620C – 01 (**40**) (Figure 37) degrades completely within 3 hours, the NIR cyanine 7 dyes **44** and **45** (Figure 42) can last up to 3 days (Figure 44).

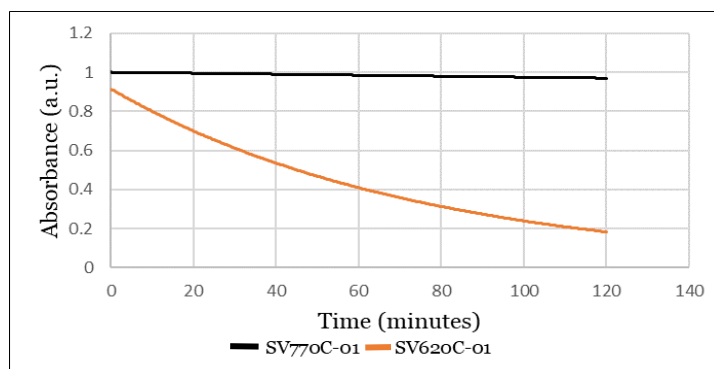


Figure 44: Photostability studies done on SV770C – 01 (**44**) and SV620C - 01 (**40**)

The new cationic NIR dye **44** (Figure 45) has its lone pair of electrons on nitrogen atom delocalised into the carbonyl group, thus removing the electron density on the amine at the *meso* position of the dye and destabilising the iminium intermediate [71]. This makes the dye a lot more photo- and chemically stable. On the other hand, compound **45** does not contain nitrogen at the *meso* position and uses a phenol ring instead (Figure 45). Additionally, the switch to the NIR region provides better signal-to-noise ratio, larger extinction coefficient and higher fluorescence quantum yields.

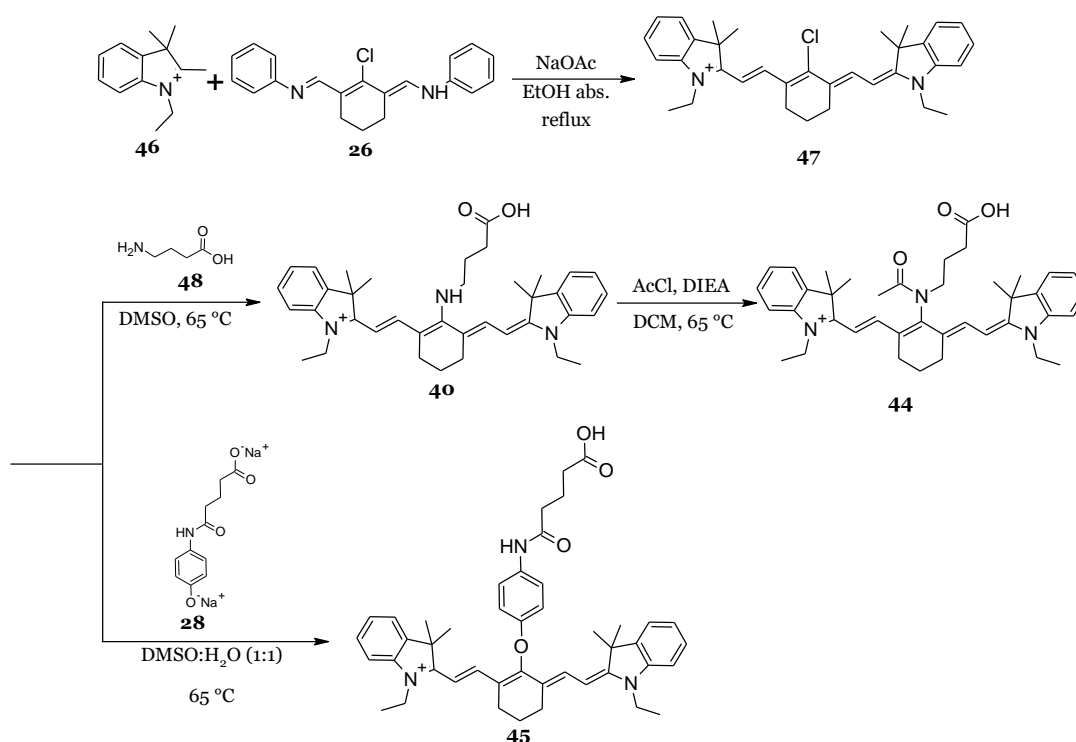


Figure 45: Reaction scheme for synthesising the cationic dyes for kidney imaging markers

The drawback with Cyanine 7 dyes is the presence of a polymethine structure with an electron-deficient iminium group that can react with protic nucleophiles. This attack on the electron-deficient iminium carbon atom renders a non-emissive dye under high-pH conditions. Therefore, for MHI148-PEI and SV620C-01-PEI (Compound **73**, Appendix), when a cyanine 7 dye is mixed with a highly basic polymer with secondary amines of pH 11, the dye is prone to a nucleophilic attack during the conjugation reaction, thereby degrading the dye and creating a non-fluorescent marker [72].

Having tackled the problems related to the dye, focus shifts to finding a replacement for PEI. As previously mentioned, PEI is toxic to cells. Besides PEI, other large polymers with positive charge are known. In search for a new polymer, two viable candidates were found:

8-arm PEG Amine (Hexaglycerol) **49** (Figure 46), with a molecular weight of 40 kDa, does not have any toxicity reported yet, and being a synthetic commercially available polymer, it does not entail the problem of batch-to-batch variation.

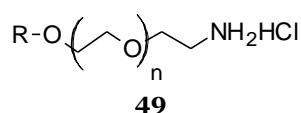


Figure 46: 8-arm PEG Amine where R is a Hexaglycerol core structure

Chitosan **50** (Figure 47) is a regularly used biological additive in food and is non-toxic. It comes in different sizes, but the small molecular weight chitosan is available with an average weight of 110 kDa, which makes it a very good candidate for our cationic marker.

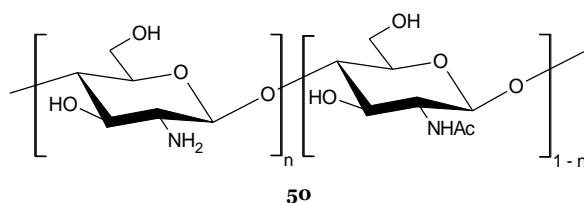


Figure 47: Chitosan with average molecular weight (M_n) = 110,000 Da and $n = 0.85$

Between the different cationic polymers, Chitosan **50** seems to be of utmost interest: (1) it is more cost effective as compared to PEG Amine **49** (Figure 46), (2) it is non-toxic compared to PEI, and (3) it is FDA approved. Moreover, in comparison to PEI, chitosan is far less basic (pKa 6.5), which is better for the cyanine dyes.

However, due to its weak basicity, chitosan is completely insoluble in water. The use of dye-polymer conjugates for biological applications requires solubilization of the marker in a water-based medium. Therefore, chitosan is modified through acetylation of the hydroxyl and the amino groups to give a water-soluble variant of the polymer **51** (Figure 48) [73].

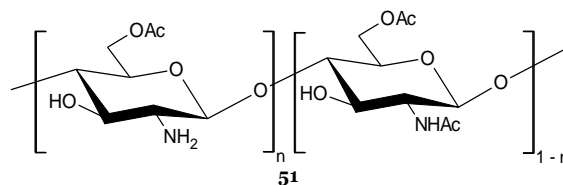


Figure 48: WS Chitosan, where $R = H$ or $R = Ac$ [73]

The acetylation of chitosan creates space in the polymer structure for water molecules to seep in. This polymer, ‘WS Chitosan’ **51** (Figure 48) is soluble in a range of pH, including neutral and slightly basic pH, as well as in organic solvents such as DMSO. The acetylation of the chitosan is carried out with AcCl with MeSO₃H as solvent. The use of MeSO₃H slows down the acetylation of the amino groups, as it protonates the free amine, thereby shifting the equilibrium towards O-acetylation (Figure 49). The partial N-acetylation of the chitosan renders free amines within the polymer that can either participate in amide bond formation with the fluorescent dyes or provide chitosan an overall cationic charge.

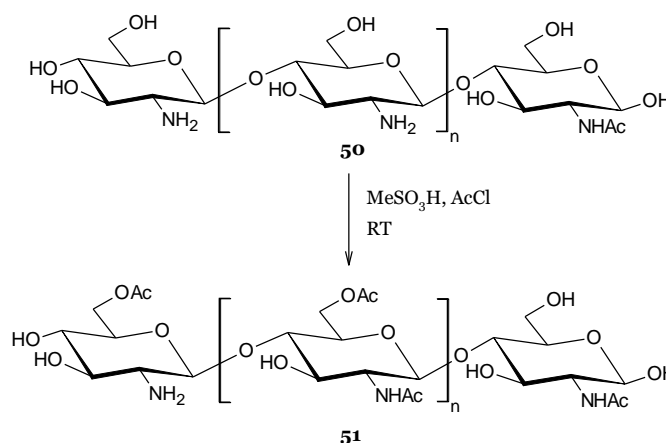


Figure 49: Reaction scheme for synthesising WS Chitosan (**51**)

The amount of AcCl used has an important role in determining the percentage of substitution for the hydroxyl and the amino groups (Table 6) [73].

AcCl equiv.	Functional group			
	OAc	OH	NHAc	NH ₂
1	27%	73%	19%	81%
3	39%	61%	46%	54%
5	40%	60%	60%	40%
10	42%	58%	74%	26%

Table 6: Effect of the amount of AcCl on the acetylation as reported in Sashiwa et al. [73]

In conclusion, the amount of AcCl used is very important, as it determines: (1) the hydrophilicity of the chitosan, and (2) the DOL and the overall cationic charge of the fluorescent polymer, which in turn is determined by the number of free amines available. Different degrees of acetylation were tried to find the perfect balance between solubility and the availability of free amines to provide cationic charge, and to form an amide bond with the cyanine dyes. Use of 10 equivalents of AcCl for each hexosamine unit of chitosan was found to be the ideal condition. It produces a water-soluble variant of the chitosan, where at least 26% of the hexosamine units have a free amine. This leaves WS chitosan **51** with enough free amines to provide cationic charge for biological staining, and enough free amines to produce a fluorescently labelled chitosan with degree of labelling ranging between 1 and 25.

WS Chitosan was therefore conjugated to previously synthesised cationic dyes **40** (Figure 37), **44** and **45** (Figure 42), via amide bond formation, as shown in Figure 50.

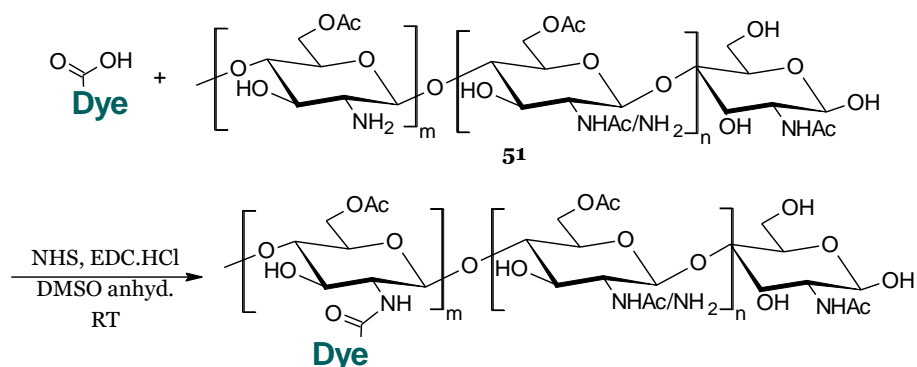


Figure 50: Reaction scheme for labelling WS chitosan with different dyes, where m is between 1 to 25 for all the kidney imaging markers.

Even with the increased chemical stability of these conjugates due to the use of a less basic polymer, these dyes are very hydrophobic. Therefore, when conjugated to WS chitosan **51**, they bring down the overall solubility of the polymer and render a largely insoluble marker. This results in use of very low concentrations of fluorescently labelled chitosan in aqueous solutions/buffers after filtering out the insoluble marker. Hence, to overcome the solubility issue, WS Chitosan was conjugated to two zwitterionic dyes (**57** and **58**, Figure 51).

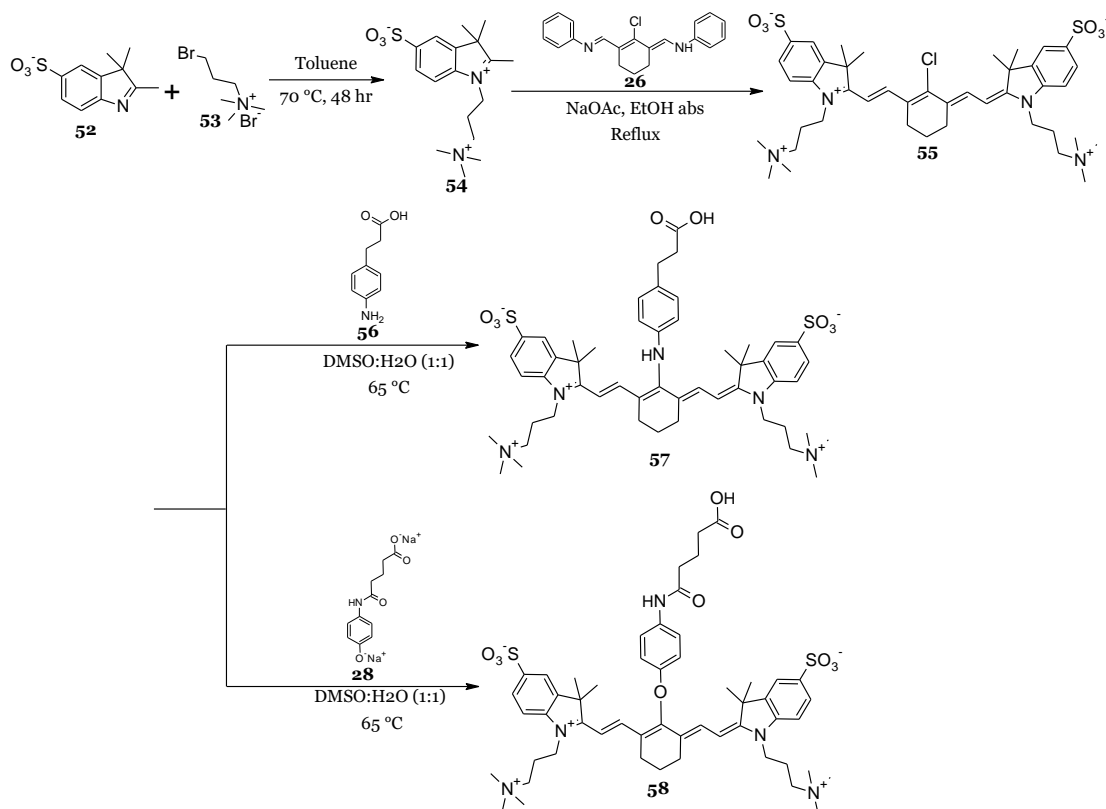


Figure 51: Reaction scheme for synthesising the zwitterionic dyes for imaging markers

While SV700 Z-01 (**57**) has a *meso* substituted aromatic amine, which gives it a large Stokes shift of 84 nm, SV770Z-01 (**58**) has *meso* substituted phenol ring. This pushes the excitation and emission wavelength for the zwitterionic cyanine 7 (**58**) further into the NIR region and gives it a higher molar extinction coefficient (Figure 51). Both these dyes have high photo- and chemical stability in comparison to SV620C-01 (**40**).

Additionally, different cyanine dyes, such as cyanine 5- (**18**, Figure 15(c)) and cyanine 5.5- derivatives (**66** and **72** in Figure 52 and 53 respectively) were conjugated to the WS Chitosan **51** since they all present the advantage of emission in a region where autofluorescence of tissue is negligible. This gives the user options to choose depending on the availability of the lasers in different microscopes and for different applications. Cyanine 5 dye **18** (Figure 15(c)), as described in section 3.1.1 was used as an anionic cyanine 5 dye to label WS chitosan. The dye was renamed to SV645A-01 for coherency between the names used for the kidney imaging markers. Cyanine 5.5 dyes were highly anionic due to the presence of multiple sulfonate groups. SV680A-03 (**66**) contains four sulfonate groups as shown in Figure 52.

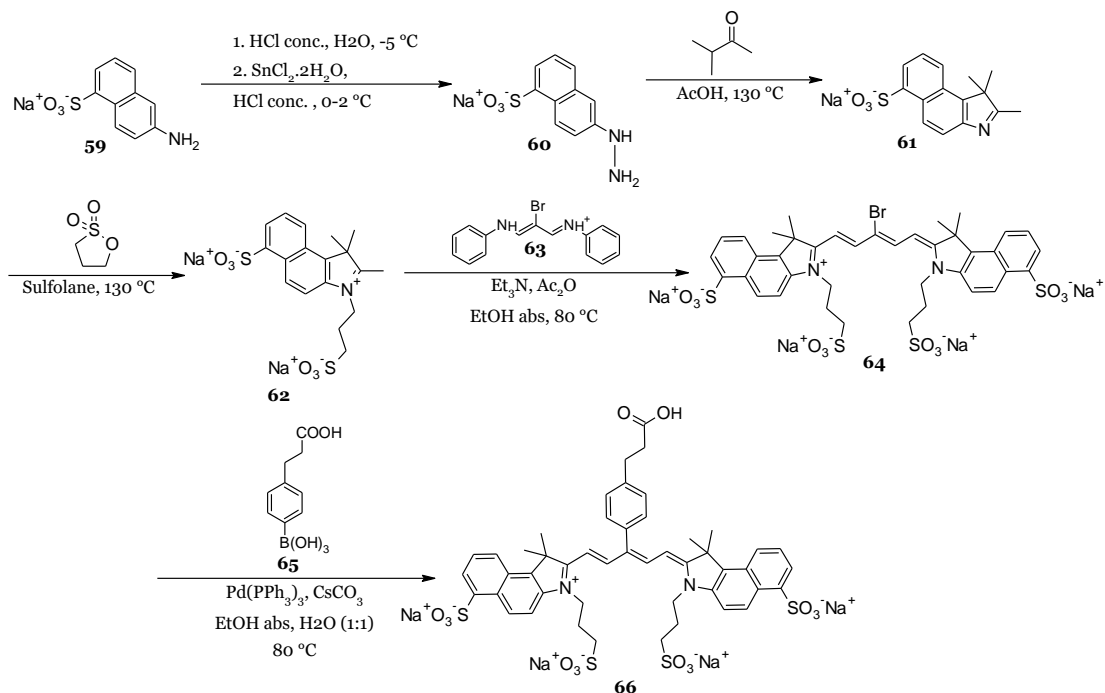


Figure 52: Reaction scheme for synthesising SV680A-03 (**66**)

In case of SV680A-02 (**72**), the dye is hexa-sulfonated (Figure 53). Since the size of the dye and the amount of negative charge carried by the dye is negligible in comparison to the polymer it was hypothesised, and later proved through biological imaging that the overall efficiency of the polymer in binding to the endothelium is not affected.

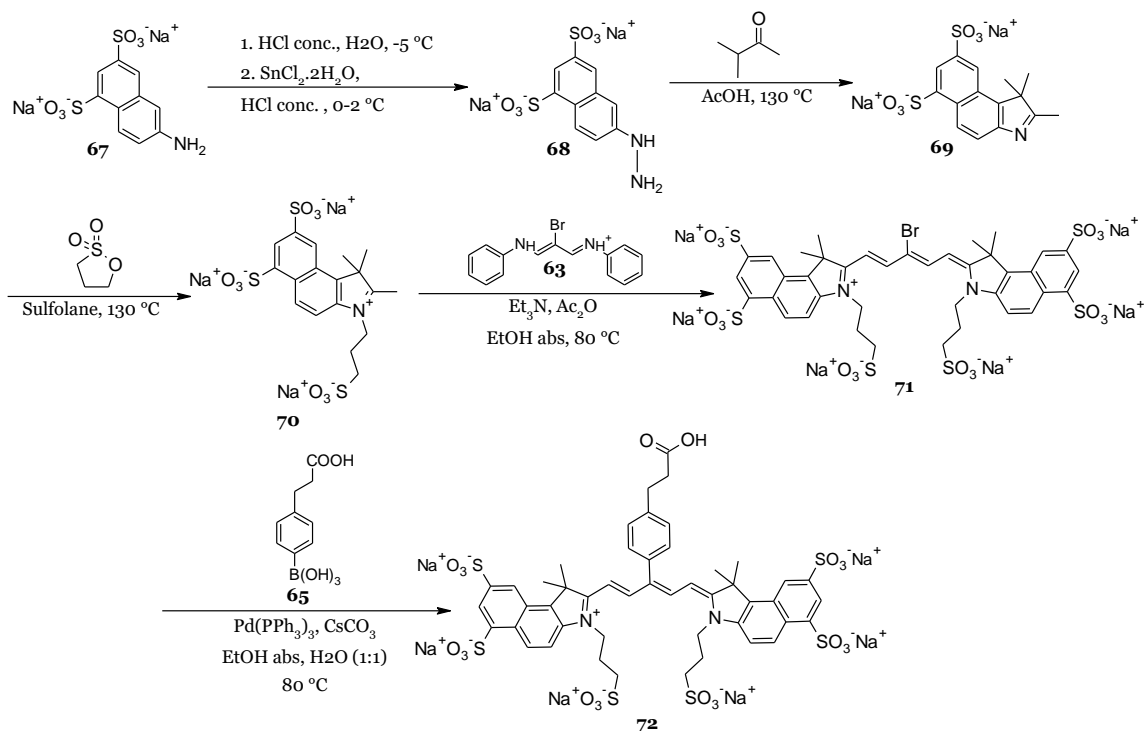


Figure 53: Reaction scheme for synthesising SV680A-02 (**72**)

Additionally, all these dyes show high photo- and chemical stability, with high molar extinction coefficient (*Table 7*).

Dye	Abs _{max} (λ)(nm)	Em _{max} (λ)(nm)	ε (M ⁻¹ cm ⁻¹)	Net charge
SV620C-01	620	750	90,000	+1
SV770C-01	770	805	270,000	+1
SV770C-02	770	805	270,000	+1
SV680A-02	677	703	240,000	-6
SV680A-03	677	703	240,000	-4
SV645A-01	641	663	250,000	-2
SV700Z-01	700	792	76,000	0
SV770Z-01	770	805	270,000	0

Table 7: Photo-physical properties of the dyes used for labelling WS chitosan

3.3.2 Physicochemical and optical properties

Figure 54 shows the electromagnetic spectrum for the various dyes used for conjugation with WS chitosan. Upon conjugation to the polymer no change is observed in the dyes' spectra and molar extinction constant.

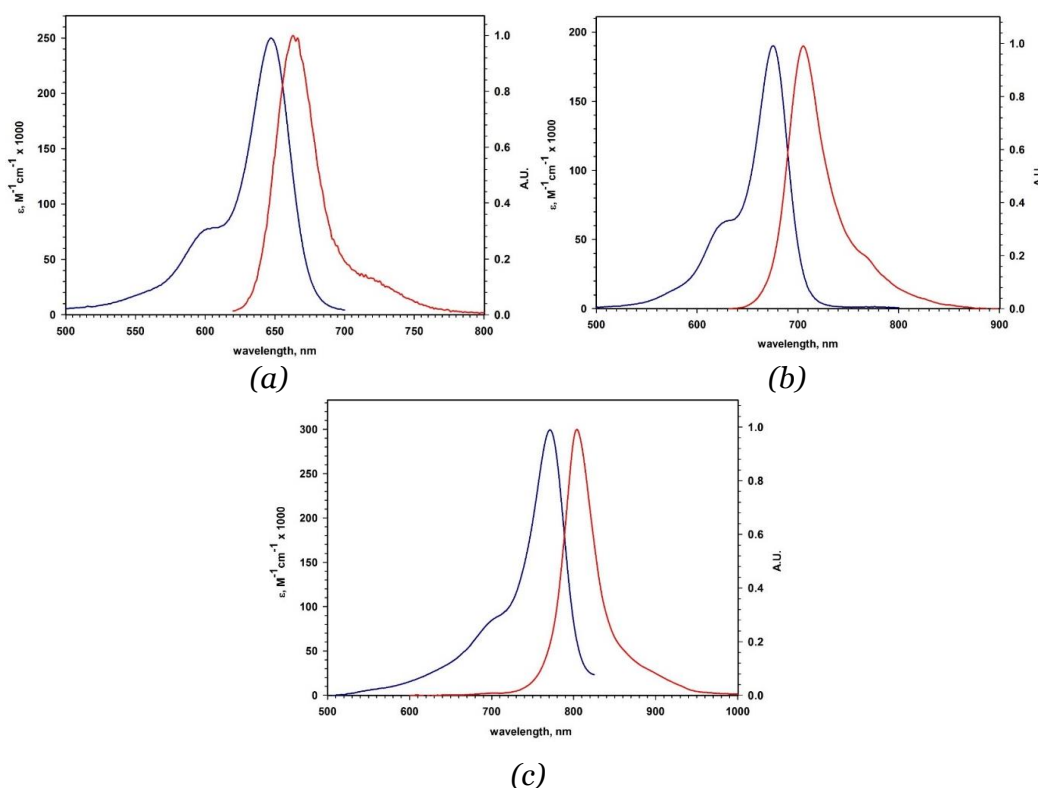
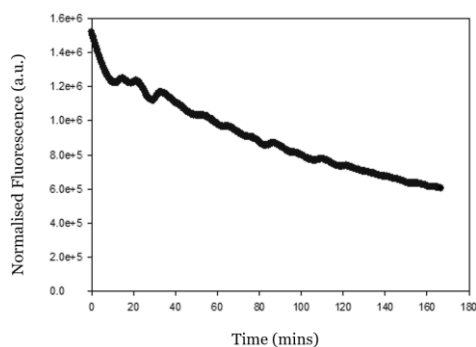


Figure 54: Electromagnetic spectrum of the dyes used for kidney imaging: (a) SV680A-02 (72), SV680A-03 (66) (b) SV645A-01 (18) (c) SV770C-01 (44), SV770C-02 (45), SV770Z-01 (58)

3.3.3 Photostability studies

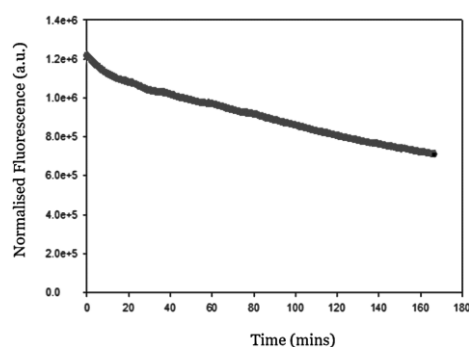
Comparative studies were carried out at University of Parma between fluorescent markers containing PEI, and the new markers designed with WS chitosan tagged to chemically stable dyes, to evaluate their photostability (*Figure 55*).



(a) **SV620C-01-PEI 73**

Fluorescence loss: 60%

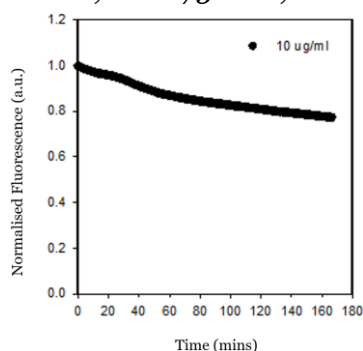
($\lambda_{ex}=620\text{ nm}$, $\lambda_{em}=750\text{ nm}$, Slit=10 nm)



(b) **SV620C-01-WS chitosan 74**

Fluorescence loss: 40%

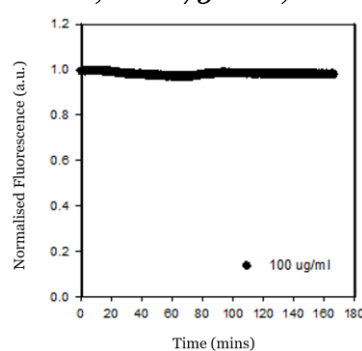
($\lambda_{ex}=620\text{ nm}$, $\lambda_{em}=750\text{ nm}$, Slit=10 nm)



(c) **SV680A-03-WS chitosan 79**

Fluorescence loss: 23%

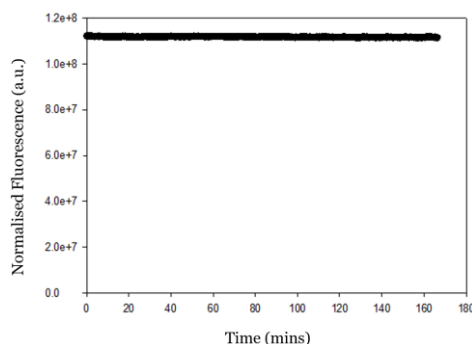
($\lambda_{ex}=677\text{ nm}$, $\lambda_{em}=703\text{ nm}$, Slit=10 nm)



(d) **SV680A-02-WS chitosan 80**

Fluorescence loss: 3%

($\lambda_{ex}=677\text{ nm}$, $\lambda_{em}=703\text{ nm}$, Slit=10 nm)



(e) **SV770Z-01-WS chitosan 78**

Fluorescence loss: <1% ($\lambda_{ex}=770\text{ nm}$, $\lambda_{em}=790\text{ nm}$, Slit=10 nm)

Figure 55: Photostability studies done on the kidney imaging markers, as provided by the University of Parma

3.3.4 DOL calculation

DOL can be varied for a given marker by differing the amount of dye used during labelling. For different biological experiments, different DOL is needed, which is based on the kind of biological application, and the sensitivity of the instrument in use. For the current research objectives, where the fluorescently labelled water-soluble chitosan was used for kidney imaging, multiple experiments were run to standardise the amount of dye that is needed to label WS chitosan, which allows imaging of the kidney vasculature. Based on these experiments, it was suggested to use 40 equivalents of dye for each equivalent of WS chitosan to produce a DOL between 15-25, which is ideal for visualisation under the fluorescent microscope (*Table 8*).

Kidney imaging marker	DOL
SV680A-02	15
SV680A-03	16
SV645A-01	25
SV700Z-01	17
SV770Z-01	17

Table 8: DOL calculation for the zwitterionic and the anionic markers for kidney imaging using equation 2 in section 2.4

DOL for SV620C-01-WS chitosan **74**, SV770C-01-WS chitosan **75** and SV770C-02-WS chitosan **76** could not be calculated as they were not fully soluble in water.

3.3.5 Fluorescent microscopy using the kidney imaging markers

Ms. Tiziana Picascia performed the imaging at the University of Heidelberg and standardised the use of the imaging markers discussed above in an ex vivo setup using the protocol developed by Gretz *et al* [53].

These markers show high efficiency in visualising the glomeruli, along with the ability to identify both, big and small blood vessels (*Figure 56*). Moreover, the use of these markers can be extended in visualising post-glomerular blood vessels something which was not possible with MHI148-PEI [53].

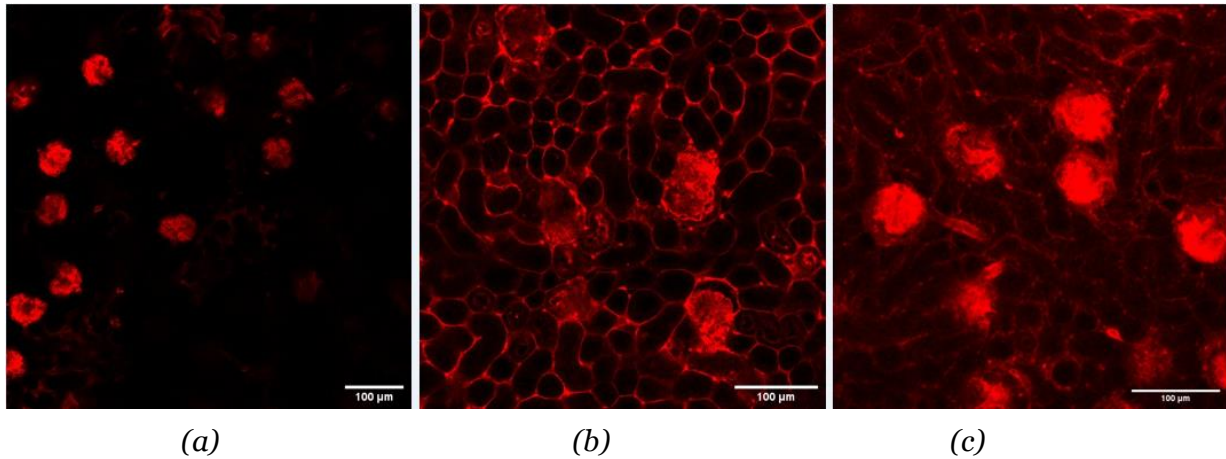


Figure 56: Renal vascular network from mouse kidney sections (cortical area) in details. (a) SV770C-02-WS Chitosan staining, (b) SV680A-02-WS Chitosan staining, and (c) MHI148-PEI staining

Hence, these markers provide a non-toxic and highly efficient approach to imaging the kidney vasculature in the NIR region with better signal-to-noise ratio and deeper tissue penetration.

4. Discussion

The objectives of this project were to develop and optimise fluorescent markers to assess the three functions of the kidneys: filtration, secretion, and reabsorption. Additionally, it was considered useful to develop fluorescent markers for visualising kidney vascularisation, to facilitate the study of disease occurrence and progression by means of histology.

For the first part of the project, to develop kidney's functional markers, extensive literature search was done to study the state of the art and to understand its shortcomings. While most of the endogenous markers suffer from variations arising due to anthropometric factors such as gender and age, or the prevalence of other diseases, great progress has been made in developing exogenous markers [20-23]. Radiotracers such as ^{51}Cr -EDTA and $^{99\text{m}}\text{Tc}$ -DTPA have found limited use due to the reservations and difficulty in using radiotracers [24-29]. Inulin and sinistrin are considered the gold standard but are very expensive and difficult to handle (see *section 1.3.2*) [20-23]. Therefore, fluorescent kidney markers have gained popularity in recent years, as a non-invasive, non-toxic, and cheap method for kidney diagnosis.

As previously discussed, most of the fluorescent markers developed in the field of kidney diagnostics have focused on assessing glomerular filtration. Current research focused on developing novel reabsorption and secretion markers, along with their optimisation to be used simultaneously with the GFR marker, which are compatible with a transcutaneous device developed by the collaborators at the University of Heidelberg (see *section 2.10*).

4. 1 GFR marker

A GFR marker was developed in the previous European Union - funded project NephroTools, where it was shown that ABZWYC Y -H β CD provides a highly efficient way for evaluating glomerular filtration [44, 46]. The use of a zwitterionic cyanine 7 dye highlighted the importance of a NIR dye, and the advantages of a large Stokes shift. The dye was compatible with the new transcutaneous device developed by Mr Mohammed Yusuf as part of the RenalToolBox project in collaboration with

Bundesministerium für Bildung und Forschung (BMBF) project. Also, Mr. James Littlewood at iThera Medical validated the clearance of ABZWICY-H β CD by the kidneys using MSOT technique in his Ph.D. project [58]. Therefore, it was decided to use ABZWICY-H β CD without further modifications and focus on the development of secretion and reabsorption markers. Having known the optical properties of one of the functional markers, it was important to develop the other two fluorescent marker types with discrete optical properties to allow simultaneous measurement.

4.2 Secretion markers

As mentioned previously, NIR dyes entail many advantages over fluorescent markers with optical properties in the visible range. However, for the final goal of this project, i.e., to have simultaneous evaluation of all three kidney functions using a transcutaneous device, it was necessary to develop markers in different regions of the electromagnetic spectrum. As described in *section 2.10*, the new transcutaneous device had a combination of three LEDs of different wavelengths: red (650 nm), near-infrared (950 nm) and green (525 nm). Therefore, the secretion markers were developed in the visible region (400 to 700 nm) of the electromagnetic spectrum, with their excitation compatible with the green channel LED.

Secretion markers were designed based on the structures of known OAT substrates. OATs, being flexible transporter proteins, mediate secretion of chemically versatile compounds. The basic requirements for an OAT substrate was to be small (less than 600 Da) and not to have an overall cationic charge (they can either be anionic or neutral) [48]. Also, studying the structures of various known OAT substrates, such as PAH and fluorescein, it was considered important that a secretion marker should also contain a carboxyl group [48].

Based on these criteria, Cy550Z – 01 (**19**), Cy645Z – 01 (**20**) and CUM450 LSS – 01 (**21**) (*Figure 14*) were tested for their biological activity. However, being hydrophobic, these dyes do not fully dissolve in water-based buffers or media, thus making their biological analysis difficult and non-reproducible. Also, hydrophobic compounds have been shown to have high affinity towards OAT₁,

which leads to blocking of these transporter proteins. Hence, these markers were not tested any further.

To solve the water-solubility issue, STAR FLUOR 488 Acid **13**, STAR FLUOR 405L Acid **8**, Cy645A-Acid-01 (**18**), Rhodamine 110 (**12**) and 500 LSS Acid – monoSO₃ (**9**) were designed (*section 3.1.1*). These markers were hydrophilic and had their optical properties compatible with the transcutaneous device. The calibration curves were studied for each marker (*section 3.1.3*), which suggested the use of 1, 2 and 4 μM concentrations for the biological tests.

The PPB is an important characteristic, as it helps in predicting the *in vivo* path a marker might take and its biological activity. The PPB assays conducted on the secretion markers showed varying results (*Figure 57*), which were highly dependent on the dyes' structure and hence interaction with albumin.

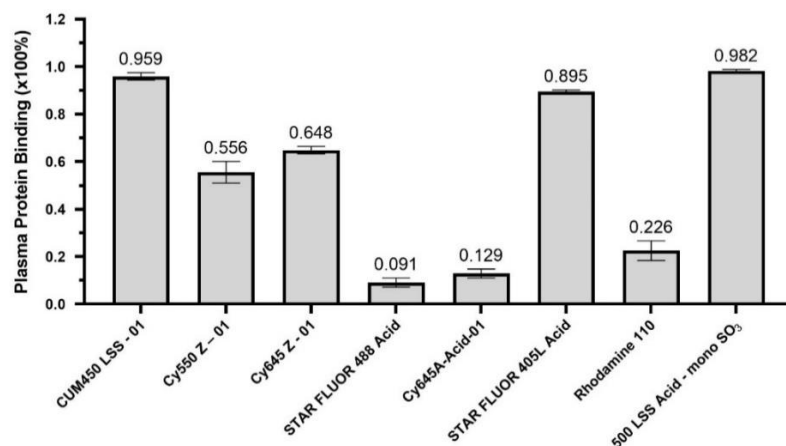


Figure 57: PPB assays performed by Ms. Yinuo Xie at the University of Heidelberg [64]

Even though PPB influences the marker's pharmacodynamics and pharmacokinetics, it cannot be used as the sole determinant for its biological activity. Especially in the case of secretion markers, where it has been shown with the example of indoxyl sulfate that their secretion could be albumin-facilitated. Indoxyl sulfate, which is a known substrate for OAT1 transporter proteins, shows reduced OAT1-mediated tubular uptake in the absence of albumin. But this cannot be generalised for all the compounds [74]. The albumin-facilitated secretion of compounds in the kidneys depends on the affinity of these compounds for albumin versus the OATs. Therefore, these compounds were further analysed for their *in vitro* uptake.

Due to the water-solubility issues encountered with compounds **19**, **20** and **21** during the PPB assays, they were not analysed further for other biological tests. The cytotoxicity assays on STAR FLUOR 488 Acid **13**, STAR FLUOR 405L Acid **8** and Cy645-Acid-01 (**18**) were conducted on 10, 20 and 40 μM concentrations (Figure 58). However, after the calibration curve studies, it was observed that these concentrations are too high. Therefore, only the results at 10 μM concentration were considered for these three markers.

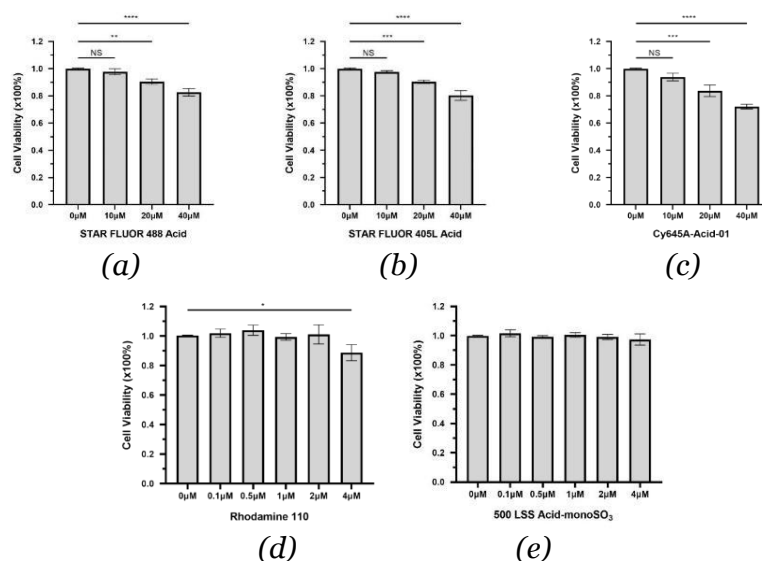
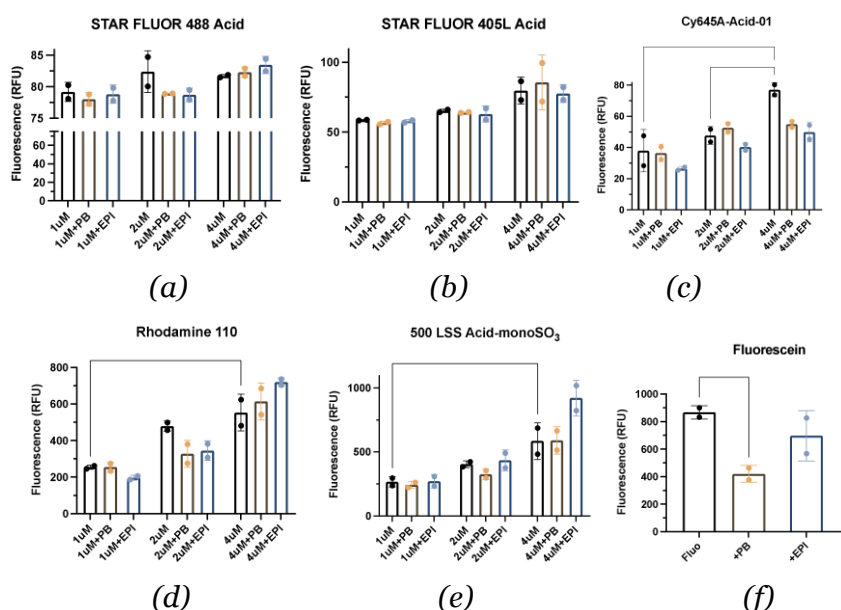


Figure 58: Cell viability assays performed by Ms. Yinuo Xie at the University of Heidelberg on *ciPTEC-OAT1* cell line when incubated with the secretion markers for 3 hr. The secretion markers consisted of (a) STAR FLUOR 488 Acid **13**, (b) STAR FLUOR 405L Acid **8**, (c) Cy645A-Acid-01 (**18**), (d) Rhodamine 110 (**12**) and (e) 500 LSS Acid-monoSO₃ (**9**). NS: no significant difference, * $p < 0.05$, ** $p < 0.01$, *** $p < 0.005$, **** $p < 0.0001$ [64]

Along with the results from Rhodamine 110 (**12**) and 500 LSS Acid-monoSO₃ (**9**) at concentrations between 0.1-4 μM , all the secretion markers showed a safe profile (Figure 58). For compounds **13**, **8** and **18** no statistically significant cytotoxicity was observed at 10 μM concentration after 3 hr of exposure. For compound **12**, only 4 μM showed statistical difference from the control group, thereby implying the use of 2 μM concentration or below. Compound **9** was not toxic at any concentration and hence is safe to use.

For the uptake assay of the secretion dyes, *ciPTECs* were incubated with the dye alone, or in combination with inhibitors (Figure 59). Fluorescein, a known OAT1

substrate, was used as a control to assess the uptake profile of the synthesised dyes as described previously [56]. STAR FLUOR 488 Acid **13** showed the highest increase in cellular uptake at 2 μM (82.44 ± 48.04) but did not respond to inhibitor (probenecid) co-incubation (*Figure 59(a)*). For all conditions, STAR FLUOR 405L Acid **8** showed overall similar fluorescence intensity values (*Figure 59(b)*). Cy645A-Acid-01 (**18**) uptake increased between the tested concentrations, with a significant increase found at 4 μM (77.06 ± 4.61 , $p < 0.0001$), however co-incubation with the inhibitors did not influence its uptake profile (*Figure 59(c)*). While 500LSS Acid-monoSO₃ (**9**) showed an uptake profile like that of fluorescein at 1 μM and 2 μM , with a decrease when co-incubated with PB and a retention with EPI, the same was not observed at 4 μM (*Figure 59(e)*). When Rhodamine 110 (**12**) was co-incubated with probenecid, its uptake decreased only at 2 μM (from 478.98 ± 28.92 to 328.52 ± 73.87), whereas its retention was more pronounced at 4 μM (*Figure 59(d)*).



*Figure 59: Comparison of uptake profiles of the different secretion markers on ciPTECs as performed by Mr. João Ferreira Faria at Utrecht University. The secretion markers consisted of (a) STAR FLUOR 488 Acid **13**, (b) STAR FLUOR 405L Acid **8**, (c) Cy645A-Acid-01 (**18**), (d) Rhodamine 110 (**12**), (e) 500 LSS Acid-monoSO₃ (**9**) and (f) fluorescein. Data are shown as mean \pm SD of three replicates from one or two independent experiments. * $p < 0.01$, ** $p < 0.01$, *** $p < 0.005$ and **** $p < 0.0001$ using one-way or two-way ANOVA analysis followed by Tukey's multiple comparison test.*

All the markers showed concentration-dependent cellular uptake, indicating OAT1 is not the only transporter involved in their secretion. While the use of probenecid showed a decrease in uptake and the use of efflux pump blockers showed a retention for some of the dyes, it was not as pronounced as seen for the control (Fluorescein, *Figure 59(f)*). This might be because these markers were substrates for OATs other than OAT1 present in the tubular cells.

Due to the unavailability of *in vitro* cell lines with other OAT proteins, the dyes could not be further tested. Nevertheless, it would be interesting to test these dyes further in *in vivo* setup, since all of them have proved to be safe for use.

4.3 Reabsorption markers

Fluorescent glucose molecules were designed and developed as reabsorption markers, using cyanine 7 dyes with their optical properties in the NIR region. The excitation and emission wavelength of these markers were significantly different from those of the secretion markers. Calibration curves for all the reabsorption markers were similar, with a fluorescence maximum between 3-3.5 μM (*Figure 60*).

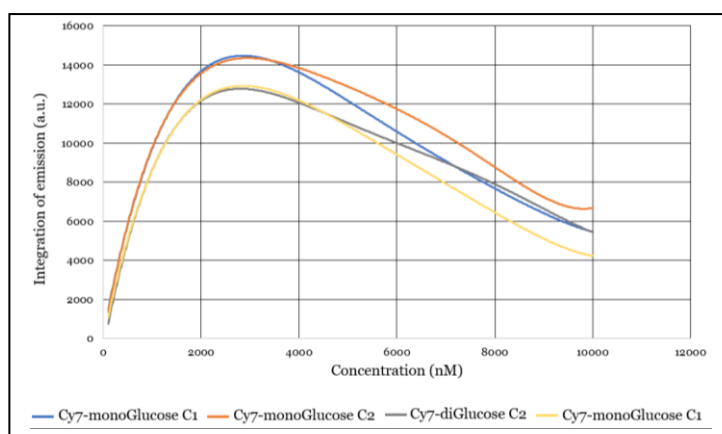


Figure 60: Calibration curves made for all the reabsorption markers

Based on the calibration curves, 1, 2 and 4 μM concentrations were chosen for the biological analysis. In case of PPB assays on the reabsorption markers (*Figure 61*), Cy7-monoGlucose C1 **36** showed 40% PPB, whereas Cy7-monoGlucose C2 (**37**) and Cy7-triGlucose C2 (**39**) exhibited low PPB (<40%). Cy7-diGlucose C2 (**38**) had a very high PPB (88.8%).

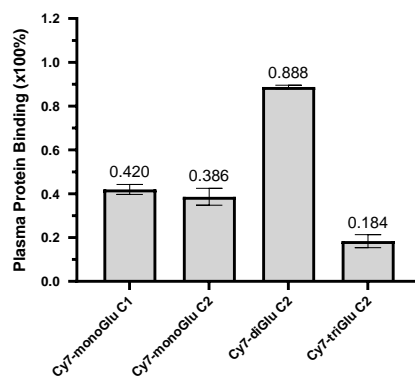


Figure 61: Plasma protein binding for reabsorption markers, as received from University of Heidelberg. All experiments were performed in triplicate and each experiment. The data shown as mean \pm standard deviation. PPB of each of the markers in [%] was determined by averaging three independent measurements [64]

The high values for PPB for these markers could be due to accessible bulky anionic groups present on the marker for albumin-interaction [62-63]. Nevertheless, as explained before, PPB cannot alone confirm the *in vivo* activity for these markers. Hence, it was necessary to test the reabsorption markers through *in vitro* and animal experiments to confirm their activity.

The cell viability assays conducted on the reabsorption markers demonstrated that only Cy7-monoGlucose C2 (**37**) and Cy7-diGlucose C2 (**38**) showed some statistical difference from the control group (Figure 62). Nevertheless, the difference was seen only at higher concentration (4 μ M), where the cell viability remains above 95%. Therefore, all the markers were safe for cellular and animal studies.

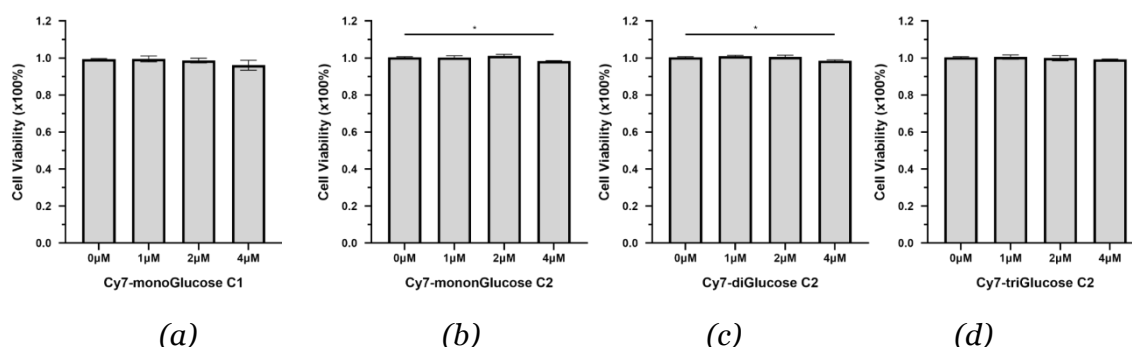
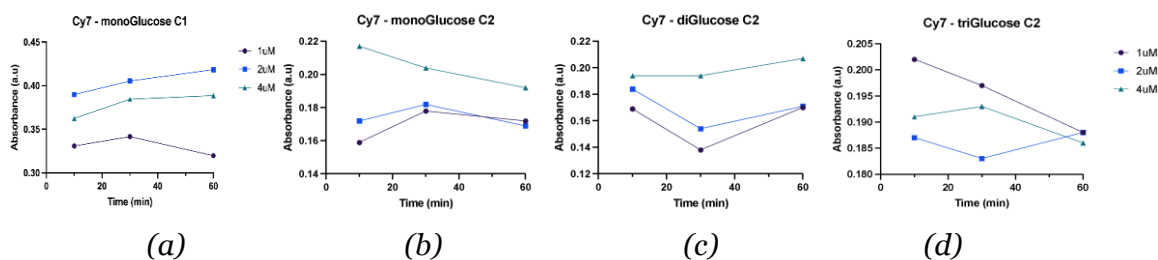


Figure 62: Cell viability assays performed on HK-2 human proximal tubular with reabsorption markers (a) Cy7-monoGlucose C1 (**36**), (b) Cy7-monoGlucose C2 (**37**), (c) Cy7-diGlucose C2 (**38**), and (d) Cy7-triGlucose C2 (**39**) for 3 hr.

NS: no significant difference, * $p < 0.05$

During the uptake assays performed on the reabsorption markers (*Figure 63*), Cy7-monoGlucose C1 (**36**) showed an increased uptake at all concentrations at the end of 30 mins and 60 mins, apart from 1 μM concentration, which decreased between 30 and 60 mins (*Figure 63(a)*). Cy7-monoGlucose C2 (**37**) showed an increased uptake at 30 mins for 1 μM (0.159 to 0.178) and 2 μM (0.172 to 0.182) concentrations, which then decreased over time (*Figure 63(b)*). At 4 μM , there was a decrease in uptake after 30 mins (0.204 to 0.192). In contrast to the previous dye, Cy7-diGlucose C2 (**38**) showed a decrease in uptake at 30 mins for all concentrations, which then increased for the remainder of the assay time (*Figure 63(c)*). Lastly, Cy7-triGlucose C2 (**39**) showed an overall decrease in uptake at 1 μM (0.202 to 0.197 to 0.188), a first decrease at 30 mins for 2 μM followed by an increase, which was opposite to the profile at 4 μM (*Figure 63(d)*).



*Figure 63: Comparison of uptake profiles of three reabsorption markers on human kidney-2 (HK-2) cells as performed by Mr. João Ferreira Faria at Utrecht University. Uptake profile was tested by incubating HK-2 cells with (a) Cy7-monoGlucose C1 (**36**), (b) Cy7-monoGlucose C2 (**37**), (c) Cy7-diGlucose C2 (**38**), or (d) Cy7-triGlucose C2 (**39**) over the course of 60 mins in HBSS at 37 °C. Data are shown as mean of three replicates from one independent experiment*

The uptake profile for reabsorption makers changed over time, which was also concentration dependent and time dependent. Cy7-monoGlucose C1 (**36**) showed an increased uptake at all concentrations and at all time points (except for 1 μM between 30 and 60 mins), which matched the results from *Hergenrother et al.*, which states that the fluorescent glucose shows better uptake when labelled with a dye at C1-position, in comparison to when labelled at C2-position [52]. The assay, like secretion dyes, was performed in Hank's buffered saline solution (HBSS). It was hypothesised that a long exposure to HBSS can be stressful for the cells, and they might require additional nutrient to perform the transport. Cy7-monoGlucose C2 (**37**) at 1 μM and 2 μM showed an initial increase and then a

subsequent decrease (even if it is minor), that can be explained by the long exposure in HBSS. In contrast, Cy7-diGlucose C2 (**38**) showed the opposite effect, which can indicate a lower affinity of this dye towards the GLUT transporter protein, which in turn can lead to a time-dependent uptake for this marker. Therefore, reabsorption marker (**38**) showed an increased uptake at the end of 60 mins for each concentration tested. For Cy7-triGlucose C2 (**39**), 1, 2 and 4 μM concentrations showed a varying uptake profile, indicating that it might not be a substrate for the GLUT transporter protein.

Therefore, the cumulative results from all the biological studies suggest Cy7-monoGlucose C1 (**36**) and Cy7-monoGlucose C2 (**37**) as viable candidates. All the markers were safe for cellular testing and can be tested further *in vivo* for their activity and biodistribution.

4.4 Markers for vascular imaging

Nephrons are made up of tiny clusters of blood capillaries, called glomeruli. Glomeruli are responsible for filtering the blood that reaches the kidney, therefore allowing the body to clear the waste while retaining important biomolecules such as proteins and glucose. Vascular damage or a reduced number of glomeruli has been associated with the progression of chronic kidney diseases, which can often lead to the development of other systemic diseases [53]. Therefore, in addition to the functional analysis, it is useful to study the histology of the kidneys to get a better grasp at disease progression.

Imaging techniques such as MRI, CT and ultrasound have been used to study vascular structures for many years, but they suffer from high costs, limited availability of the instruments, and poor resolution. The contrast agents used for these techniques, in addition to their high costs, cannot distinguish between capillary tuft and bowman's capsule sufficiently [53]. A substantial improvement is the use of optical imaging with fluorescence-based staining of intra- and extracellular biomolecules. Fluorescent markers such as Alcian Blue, indocyanine green dye, green fluorescent proteins and various synthetic chromophores have been used for the vascular visualisation [53]. Fluorescently labelled antibodies are another example for using fluorescence based vascular visualisation. For

example, Alexa Fluor 647 labelled anti-CD31 is used for staining the endothelial cell lining of the vessels [53]. This remains an expensive technique and finds limited use in the clinics.

Therefore, to expand the scope of optical imaging, new fluorescently labelled molecules are being developed, that are cheaper, provide higher resolution, stain the vessels uniformly, and provide a readily available easy assessment of the vascular system. The fluorescent staining of the vasculature is often preceded by ‘clearing’ of the organs [53]. A cleared organ does not have lipids, cell organelles or protein clusters present in the tissues. This ensures deeper tissue penetration as the light does not get refracted by the body tissues. In addition, haemoglobin can absorb light at wavelengths below 600 nm. Therefore, a cleared organ allows better signal-to-noise ratio and better imaging of the vasculature.

All blood vessels are composed of an endothelial lining, which is fenestrated and carries a negative charge on the surface due to the presence of highly anionic glycosaminoglycans (GAGs). Different layers of the vessels have different sizes of the fenestrations: endothelial layer has 70-90 nm wide fenestrations, while the basement membrane and podocyte extensions are 2-8 nm and 4-11 nm wide respectively. Based on this information, MHI148-PEI was developed by *Gretz et al*, which consisted of a highly cationic polymer with a molecular weight of 70 kDa and labelled with a cyanine 7 dye (*Figure 9*) [53]. As previously discussed, this fluorescent marker has many shortcomings, including, and most importantly, the toxicity of PEI [54]. Therefore, development of fluorescent water-soluble chitosan (*Figure 64*) as a marker to visualise kidney vasculature proved to be a novel, non-toxic and more efficient way for kidney imaging.

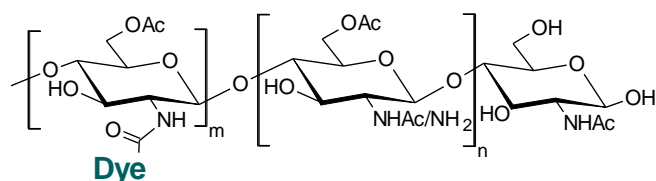


Figure 64: Fluorescent water-soluble chitosan labelled with different dyes mentioned in Table 7, and where m is between 1 to 25 for all the kidney imaging markers.

These new markers were tested for their photostability (*Figure 65*), where it was observed that SV620C-01-WS chitosan (compound **74**, *Appendix*) is more stable than SV620C-01-PEI (compound **73**, *Appendix*), with 40% degradation as

compared to 60% degradation of the PEI conjugate. This indicated that WS chitosan offers higher stability to the marker, as compared to PEI.

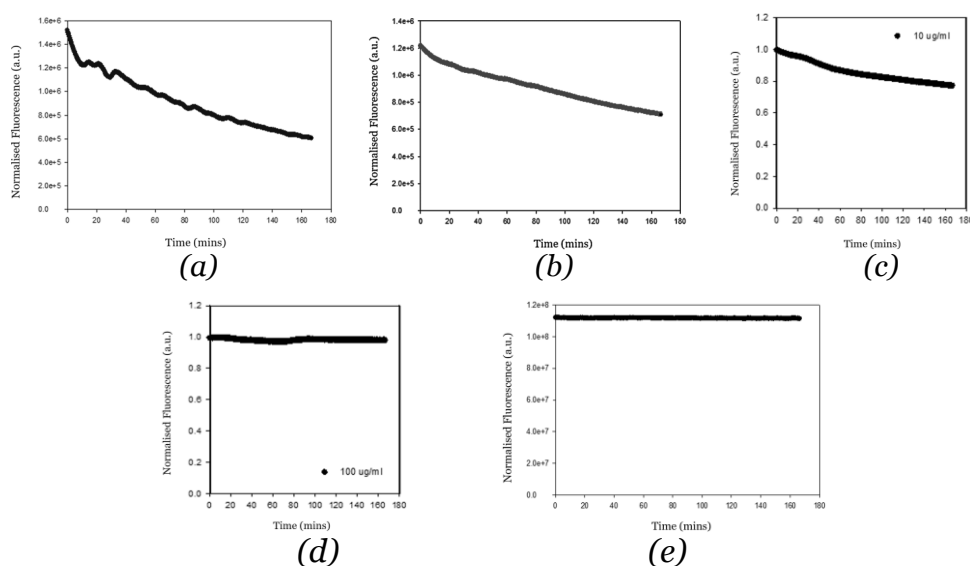


Figure 65: Photostability studies done on the kidney imaging markers, as provided by the University of Parma: (a) SV620C-01-PEI **73** with 60% fluorescence loss, (b) SV620C-01-WS chitosan **74** with 40% fluorescence loss, (c) SV680A-03-WS chitosan **79** with 23% fluorescence loss, (d) SV680A-02-WS chitosan **80** with 3% fluorescence loss, and (e) SV770Z-01-WS chitosan **78** with <1% fluorescence loss

Moreover, it was observed that the new dyes (SV680A-03, SV680A-02 and SV770Z-01) were more photostable, showing far less degradation under continuous illumination, when compared with SV620C-01 (Figure 65).

These markers also provided the users a variety of options in their excitation wavelength and their fluorescence intensity. This is because different dyes with varying optical properties were used for labelling WS Chitosan **51**. Therefore, by varying the amount of dye and the choice of dye used for labelling WS Chitosan **51**, we could obtain a range of markers for the users.

To study the kidney vasculature, the *in vivo* dosage was standardised at University of Heidelberg. These novel fluorescent markers can image the smaller vessels, as well as the larger ones, including the post-glomerular capillaries. Moreover, being non-toxic, these markers have a scope of extended use *in vivo* in the future for visualising vasculature of other organs as well.

4.5 Conclusion

To conclude, we developed novel markers for assessing kidney's tubular secretion and reabsorption. These markers were designed with respect to the new transcutaneous device developed at University of Heidelberg. The three kidney functional markers (GFR, secretion and reabsorption) had distinct optical properties that allow simultaneous measurement of their individual fluorescence. All the markers were tested for their PPB, cell viability and *in vitro*, where they proved to be safe for *in vivo* use and showed biological activity *in vitro*.

For secretion markers, Rhodamine 110 (**12**) and 500 LSS Acid – monoSO₃ (**9**) showed promising results at 2 μM concentrations. Further, Cy7-monoGlucose C1 (**36**) was a viable candidate for reabsorption marker at 2 and 4 μM concentrations, while Cy7-monoGlucose C2 **37** showed promising results at 1 and 2 μM concentrations.

In case of vascular staining, various dyes were used to label modified water-soluble chitosan. These fluorescent markers showed good results in biological experiments, with the added advantages of being non-toxic, highly photostable and chemically stable with reproducible results. These markers were developed in the NIR range, which provided better signal-to-noise ratio and a deeper tissue penetration.

Hence, together, the functional and the imaging markers paved way for a novel, more accurate and non-invasive way for kidney diagnosis at an early stage.

5. Summary

Chronic kidney diseases (CKDs) affect a huge population world-wide, where most of these patients do not know they are suffering from a CKD until the later stage. At this point, the treatment options available often lead to poor quality of life without full recovery of the kidney's functioning. The current clinical diagnostic techniques are expensive, cumbersome, invasive and many-a-times not accurate. This creates a need for an early detection way.

Glomerular filtration rate (GFR) to date is still the most used parameter for diagnosing kidney diseases. Nevertheless, tubular secretion and reabsorption play as much a role in healthy functioning of the kidney as does the filtration. The primary focus of this thesis has been to synthesise novel fluorescent markers for evaluating all three physiological processes of the kidneys. This would help diagnosing function-/location-specific abnormality in kidneys. These markers are tested for their use together in evaluating the three kidney functions simultaneously using a transcutaneous device. The detection can be done in parallel with multiple light-emitting diodes (LEDs), or successively. Since the ideal goal would be to measure all the kidney parameters together in a patient, the absorbance and emission wavelength for each marker is designed to be significantly different to evaluate each function distinctly.

Fluorescently labelled cyclodextrin (ABZWYC-H β CD) was previously deigned as a GFR marker in the red-NIR region. The secretion markers have been designed analogous to the known organic anion transporter (OAT) substrates in the blue-green region of the visible light of the electromagnetic spectrum. Fluorescent glucose molecules have been designed as reabsorption markers in the near-infrared (NIR) region. All these functional markers altogether pave way for a wholesome, rapid, and non-invasive technique for kidney diagnosis at an early stage.

In addition, fluorescent markers that can assist in kidney imaging were developed, to study its histology using confocal and light sheet microscopy. Fluorescent water-soluble chitosan was developed as a tool for staining kidney

vasculature, allowing us to visualise pre- and post-glomerular capillaries along with large blood vessels.

Preliminary results on all the markers show scope for their future biomedical application. Nevertheless, further *in vivo* experiments are needed on the kidney functional markers to confirm their biological activity. Also the use of kidney imaging markers could be extended to other organs. Therefore, follow-up biological experiments are needed on other organs, such as heart, lungs, and muscles to test the markers' efficiency.

6. References

1. Eknoyan, G: Sir William Bowman: his contributions to physiology and nephrology. *Kidney Int*, 50: 2120-2128, 1996.
<https://doi.org/10.1038/ki.1996.538>
2. Grollman, A: Present concepts of the mechanism of urine formation and of diuretic action*. *Ann Ny Acad Sci*, 88: 773-784, 2006.
<https://doi.org/10.1111/j.1749-6632.1960.tb20070.x>
3. Lepowsky, E, Ghaderinezhad, F, Knowlton, S, Tasoglu, S: Paper-based assays for urine analysis. *Biomicrofluidics*, 11: 051501, 2017.
<https://doi.org/10.1063/1.4996768>
4. Launay-Vacher, V, Izzedine, H, Karie, S, Hulot, JS, Baumelou, A, Deray, G: Renal tubular drug transporters. *Nephron Physiol*, 103: p97-106, 2006.
<https://doi.org/10.1159/000092212>
5. Kellum, JA, Romagnani, P, Ashuntantang, G, Ronco, C, Zarbock, A, Anders, H-J: Acute kidney injury. *Nat Rev Dis Primers*, 7: 52, 2021.
<https://doi.org/10.1038/s41572-021-00284-z>
6. Coresh, J, Astor, BC, Greene, T, Eknoyan, G, Levey, AS: Prevalence of chronic kidney disease and decreased kidney function in the adult US population: Third National Health and Nutrition Examination Survey. *Am J Kidney Dis*, 41: 1-12, 2003. <https://doi.org/10.1053/ajkd.2003.50007>
7. Thomas, R, Kanso, A, Sedor, JR: Chronic kidney disease and its complications. *Prim Care*, 35: 329-344, 2008.
<https://doi.org/10.1016/j.pop.2008.01.008>
8. Levey, AS, Atkins, R, Coresh, J, Cohen, EP, Collins, AJ, Eckardt, KU, Nahas, ME, Jaber, BL, Jadoul, M, Levin, A, Powe, NR, Rossert, J, Wheeler, DC, Lameire, N, Eknoyan, G: Chronic kidney disease as a global public health problem: approaches and initiatives - a position statement from Kidney Disease Improving Global Outcomes. *Kidney Int*, 72: 247-259, 2007.
<https://doi.org/10.1038/sj.ki.5002343>
9. Jha, V, Garcia-Garcia, G, Iseki, K, Li, Z, Naicker, S, Plattner, B, Saran, R, Wang, AY, Yang, CW: Chronic kidney disease: global dimension and perspectives. *Lancet*, 382: 260-272, 2013.
[https://doi.org/10.1016/s0140-6736\(13\)60687-x](https://doi.org/10.1016/s0140-6736(13)60687-x)
10. McClellan, W, Aronoff, SL, Bolton, WK, Hood, S, Lorber, DL, Tang, KL, Tse, TF, Wasserman, B, Leiserowitz, M: The prevalence of anemia in patients with chronic kidney disease. *Curr Med Res Opin*, 20: 1501-1510, 2004.
<https://doi.org/10.1185/030079904x2763>
11. Gansevoort, RT, Correa-Rotter, R, Hemmelgarn, BR, Jafar, TH, Heerspink, HJ, Mann, JF, Matsushita, K, Wen, CP: Chronic kidney disease and cardiovascular risk: epidemiology, mechanisms, and prevention. *Lancet*, 382: 339-352, 2013. [https://doi.org/10.1016/s0140-6736\(13\)60595-4](https://doi.org/10.1016/s0140-6736(13)60595-4)
12. de Boer, IH, Rue, TC, Hall, YN, Heagerty, PJ, Weiss, NS, Himmelfarb, J: Temporal trends in the prevalence of diabetic kidney disease in the United States. *Jama-J Am Med Assoc*, 305: 2532-2539, 2011.
<https://doi.org/10.1001/jama.2011.861>

13. Fox, CS, Matsushita, K, Woodward, M, Bilo, HJ, Chalmers, J, Heerspink, HJ, Lee, BJ, Perkins, RM, Rossing, P, Sairenchi, T, Tonelli, M, Vassalotti, JA, Yamagishi, K, Coresh, J, de Jong, PE, Wen, CP, Nelson, RG: Associations of kidney disease measures with mortality and end-stage renal disease in individuals with and without diabetes: a meta-analysis. *Lancet*, 380: 1662-1673, 2012. [https://doi.org/10.1016/s0140-6736\(12\)61350-6](https://doi.org/10.1016/s0140-6736(12)61350-6)
14. Mahmoodi, BK, Matsushita, K, Woodward, M, Blankestijn, PJ, Cirillo, M, Ohkubo, T, Rossing, P, Sarnak, MJ, Stengel, B, Yamagishi, K, Yamashita, K, Zhang, L, Coresh, J, de Jong, PE, Astor, BC: Associations of kidney disease measures with mortality and end-stage renal disease in individuals with and without hypertension: a meta-analysis. *Lancet*, 380: 1649-1661, 2012. [https://doi.org/10.1016/s0140-6736\(12\)61272-0](https://doi.org/10.1016/s0140-6736(12)61272-0)
15. Gounden, V, Jialal, I. *Renal Function Tests*. StarPearls Publishing, 2020.
16. Beierwaltes, WH, Harrison-Bernard, LM, Sullivan, JC, Mattson, DL: Assessment of renal function; clearance, the renal microcirculation, renal blood flow, and metabolic balance. *Compr Physiol*, 3: 165-200, 2013. <https://doi.org/10.1002/cphy.c120008>
17. Ferguson, MA, Waikar, SS: Established and emerging markers of kidney function. *Clin Chem*, 58: 680-689, 2012. <https://doi.org/10.1373/clinchem.2011.167494>
18. Filler, G, Bökenkamp, A, Hofmann, W, Le Bricon, T, Martínez-Brú, C, Grubb, A: Cystatin C as a marker of GFR-history, indications, and future research. *Clin Biochem*, 38: 1-8, 2005. <https://doi.org/10.1016/j.clinbiochem.2004.09.025>
19. Westhuyzen, J: Cystatin C: a promising marker and predictor of impaired renal function. *Ann Clin Lab Sci*, 36: 387-394, 2006. PMID: 17127725
20. Guignard, J-P: *Postnatal Development of Glomerular Filtration Rate in Neonates*. Fetal and Neonatal Physiology (Fifth Edition), 2017.
21. Buclin, T, Pechère-Bertschi, A, Séchaud, R, Décosterd, LA, Munafo, A, Burnier, M, Biollaz, J: Sinistrin clearance for determination of glomerular filtration rate: a reappraisal of various approaches using a new analytical method. *J Clin Pharmacol*, 37: 679-692, 1997. <https://doi.org/10.1002/j.1552-4604.1997.tb04355.x>
22. Nitsch, E, Iwanov, W, Lederer, K: Molecular characterization of sinistrin. *Carbohydr Res*, 72: 1-12, 1979. [https://doi.org/https://doi.org/10.1016/S0008-6215\(00\)83918-X](https://doi.org/https://doi.org/10.1016/S0008-6215(00)83918-X)
23. Mohammed, Y, Vajpayee, S, Picascia, T, Gretz, N, Perciaccante, R: An overview of non-invasive methods for transcutaneous measurements of glomerular filtration. *J Exp Nephrol*, 2: 7-14, 2021. <https://doi.org/10.46439/nephrology.2.008>
24. Stacy, BD, Thorburn, GD: Chromium-51 ethylenediaminetetraacetate for estimation of glomerular filtration rate. *Science*, 152: 1076-1077, 1966. <https://doi.org/10.1126/science.152.3725.1076>
25. Winter, CC, Myers, WG: Three new test agents for the radioisotope renogram: DISA-I-131; EDTA-Cr51; and Hippuran-I-125. *J Nucl Med*, 3: 273-281, 1962. PMID: 14007586

26. Chervu, LR, Blaufox, MD: Renal radiopharmaceuticals-an update. *Semin Nucl Med*, 12: 224-245, 1982. [https://doi.org/10.1016/s0001-2998\(82\)80038-x](https://doi.org/10.1016/s0001-2998(82)80038-x)
27. Stevens, LA, Levey, AS: Measured GFR as a confirmatory test for estimated GFR. *J Am Soc Nephrol*, 20: 2305-2313, 2009. <https://doi.org/10.1681/asn.2009020171>
28. Rehling, M, Møller, ML, Thamdrup, B, Lund, JO, Trap-Jensen, J: Simultaneous measurement of renal clearance and plasma clearance of ^{99m}Tc-labelled diethylenetriaminepenta-acetate, ⁵¹Cr-labelled ethylenediaminetetra-acetate and inulin in man. *Clin Sci*, 66: 613-619, 1984. <https://doi.org/10.1042/cs0660613>
29. Assadi, M, Eftekhari, M, Hozhabrosadati, M, Saghari, M, Ebrahimi, A, Nabipour, I, Abbasi, MZ, Moshtaghi, D, Abbaszadeh, M, Assadi, S: Comparison of methods for determination of glomerular filtration rate: low and high-dose Tc-99m-DTPA renography, predicted creatinine clearance method, and plasma sample method. *Int Urol Nephrol*, 40: 1059-1065, 2008. <https://doi.org/10.1007/s11255-008-9446-4>
30. Gaspari, F, Perico, N, Ruggenenti, P, Mosconi, L, Amuchastegui, CS, Guerini, E, Daina, E, Remuzzi, G: Plasma clearance of nonradioactive iohexol as a measure of glomerular filtration rate. *J Am Soc Nephrol*, 6: 257-263, 1995. <https://doi.org/10.1681/asn.V62257>
31. Delanaye, P, Ebert, N, Melsom, T, Gaspari, F, Mariat, C, Cavalier, E, Björk, J, Christensson, A, Nyman, U, Porrini, E, Remuzzi, G, Ruggenenti, P, Schaeffner, E, Soveri, I, Sterner, G, Eriksen, BO, Bäck, SE: Iohexol plasma clearance for measuring glomerular filtration rate in clinical practice and research: a review. Part 1: How to measure glomerular filtration rate with iohexol? *Clin Kidney J*, 9: 682-699, 2016. <https://doi.org/10.1093/ckj/sfw070>
32. Edelson, J, Shaw, D, Palace, G: Pharmacokinetics of iohexol, a new nonionic radiocontrast agent, in humans. *J Pharm Sci*, 73: 993-995, 1984. <https://doi.org/10.1002/jps.2600730735>
33. Mützel, W, Siefert, HM, Speck, U: Biochemical-pharmacologic properties of iohexol. *Acta Radiol Suppl*, 362: 111-115, 1980. <https://doi.org/10.1177/0284185180021362S20>
34. Chinen, LK, Galen, KP, Kuan, KT, Dyszlewski, ME, Ozaki, H, Sawai, H, Pandurangi, RS, Jacobs, FG, Dorshow, RB, Rajagopalan, R: Fluorescence-enhanced europium-diethylenetriaminepentaacetic (DTPA)-monoamide complexes for the assessment of renal function. *J Med Chem*, 51: 957-962, 2008. <https://doi.org/10.1021/jmo70842+>
35. Hiroaki, O, Emiko, S, Toshihisa, N, Hiroaki, S: Sensitization of Europium(III) Luminescence by DTPA Derivatives. *Chem Lett*, 29: 312-313, 2000. <https://doi.org/10.1246/cl.2000.312>
36. Dorshow, RB, Bugaj, JE: Next tier in vitro and in vivo nonclinical studies further elucidating the safety and toxicity profile of MB-102, a novel fluorescent tracer agent for measurement of glomerular filtration rate. *Regul Toxicol Pharmacol*, 107: 104417, 2019. <https://doi.org/10.1016/j.yrtph.2019.104417>

37. Poreddy, AR, Neumann, WL, Freskos, JN, Rajagopalan, R, Asmelash, B, Gaston, KR, Fitch, RM, Galen, KP, Shieh, JJ, Dorshow, RB: Exogenous fluorescent tracer agents based on pegylated pyrazine dyes for real-time point-of-care measurement of glomerular filtration rate. *Bioorg Med Chem*, 20: 2490-2497, 2012. <https://doi.org/10.1016/j.bmc.2012.03.015>
38. Huang, J, Gretz, N: Light-Emitting Agents for Noninvasive Assessment of Kidney Function. *ChemistryOpen*, 6: 456-471, 2017. <https://doi.org/10.1002/open.201700065>
39. Lorenz, JN, Gruenstein, E: A simple, nonradioactive method for evaluating single-nephron filtration rate using FITC-inulin. *Am J Physiol*, 276: F172-177, 1999. <https://doi.org/10.1152/ajprenal.1999.276.1.F172>
40. Pill, J, Issaeva, O, Woderer, S, Sadick, M, Kränzlin, B, Fiedler, F, Klötzer, HM, Krämer, U, Gretz, N: Pharmacological profile and toxicity of fluorescein-labelled sinistrin, a novel marker for GFR measurements. *Naunyn Schmiedebergs Arch Pharmacol*, 373: 204-211, 2006. <https://doi.org/10.1007/s00210-006-0067-0>
41. Ellery, SJ, Cai, X, Walker, DD, Dickinson, H, Kett, MM: Transcutaneous measurement of glomerular filtration rate in small rodents: through the skin for the win? *Nephrology*, 20: 117-123, 2015. <https://doi.org/10.1111/nep.12363>
42. Gould, S, Scott, RC: 2-Hydroxypropyl-beta-cyclodextrin (HP-beta-CD): a toxicology review. *Food Chem Toxicol*, 43: 1451-1459, 2005. <https://doi.org/10.1016/j.fct.2005.03.007>
43. Huang, J, Weinfurter, S, Pinto, PC, Pretze, M, Kränzlin, B, Pill, J, Federica, R, Perciaccante, R, Ciana, LD, Masereeuw, R, Gretz, N: Fluorescently Labeled Cyclodextrin Derivatives as Exogenous Markers for Real-Time Transcutaneous Measurement of Renal Function. *Bioconj Chem*, 27: 2513-2526, 2016. <https://doi.org/10.1021/acs.bioconjchem.6b00452>
44. Huang, J, Weinfurter, S, Daniele, C, Perciaccante, R, Federica, R, Della Ciana, L, Pill, J, Gretz, N: Zwitterionic near infrared fluorescent agents for noninvasive real-time transcutaneous assessment of kidney function. *Chem Sci*, 8: 2652-2660, 2017. <https://doi.org/10.1039/c6sc05059j>
45. Hauser-Kawaguchi, A, Milne, M, Li, F, Lee, TY, Luyt, LG: The development of a near infrared inulin optical probe for measuring glomerular filtration rate. *Int J Biol Macromol*, 123: 255-260, 2019. <https://doi.org/10.1016/j.ijbiomac.2018.11.034>
46. Ciana, LD, Gretz, N, Perciaccante, R, Rodeghiero, F, Geraci, S, Huang, J, Pérez, ZH, Pill, J, Weinfurter, S: Tricarbocyanine-cyclodextrin(s) conjugates and uses thereof. Italy, Cyanagen Srl, 2015 pp 54.
47. Sweet, DH, Eraly, SA, Vaughn, DA, Bush, KT, Nigam, SK: Organic anion and cation transporter expression and function during embryonic kidney development and in organ culture models. *Kidney Int*, 69: 837-845, 2006. <https://doi.org/10.1038/sj.ki.5000170>
48. Maeda, K, Tian, Y, Fujita, T, Ikeda, Y, Kumagai, Y, Kondo, T, Tanabe, K, Nakayama, H, Horita, S, Kusuhara, H, Sugiyama, Y: Inhibitory effects of p-aminohippurate and probenecid on the renal clearance of adefovir and

- benzylpenicillin as probe drugs for organic anion transporter (OAT) 1 and OAT3 in humans. *Eur J Pharm Sci*, 59: 94-103, 2014.
<https://doi.org/10.1016/j.ejps.2014.04.004>
49. Martin, MM, Lindqvist, L: The pH dependence of fluorescein fluorescence. *J Lumin*, 10: 381-390, 1975.
[https://doi.org/https://doi.org/10.1016/0022-2313\(75\)90003-4](https://doi.org/https://doi.org/10.1016/0022-2313(75)90003-4)
50. Hodgson, E: *Pesticide Excretion*. Pesticide Biotransformation and Disposition. Academic Press, 2012.
51. Mather, A, Pollock, C: Glucose handling by the kidney. *Kidney Int Suppl*: S1-6, 2011. <https://doi.org/10.1038/ki.2010.509>
52. Calvaresi, EC, Hergenrother, PJ: Glucose conjugation for the specific targeting and treatment of cancer. *Chem Sci*, 4: 2319-2333, 2013.
<https://doi.org/10.1039/c3sc22205e>
53. Huang, J, Brenna, C, Khan, AuM, Daniele, C, Rudolf, R, Heuveline, V, Gretz, N: A cationic near infrared fluorescent agent and ethyl-cinnamate tissue clearing protocol for vascular staining and imaging. *Sci Rep*, 9: 521, 2019.
<https://doi.org/10.1038/s41598-018-36741-1>
54. Kafil, V, Omid, Y: Cytotoxic impacts of linear and branched polyethylenimine nanostructures in a431 cells. *Bioimpacts*, 1: 23-30, 2011.
<https://doi.org/10.5681/bi.2011.004>
55. Wypych, G: *Photophysics*. Handbook of UV Degradation and Stabilization (Second Edition). ChemTec Publishing, 2015.
56. Nieskens, TT, Peters, JG, Schreurs, MJ, Smits, N, Woestenenk, R, Jansen, K, van der Made, TK, Röring, M, Hilgendorf, C, Wilmer, MJ, Masereeuw, R: A Human Renal Proximal Tubule Cell Line with Stable Organic Anion Transporter 1 and 3 Expression Predictive for Antiviral-Induced Toxicity. *Aaps j*, 18: 465-475, 2016. <https://doi.org/10.1208/s12248-016-9871-8>
57. Mihaila, SM, Faria, J, Stefens, MFJ, Stamatialis, D, Verhaar, MC, Gerritsen, KGF, Masereeuw, R: Drugs Commonly Applied to Kidney Patients May Compromise Renal Tubular Uremic Toxins Excretion. *Toxins*, 12, 2020.
<https://doi.org/10.3390/toxins12060391>
58. Littlewood, J: *Innovative Multispectral Optoacoustic Tomography Strategies for Evaluating Different Aspects of Renal Function*. Med. Dissertation. Faculty of Health and Life Sciences, University of Liverpool, 2022.
59. Sekine, T, Cha, SH, Endou, H: The multispecific organic anion transporter (OAT) family. *Eur J Physiol*, 440: 337-350, 2000.
<https://doi.org/10.1007/s004240000297>
60. Ren, TB, Xu, W, Zhang, W, Zhang, XX, Wang, ZY, Xiang, Z, Yuan, L, Zhang, XB: A General Method To Increase Stokes Shift by Introducing Alternating Vibronic Structures. *J Am Chem Soc*, 140: 7716-7722, 2018.
<https://doi.org/10.1021/jacs.8b04404>
61. Xia J: Preparation method of rhodamine 110. China, Suzhou Youyi landi Biotechnology Co.,Ltd., 2015 pp 12.
62. Smith, DA, Di, L, Kerns, EH: The effect of plasma protein binding on in vivo efficacy: misconceptions in drug discovery. *Nat Rev Drug Discov*, 9: 929-939, 2010. <https://doi.org/10.1038/nrd3287>

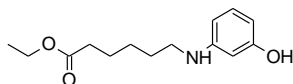
63. Bteich, M: An overview of albumin and alpha-1-acid glycoprotein main characteristics: highlighting the roles of amino acids in binding kinetics and molecular interactions. *Heliyon*, 5: e02879, 2019. <https://doi.org/10.1016/j.heliyon.2019.e02879>
64. Xie, Y: *Validation of new markers for the transcutaneous determination of tubular secretion and tubular reabsorption in in-vitro systems*. Med. Dissertation. Medizinische Fakultät Mannheim, Universität Heidelberg, Personal communication.
65. Reux, B, Weber, V, Galmier, MJ, Borel, M, Madesclaire, M, Madelmont, JC, Debiton, E, Coudert, P: Synthesis and cytotoxic properties of new fluorodeoxyglucose-coupled chlorambucil derivatives. *Bioorg Med Chem*, 16: 5004-5020, 2008. <https://doi.org/10.1016/j.bmc.2008.03.038>
66. Ren, B, Wang, M, Liu, J, Ge, J, Zhang, X, Dong, H: Zemplén transesterification: a name reaction that has misled us for 90 years. *Green Chem*, 17: 1390-1394, 2015. <https://doi.org/10.1039/C4GC02006E>
67. Mujumdar, SR, Mujumdar, RB, Grant, CM, Waggoner, AS: Cyanine-labeling reagents: sulfobenzindocyanine succinimidyl esters. *Bioconj Chem*, 7: 356-362, 1996. <https://doi.org/10.1021/bc960021b>
68. Lu, YT, Ma, XL, Xu, YH, Hu, J, Wang, F, Qin, WY, Xiong, WY: A Fluorescent Glucose Transport Assay for Screening SGLT2 Inhibitors in Endogenous SGLT2-Expressing HK-2 Cells. *Nat Prod Bioprospect*, 9: 13-21, 2019. <https://doi.org/10.1007/s13659-018-0188-4>
69. Gao, Z, Hao, Y, Zheng, M, Chen, Y: A fluorescent dye with large Stokes shift and high stability: synthesis and application to live cell imaging. *RSC Adv*, 7: 7604-7609, 2017. <https://doi.org/10.1039/C6RA27547H>
70. Todorov, MI, Paetzold, JC, Schoppe, O, Tetteh, G, Shit, S, Efremov, V, Todorov-Völgyi, K, Düring, M, Dichgans, M, Piraud, M, Menze, B, Ertürk, A: Machine learning analysis of whole mouse brain vasculature. *Nat Methods*, 17: 442-449, 2020. <https://doi.org/10.1038/s41592-020-0792-1>
71. Samanta, A, Vendrell, M, Das, R, Chang, YT: Development of photostable near-infrared cyanine dyes. *Chem Commun*, 46: 7406-7408, 2010. <https://doi.org/10.1039/c0cc02366c>
72. Exner, RM, Cortezon-Tamarit, F, Pascu, SI: Explorations into the Effect of meso-Substituents in Tricarbocyanine Dyes: A Path to Diverse Biomolecular Probes and Materials. *Angew Chem Int Ed Engl*, 60: 6230-6241, 2021. <https://doi.org/10.1002/anie.202008075>
73. Sashiwa, H, Kawasaki, N, Nakayama, A, Muraki, E, Yamamoto, N, Aiba, S: Chemical modification of chitosan. 14:(1) Synthesis of water-soluble chitosan derivatives by simple acetylation. *Biomacromolecules*, 3: 1126-1128, 2002. <https://doi.org/10.1021/bm0200480>
74. van der Made, TK, Fedecostante, M, Scotcher, D, Rostami-Hodjegan, A, Sastre Toraño, J, Middel, I, Koster, AS, Gerritsen, KG, Jankowski, V, Jankowski, J, Hoenderop, JGJ, Masereeuw, R, Galetin, A: Quantitative Translation of Microfluidic Transporter in Vitro Data to in Vivo Reveals Impaired Albumin-Facilitated Indoxyl Sulfate Secretion in Chronic Kidney Disease. *Mol Pharmaceut*, 16: 4551-4562, 2019.

<https://doi.org/10.1021/acs.molpharmaceut.9b00681>

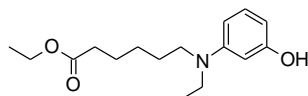
75. Jansen, TP, Rodeghiero, G., Foglietta, D., Perciaccante, R., Ciana, L.P.: Coumarin dyes and conjugates thereof. Italy, Cyanagen Srl, 2016 pp 53.
76. Xu, X, Draney, D.R.: Fluorescent imaging with substituted cyanine dyes. US, Li Cor Inc, 2010 pp 89.

7. Appendix

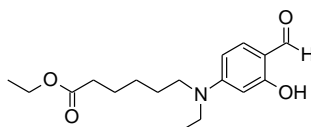
Synthesis, purification, and characterisation of all the markers was carried out as follows:



Ethyl 6-[(3-hydroxyphenyl)amino] hexanoate (3): In a 100 mL round bottom, one necked flask set up with a magnetic stir bar and a reflux condenser, 3-aminophenol **1** (40.0 g, 367 mmol, 5 eq) was dissolved in dimethylformamide. Ethyl-6-bromo hexanoate **2** (16.4 g, 73 mmol, 1 eq) was added. The reaction mixture was stirred at 50 °C for 20 hr. Solvent was removed under vacuum to give a crude oil. The crude oil was purified on a silica gel column with a gradient of hexane/ethyl acetate as eluent to yield the desired product as a colourless oil **3** (13.7 g, yield 74%). ¹H-NMR (CDCl₃, 600 MHz): δ 1.26 (t, J = 7.0 Hz, 3H), 1.38-1.46 (m, 2H), 1.58-1.71 (m, 4H), 2.30 (t, J = 7.4 Hz, 2H), 3.08 (t, J = 7.0 Hz, 2H), 4.13 (q, J = 7.4 Hz, 2H), 6.09 (t, J = 2.3 Hz, 1H), 6.17 (m, 2H), 7.00 (t, J = 8.2 Hz, 1H) [75].

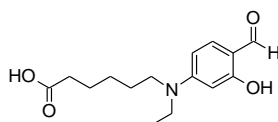


Ethyl 6-[ethyl(3-hydroxyphenyl)amino]hexanoate (4): In a 100 mL round bottom, one necked flask set up with a magnetic stir bar and a reflux condenser, **3** (5.3 g, 21.1 mmol, 1 eq) was dissolved in dimethylformamide. Ethyl iodide (3.29 g, 21.1 mmol, 1 eq) and potassium carbonate (2.92 g, 21.1 mmol, 1 eq) were added. The reaction mixture was stirred at 50 °C for 20 hr. Solvent was removed under vacuum to give a crude oil. The crude oil was dissolved in ethyl acetate (250 mL) and extracted with aqueous hydrochloric acid (0.05 M, 2 x 200 ml). The organic phase was dried over sodium sulfate and solvent was removed under vacuum to give a crude oil. The crude oil was purified on a silica gel column with a gradient of hexane/ethyl acetate as eluent to yield the desired product as a colourless oil **4** (5.1 g, yield 86%). ¹H-NMR (CDCl₃, 600 MHz): δ 1.13 (t, J = 7.0 Hz, 3H), 1.26 (t, J = 7.0 Hz, 3H), 1.33-1.38 (m, 2H), 1.57-1.62 (m, 2H), 1.66-1.70 (m, 2H), 2.32 (t, J = 7.0 Hz, 2H), 3.21 (t, J = 7.6 Hz, 2H), 3.31 (q, J = 7.0 Hz, 2H), 4.14 (q, J = 7.0 Hz, 2H), 5.13 (broad band, 1H), 6.12 (d, J = 7.6 Hz, 1H), 6.16 (s, 1H), 6.23 (d, J = 8.2 Hz, 1H), 7.04 (t, J = 8.2 Hz, 1H) [75].

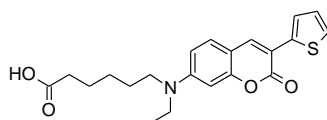


Ethyl 6-[ethyl(4-formyl-3-hydroxyphenyl)amino]hexanoate (5): A flame-dried two-necked round bottom flask equipped with stir bar was cooled to 0 °C. Anhydrous dimethyl-

formamide (14.5 mL, 188 mmol, 15 eq) was added, followed by slow addition of phosphoryl chloride (8.7 mL, 94 mmol, 7.5 eq). The reaction mixture was then stirred at 0 °C for 30 min and an additional 30 min at room temperature. A solution of **4** (3.5 g, 12.5 mmol, 1 eq) in anhydrous dimethylformamide (10 mL) was slowly added and the reaction mixture was stirred at room temperature for 20 hr. The reaction mixture was cooled to 0 °C and quenched by addition of small pieces of ice at a time. The pH was neutralized to pH 8-10 with 1 M sodium hydroxide. The aqueous solution was extracted with dichloromethane (2 x 250 mL). Solvent was removed under vacuum to give a crude oil. The crude oil was purified on a silica gel column with a gradient of hexane/ethyl acetate as eluent to yield the desired product as a colourless oil **5** (2 g, yield 53%). ¹H-NMR (CDCl₃, 600MHz): δ 1.19 (t, J=7.0 Hz, 3H), 1.25 (t, J=7.6 Hz, 3H), 1.37 (m, 2H), 1.60-1.70 (m, 4H), 2.31 (t, J=7.6 Hz, 2H), 3.30 (t, J=7.6 Hz, 2H), 3.40 (q, J=7.0 Hz, 2H), 4.13 (q, J=7.0 Hz, 2H), 6.04 (d, J=2.3 Hz, 1H), 6.23 (dd, J=8.8, 2.3 Hz, 1H), 7.25 (d, J=8.8 Hz, 1H), 9.48 (s, 1H), 11.62 (s, 1H) [75].

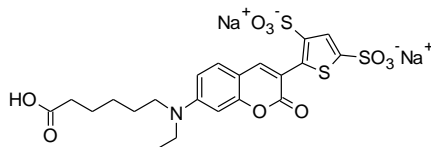


6-[ethyl(4-formyl-3-hydroxyphenyl)amino]hexanoic acid (6): In a one-necked round bottom flask, **5** (2 g, 6.5 mmol, 1 eq) was dissolved in 20 mL tetrahydrofuran. Sodium hydroxide (0.78 g, 19.5 mmol, 3 eq) dissolved in water (20 mL) was added and the mixture was stirred at room temperature for one hour. Tetrahydrofuran was evaporated and the mixture was neutralized with hydrochloric acid until it reached pH 6. The organic material was extracted with ethyl acetate. The solvent was evaporated after drying over magnesium sulphate to give an off-white powder **6** (1.72 g, 95%). ¹H-NMR (CDCl₃, 600MHz): δ 1.19 (t, J=7.0 Hz, 3H), 1.34-1.45 (m, 2H), 1.59-1.74 (m, 4H), 2.39 (t, J=7.3 Hz, 2H), 3.32 (t, J=7.6 Hz, 2H), 3.41 (q, J=7.0 Hz, 2H), 6.05 (d, J=2.4 Hz, 1H), 6.23 (d, J=2.4 Hz, 1H), 6.25 (d, J=2.4 Hz, 1H), 9.48 (s, 1H), 11.61 (s, 1H) [75].

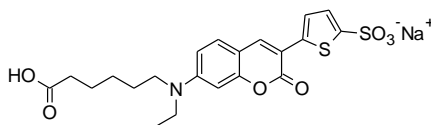


6-[ethyl{2-oxo-3-(thiophen-2-yl)-2H-chromen-7-yl}amino]hexanoic acid (7): In a two necked round bottom flask equipped with magnetic stirring bar and a condenser, a mixture of **6** (1.2 g, 4.15 mmol, 1 eq) and 2-(thiophen-2-yl) acetonitrile (0.486 mL, 4.565 mmol, 1.1 eq) in dimethylformamide (15 mL) and acetic acid (4 mL) was added with piperidine (1.626 mL, 16.6 mmol, 4 eq). The reaction mixture was stirred at reflux under argon for 24 hr. After being cooled to room temperature, water (100 mL) was added, and the mixture was extracted with ethyl acetate (3 x 70 mL). The combined organic phase was washed with water (100 mL), brine solution (100 mL) and dried over anhydrous sodium sulphate. It was then filtered, and the solvents were removed to dryness. The crude oil was purified on a silica gel column with a

gradient of hexane/ethyl acetate as eluent to yield the desired product as an orange solid **7** (0.7 g, yield 44%). **¹H-NMR** (CDCl₃, 600 MHz): δ 1.21 (t, J = 7.0 Hz, 3H), 1.39-1.46 (m, 2H), 2.40 (t, J = 7.4 Hz, 2H), 3.34 (t, J = 7.8 Hz, 2H), 3.43 (quartet, J=7.0 HZ, 2H), 6.51 (d, J = 2.3 Hz, 1H), 6.59 (dd, J = 8.9, 2.3 Hz, 1H), 7.08 (dd, J = 5.1, 3.5 Hz, 1H), 7.31 (d, J = 8.6 Hz, 1H), 7.65 (dd, J = 3.5, 1.2 Hz, 1H), 7.88 (s, 1H). **ε**: 26000-27000 M⁻¹ cm⁻¹. **λ_{ab}**: 412 nm, **λ_{em}**: 507 nm [75].

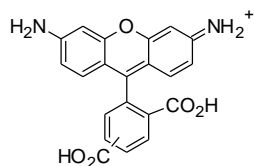


STAR FLUOR 405L Acid (8): In a flame-dried two-necked round bottom flask, set up with a magnetic stir bar and argon inlet, **7** (0.090 g, 0.23 mmol, 1 eq) was dissolved in anhydrous dimethylformamide (5 mL). Sulfur trioxide dimethyl-formamide complex (1.49 g, 9.34 mmol, 40 eq) was added and the reaction mixture was stirred at 60 °C for 20 hr under an inert argon atmosphere. The reaction mixture was cooled to room temperature and quenched by addition of saturated sodium bicarbonate solution (5 mL). Solvents were removed under vacuum to give a crude oil. The crude oil was purified on a reverse phase C18 column with a gradient of water/ methanol as eluent to yield the desired product, as a dark orange oil. The obtained dark orange oil was then passed through a Sephadex LH20 column with an isocratic gradient of water as eluent to yield the desired product as a dark orange solid **8** (STAR FLUOR 405L Acid, 0.07 g, yield 55%). **¹H-NMR** (D₂O, 600MHz): δ 1.13 (t, J = 7.0 Hz, 3H), 1.28-1.33 (m, 2H), 1.47-1.52 (m, 2H), 1.52-1.58 (m, 2H), 1.89 (t, J = 7.0 Hz, 1H), 3.34 (t, J = 7.4 Hz, 2H), 3.45 (quartet, J = 7.0 Hz, 2H), 6.52 (d, J = 2.3 Hz, 1H), 6.71 (dd, J = 8.4, 2.3 Hz, 1H), 7.21 (s, 1H), 7.34 (d, J = 8.8 Hz, 1H), 8.78 (s, 1H). **ε**: 26000-27000 M⁻¹ cm⁻¹. **λ_{ab}**: 412 nm, **λ_{em}**: 507 nm [75].

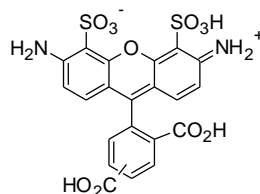


500 LSS Acid – monoSO₃ (9): In a flame-dried two-necked round bottom flask set up with a magnetic stir bar and argon inlet, **7** (0.2 g, 0.499 mmol, 1 eq) was dissolved in anhydrous dimethylformamide (12 mL). Sulfur trioxide dimethyl-formamide complex (1.556 g, 9.98 mmol, 20 eq) was added and the reaction mixture was stirred at 60 °C for 1 hr under an inert argon atmosphere. The reaction mixture was cooled to room temperature and quenched by addition of saturated sodium bicarbonate solution (5 mL). Solvents were removed under vacuum to give a crude oil. The crude oil was purified on a reverse phase C18 column with a gradient of water/ methanol as eluent to yield the desired product, as a dark orange oil. The obtained dark orange oil was then passed through a Sephadex LH20 column with an isocratic gradient of water as eluent to yield the desired product as a dark orange solid **9** (500 LSS Acid – monoSO₃, 0.025 g, yield 55%). **¹H-NMR** (D₂O, 600MHz): δ 0.96 (t, J = 7.0 Hz, 3H), 1.12-1.27 (m, J=6.9 Hz, 2H), 1.25-1.41 (m, 2H), 1.43-1.63 (m, J=14.9, 7.5 Hz, 2H), 2.34 (t, J = 7.4 Hz, 2H), 2.9 (t, J

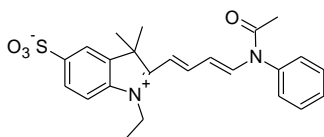
= 7.8 Hz, 2H), 3.08 (quartet, $J=7.0$ HZ, 2H), 5.92 (s, 1H), 6.22 (d, $J = 7.8$ Hz, 1H), 6.85 (d, $J = 8.9$ Hz, 1H), 7.12 (d, $J = 3.9$ Hz, 1H), 7.37 (d, $J = 8.8$ Hz, 1H), 7.59 (s, 1H). ϵ : 44000 $M^{-1} cm^{-1}$. λ_{ab} : 444 nm, λ_{em} : 518 nm.



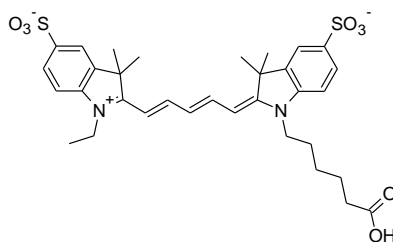
Rhodamine 110 (12): In a two-necked round-bottom flask, ethyl (3-hydroxyphenyl) carbamate **11** (10 g, 55.24 mmol, 2 eq), Phthalic anhydride **10** (5.2 g, 27.08 mmol, 1 eq) and zinc chloride (15 g, 110.1 mmol, 4 eq) were added under argon and the mixture was stirred in methane sulfonic acid (50 mL) for 24 hr at 90 °C. The mixture was cooled down and added to ice water and vigorously stirred for 10 mins. The obtained red precipitated was filtered and added to hydrogen bromide 48% overnight at 120 °C. Ice water was added and the obtained solid was filtered and added to a solution of a semi-saturated of brine (25 mL saturated solution + 25 mL water). The suspension was stirred for one hour at 90 °C and subsequently cooled down. The red suspension was filtered and washed with cold water. Compound **12** was obtained as a red solid in an isomeric mixture (Rhodamine 110, 4.9 g, yield 42%). 1H -NMR (DMSO, 600MHz): δ 6.75-6.85 (m, 8H), 6.97 (d, $J = 9.4$ Hz, 4H), 7.55 (d, $J = 7.6$ Hz, 2H), 7.86 (s, 1H), 8.3-8.4 (m, 3H), 8.7 (s, 1H). ϵ : 80000 $M^{-1} cm^{-1}$. λ_{ab} : 488 nm, λ_{em} : 515 nm [61].



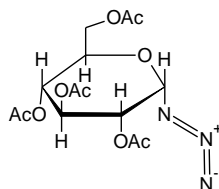
STAR FLUOR 488 Acid (13): In a one-necked round-bottom flask fuming sulfuric acid 30% (15 mL) was cooled at 0 °C and Rhodamine 110 **12** (1 g, 2.04 mmol, 1 eq) was subsequently added. The mixture was stirred for 10 hr at 0 °C. The obtained viscous oil was dropwise added to fresh dioxane (100 mL) and subsequently diethyl ether was added and stirred at 0 °C for 10 mins. The obtained reddish solid was filtered, dissolved in methanol, and quenched with triethylamine (until basic pH was reached). The solvent was removed, and the solid was purified by reverse phase C18 column chromatography to give a red solid **13** (STAR FLUOR 488 Acid, 1 g, yield 88%). 1H -NMR (DMSO, 600MHz): δ 6.30 (dt, $J = 5.9, 2.9$ Hz, 3 Hz), 6.39-6.43 (m, 2H), 7.17 (d, $J = 7.6$ Hz, 1H), 7.54 (s, 1H), 7.85 (d, $J = 7.6$ Hz, 1H), 8.08 (m, 1H), 8.19-8.22 (m, 1H), 8.31 (s, 1H). ϵ : 73000 $M^{-1} cm^{-1}$. λ_{ab} : 488 nm, λ_{em} : 515 nm.



2-[4-(acetylphenylamino)-1,3-butadien-1-yl]-1-ethyl-3,3-dimethyl-5-sulfo-3*H*-Indo-*lium* (16**):** In a 1 L 3-necked round bottom flask equipped with a magnetic stirrer and under argon atmosphere, 1-ethyl-2,3,3-trimethylindoleninium-5-sulfonate **14** (10 g, 37.45 mmol, 1 eq) was suspended in acetic anhydride. Malonaldehyde dianlyde hydrochloride **15** (10.7 g, 41.2 mmol, 1.1 eq) was added to the flask, followed by acetyl chloride (58.8 g, 749 mmol, 20 eq) and heated at 100 °C for 1.5 hr. The reaction flask was cooled to room temperature and then slowly precipitated in ethyl acetate. The solid was filtered over Gooch funnel and washed with excess ethyl acetate/diethyl ether to yield a greenish-brown solid **16**, which was directly used for the next step (15.5 g, yield 94%).

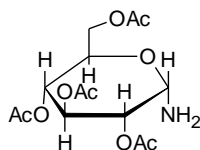


Cy645A-Acid-01 (18**):** In a 1 L flask, **16** (15.5 g, 35.4 mmol, 1 eq) was suspended in acetic anhydride. 1-(5-carboxypentyl)-2,3,3-trimethylindolium-5-sulfonate **17** (12.5 g, 35.4 mmol, 1 eq) and potassium acetate (9.4 g, 95.5 mmol, 2.7 eq) were added and the reaction was stirred at room temperature for 3 hr. The reaction mixture was slowly precipitated in ethyl acetate. The solid was filtered over Gooch funnel and washed with excess ethyl acetate/diethyl ether. The crude was purified over silica column in methanol and dichloromethane. The column was prepared in 30% methanol and was run from 10 to 100% methanol. Fractions collected were checked using TLC and combined and dried to get pure product. The solvent was dried under vacuum to yield a blue solid **18** (Cy645A-Acid-01, 22 g, yield 95%). **¹H-NMR** (DMSO, 400MHz): δ 1.24 (t, $J = 7.2$ Hz, 3H), 1.31-1.37 (m, 2H), 1.45-1.54 (m, 2H), 1.65 (s, 12H), 2.02-2.09 (m, 2H), 4.04-4.14 (m, 2H), 6.28 (m, 2H), 6.56 (dd, $J = 29.2, 16.8$ Hz, 1H), 7.30 (dd, $J = 8.3, 2.7$ Hz, 2H), 7.61 (ddd, $J = 8.2, 5.1, 1.6$ Hz, 2H), 7.73 – 7.83 (m, 2H), 8.33 (t, $J = 13.1$ Hz, 2H). **ϵ** : 240,000 M⁻¹ cm⁻¹. **λ_{ab}** : 648 nm, **λ_{em}** : 667 nm.

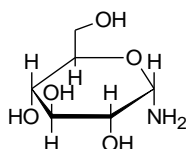


Acetylated glucose β -anomeric azide (20**):** A cold (0 °C) solution of sodium azide (1.57 g, 24.32 mmol, 4 eq) in water (20 mL) was added dropwise, in 20 mins, to 2,3,4,6-tetra-O-acetyl- α -D-glucopyranosyl bromide **19** (2.5 g, 6.08 mmol, 1 eq), dissolved in acetone (20 mL). After stirring at room temperature for 1 hr, the white precipitate was filtered, washed thoroughly with water, and dried under vacuum to give a white solid, which was used directly for the next step **20** (1.838 g, yield 82%). **¹H-NMR** (400 MHz, DMSO): δ 1.93 (s, 3H), 1.97 (s, 3H), 2.01 (s,

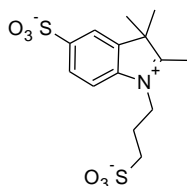
3H), 2.02 (s, 3H), 4.03-4.18 (m, 3H), 4.8 (dd, $J=9.7, 8.9$ Hz, 1H), 4.96 (t, $J=9.5$ Hz, 1H), 5.12 (d, $J=8.9$ Hz, 1H), 5.30 (t, $J=9.6$ Hz, 1H) [65].



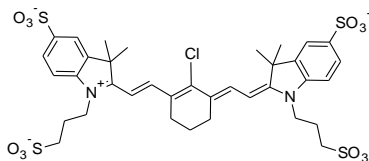
Acetylated 1-aminoglucose (21): Platinum on charcoal (0.36 g, 10% by weight) was added to a solution of **20** (1.83 g, 4.9 mmol, 1 eq) in tetrahydrofuran/methanol (40/50 mL), and the suspension was shaken with hydrogen gas for 1 hr at atmospheric pressure and room temperature. After filtration of the suspension on celite, the filtrate was evaporated to dryness to give a white solid, which was used directly for the next step **21** (1.126 g, yield 67%). **¹H-NMR** (600 MHz, DMSO): δ 1.88 (s, 3H), 1.93 (s, 6H), 1.98 (s, 3H), 3.84 (ddd, $J=9.9$ Hz, $J=4.9$ Hz, 2.7 Hz, 1H), 3.96 (dd, $J=12.1$ Hz, $J=2.5$ Hz, 1H), 4.09 (dd, $J=12.1$ Hz, $J=2.5$ Hz, 1H), 4.26 (dd, $J=12.1$ Hz, $J=4.9$ Hz, 1H), 4.6 (t, $J=9.9$ Hz, 1H), 4.82 (t, $J=9.3$ Hz, 1H), 5.18 (t, $J=9.3$ Hz, 1H) [65].



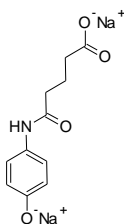
1-aminoglucose (22): DEAE-Sephadex A-25 chloride resin (10 g) was soaked overnight in 250 mL of 1M sodium hydroxide solution. The resin was then stirred in 1 M sodium hydroxide solution for 1 hr to exchange the chloride ions with hydroxide ions. The resin was washed with excess water till it reached neutral pH. The resin was stirred with **21** (1 g, 2.8 mmol, 1 eq) in 10 mL methanol for 1 hr at room temperature. The reaction was filtered, and the filtrate was dried to yield **22** as a white solid in pure form (1-aminoglucose, 0.43 g, yield 87%). **¹H-NMR** (400 MHz, DMSO): δ 2.76 (t, 1H), 2.93-3.18 (m, 3H), 3.36 (dd, $J=6.1$ Hz, 2H), 3.62 (d, $J=10.9$ Hz, 1H), 3.72 (d, $J=8.1$ Hz, 1H) [66].



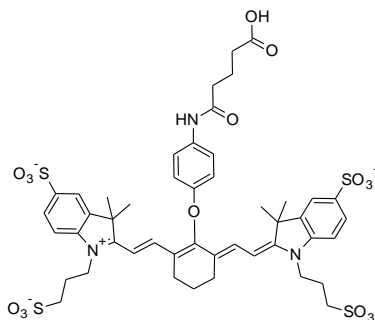
Di-sulfonate indolium salt (25): 2,3,3-Trimethyl-3*H*-indolenine-5-sulfonate potassium salt **23** (25 g, 90 mmol, 1 eq) was taken in a round-bottom flask along with 1,3-propanesultone **24** (12.25 mL, 135 mmol, 1.5 eq) in 1,2-dichlorobenzene (65 mL) and refluxed at 130 °C for 16 hr under argon. The reaction was then cooled down and the solvent was decanted. The crude was dissolved in methanol/water 30/70 and dropped in 2 L of acetone. The pink solid was filtered over Gooch funnel and washed with excess acetone. The solid precipitate **25** was dried under vacuum and used directly for the next step (38 g, yield 100 %).



Meso-chloro tetra-sulfonate Cyanine 7 (27): A mixture of **25** (5 g, 12.5 mmol, 2 eq), *N*-((2-chloro-3-((phenylamino)methylene)-1-cyclohexen-1-yl) methylene] benzenamine **26** (2.4 g, 6.25 mmol, 1 eq) and anhydrous sodium acetate (2.461 g, 30 mmol, 4 eq) in 100 mL of absolute ethanol was refluxed for 6 hr under argon. The reaction mixture was cooled to room temperature, and then filtered over Gooch funnel with pore size 4 to give a brownish green residue. The crude product was washed with excess of absolute ethanol and a mixture of absolute ethanol and methanol 50/50. The crude product was purified by reverse phase C18 chromatography in methanol and water. The pure fractions, as indicated by HPLC and TLC, were combined and dried under vacuum to yield a golden-green solid **27** (2.43 g, yield 46 %). **¹H-NMR** (400 MHz, D₂O): δ 1.68 (s, 12H), 1.84 (m, 2H), 2.04 (m, 4H), 2.60 (t, J = 6 Hz, 4H), 2.75 (m, 4H), 4.38 (m, 4H), 6.54 (d, J = 14 Hz, 2H), 7.46 (d, J = 9 Hz, 1H), 7.68 (d, J = 9 Hz, 1H), 7.80 (s, 1H), 8.26 (d, J = 14 Hz, 2H). **ε**: 270,000 M⁻¹ cm⁻¹. **λ_{ab}**: 790 nm, **λ_{em}**: 805 nm.

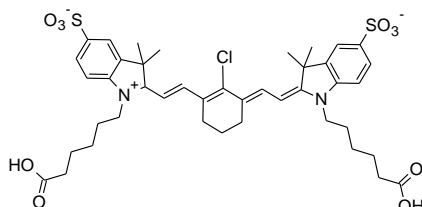


Disodium 4-[(4-hydroxyphenyl)amino]-4-oxobutanoic acid (28): In a 100 mL round-bottom flask, sodium pellets (1.8 g, 45 mmol, 2 eq) were dissolved completely in 60 mL methanol, and then 4-[(4-hydroxyphenyl)amino]-4-oxobutanoic acid (5 g, 22.5 mmol, 1 eq) was added and stirred altogether at room temperature for 2.5 hr. The reaction was stopped and precipitated in diethyl ether. The precipitate was filtered and dried to obtain a white solid **28**, which was directly used for the next step (5 g, 85% yield).

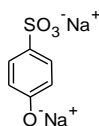


Tetra-sulfonate Cyanine 7 (29): A mixture of compound **27** (1.2 g, 1.395 mmol, 1 eq) and **28** (1.912 g, 6.975 mmol, 5 eq) in DMSO and water 50/50 was heated at 65 °C for 3 hr. The reaction mixture was cooled to room temperature and precipitated slowly in ethyl acetate and

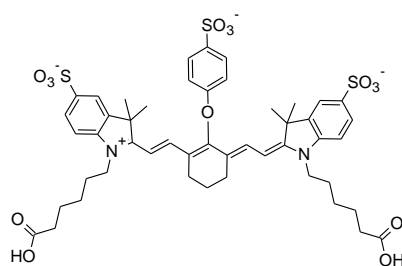
absolute ethanol 50/50 with 0.1% formic acid. The precipitate was filtered and washed with excess ethanol. The crude product was purified by reverse phase C18 chromatography to yield a golden-green solid **29** (0.5 g, yield 35%). ¹H-NMR (400 MHz, D₂O): δ 1.32 (s, 12H), 1.94 (m, 4H), 2.20 (m, 4H), 2.27 (t, 2H), 2.27 (t, 2H), 2.69 (m, 4H), 3.02 (t, 4H), 4.21 (t, 4H), 6.22 (d, J= 14 Hz, 2H), 7.14-7.20 (m, 2H), 7.32 (d, J= 8.4 Hz, 2H), 7.46 (d, 9.2 Hz, 2H), 7.73 – 7.81 (m, 2H), 7.91 (d, 14 Hz, 2H). ε: 270,000 M⁻¹ cm⁻¹. λ_{ab}: 779 nm, λ_{em}: 805 nm.



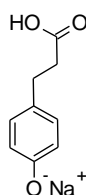
Meso-chloro di-sulfonate di-carboxylic acid Cyanine 7 (31): A mixture of 1-(5-Carboxypentyl)-2,3,3-trimethylindolium-5-sulfonate **30** (2.45 g, 6.95 mmol, 2.5 eq), *N*-[[2-chloro-3-[(phenylamino)methylene]-1-cyclohexen-1-yl] methylene] benzen- amine **26** (1 g, 2.78 mmol, 1 eq) and anhydrous sodium acetate (0.651 g, 7.5 mmol, 2.7 eq) in 45 mL of absolute ethanol was refluxed for 1 hr under argon. The reaction mixture was cooled to room temperature, and then precipitated in 1 L of ethyl acetate. The precipitate was filtered over Gooch funnel and washed with excess ethyl acetate. It was dried under vacuum to yield a golden-green solid **31** (2.3 g, yield 46 %). ¹H-NMR (400 MHz, DMSO): δ 1.54 (m, 4H), 1.66 (s, 12H), 1.71 (m, 4H), 1.80 (m, 2H), 2.17 (t, 4H), 2.69 (m, 4H), 4.19 (t, 4H), 6.3 (d, J=14.1 Hz, 2H), 7.36 (d, J=8.4 Hz, 2H), 7.64 (d, J=8.3 Hz, 2H), 7.78 (s, 2H), 8.23 (d, J=14.3 Hz, 2H). ε: 270,000 M⁻¹ cm⁻¹. λ_{ab}: 791 nm, λ_{em}: 805 nm.



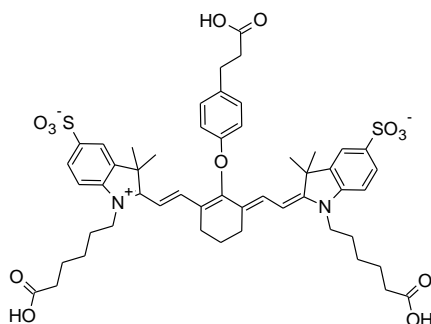
Disodium 4-hydroxybenzylsulfonate (32): In a 100 mL round-bottom flask, sodium pellets (0.86 g, 21.5 mmol, 1 eq) were dissolved completely in 60 mL methanol, and then sodium-4-hydroxybenzylsulfonatedihydrate (5 g, 21.5 mmol, 1 eq) was added and stirred altogether at room temperature for 2 hr. The reaction was stopped and precipitated in acetone. The precipitate was filtered and dried to obtain a white solid **32**, which was directly used for the next step (4.1 g, 100% yield).



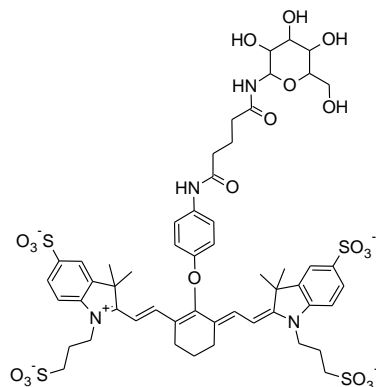
Di-sulfonate di-carboxylic acid Cyanine 7 (33): A mixture of compound **31** (0.5 g, 0.6 mmol, 1 eq) and **32** (0.7 g, 3 mmol, 5 eq) in DMSO and water 50/50 was heated at 65 °C for 2 hr. The reaction mixture was cooled to room temperature and precipitated slowly in ethyl acetate and absolute ethanol 50/50 with 0.1% formic acid. The precipitate was dried overnight under vacuum to yield a golden-green solid **33** (0.541 g, yield 92%). **¹H-NMR** (400 MHz, D₂O): δ 1.07 (s, 12H), 1.12-1.22 (m, 4H), 1.35-1.44 (m, 4H), 1.45-1.56 (m, 4H), 1.57-1.69 (m, 2H), 2.14 (t, J = 7.3 Hz, 4H), 2.29-2.37 (m, 4H), 3.74 (m, 4H), 5.83 (d, J=14.4 Hz, 2H), 6.84 (d, J = 9 Hz, 2H), 6.97 (d, J = 8.6 Hz, 2H), 7.51-7.62 (m, 6H), 7.68 (d, J=8.4 Hz, 2H). **ε**: 270,000 M⁻¹ cm⁻¹. **λ_{ab}**: 775 nm, **λ_{em}**: 805 nm.



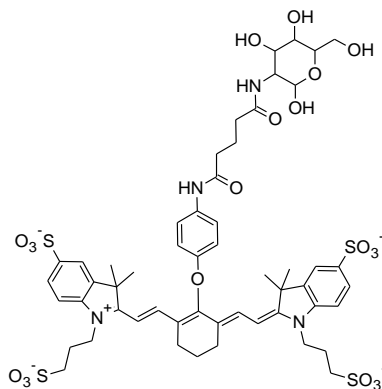
Sodium-3-(4-hydroxyphenyl) propanoic acid (34): In a 250 mL round-bottom flask, sodium pellets (2 g, 50 mmol, 2 eq) were dissolved completely in 100 mL methanol, and then 3-(4-hydroxyphenyl) propanoic acid (4.2 g, 25 mmol, 1 eq) was added and stirred altogether at room temperature for 2 hr. The reaction was stopped and precipitated in acetone. The precipitate was filtered and dried to obtain a yellow solid **34**, which was directly used for the next step (4.7 g, 100% yield).



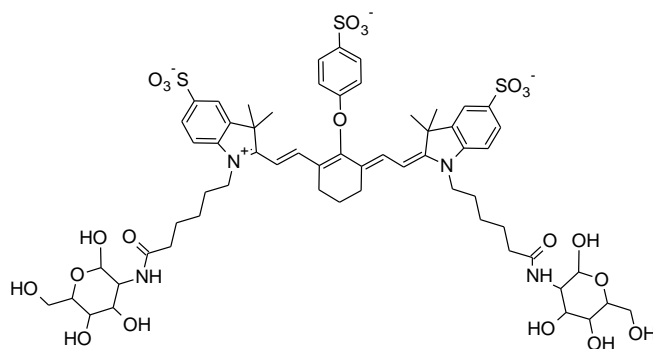
Di-sulfonate tri-carboxylic acid Cyanine 7 (35): A mixture of compound **31** (1.338 g, 1.64 mmol, 1 eq) and **34** (1.374 g, 6.56 mmol, 4 eq) in DMSO and water 50/50 was heated at 65 °C for 2 hr. The reaction mixture was cooled to room temperature and precipitated slowly in ethyl acetate with 0.1% formic acid. The precipitate was filtered over Gooch funnel and then dried under vacuum. The crude compound was purified using reverse phase c18 column chromatography to yield a golden-green solid **35** (0.777 g, yield 49%). **¹H-NMR** (600 MHz, DMSO): δ 1.24 (s, 12H), 1.32 (dt, J=15.2 Hz, 4H), 1.51 (dt, J=15 Hz, 4H), 1.65 (dd, J=15.6 Hz, 4H), 2.16 (t, 4H), 2.38-2.43 (m, 4H), 2.66 (t, 4H), 4.08 (t, 4H), 6.11 (d, J=14.3 Hz, 2H), 6.59-6.63 (d, 2H), 6.96 (d, J=8.5 Hz, 1H), 7.01 (d, J=8.7 Hz, 1H), 7.18-7.24 (m, 2H), 7.26 (d, 2H), 7.58 (d, 2H), 7.76 (d, J=14 Hz, 2H). **ε**: 270,000 M⁻¹ cm⁻¹. **λ_{ab}**: 775 nm, **λ_{em}**: 805 nm.



Cy7-monoGlucose C1 (36): In a 50 mL round-bottom flask, compound **29** (0.25 g, 0.239 mmol, 1 eq) was stirred with triethylamine (0.057 mL, 0.431 mmol, 1.8 eq) and 2-(2,5-Dioxopyrrolidin-1-yl)-1,1,3,3-tetramethylisouronium tetrafluoroborate (0.13 g, 0.431 mmol, 1.8 eq) in anhydrous DMSO at room temperature for 15 mins under argon. Once the ester formation was complete, a solution of 1-aminoglucose **22** (0.1 g, 0.558 mmol, 2.3 eq) in 0.1 M sodium bicarbonate buffer pH 9.2 (1.5 mL) was added and stirred altogether overnight. After 21 hr the reaction was stopped, and the water was removed using rotary evaporator. The remaining reaction mixture in DMSO was precipitated in ethyl acetate and filtered. The crude was purified over silica column in methanol and dichloromethane. The column was prepared in 30% methanol and was run from 30 to 100% methanol. Fractions collected were checked using HPLC and combined to get pure product. The solvent was dried under vacuum to yield a golden-green solid **36** (Cy7-monoGlucose C1, 0.1 g, yield 35%). **¹H-NMR** (400 MHz, D₂O): δ 1.12 (s, 12H), 1.94-2.07 (m, 4H), 2.24-2.38 (m, 4H), 2.44-2.58 (m, 4H), 2.84 (t, J = 7 Hz, 4H), 3.055-3.80 (m, 7H), 4.01 (t, 4H), 4.16 (d, J = 8.9 Hz, 1H), 4.83 (d, J = 9.2 Hz, 1H), 6.04 (d, J=13.8 Hz, 2H), 6.98 (d, J = 9 Hz, 2H), 7.15 (d, J=8.1 Hz, 2H), 7.31 (d, J=8.1 Hz, 2H), 7.58 (s, 2H), 7.64 (d, J=8.4 Hz, 2H), 7.72 (d, J=13.8 Hz, 2H). **¹³C-NMR** (101 MHz, D₂O): δ 178.92, 178.64, 176.69, 175.34, 166.65, 159.47, 146.35, 144.98, 144.03, 141.53, 134.27, 129.09, 126.87, 126.23, 122.18, 117.56, 113.24, 103.26, 97.43, 93.36, 78.38, 76.29, 74.03, 73.14, 72.63, 72.41, 63.23, 63.11, 59.12, 56.53, 51.31, 50.26, 49.16, 44.97, 37.84, 37.65, 37.34, 29.49, 26.38, 24.59, 24.21, 23.20, 10.74. **LRMS (m/z):** calcd: 1204.34, found: 1204.29. **ε:** 270,000 M⁻¹ cm⁻¹. **λ_{ab}:** 771 nm, **λ_{em}:** 805 nm.

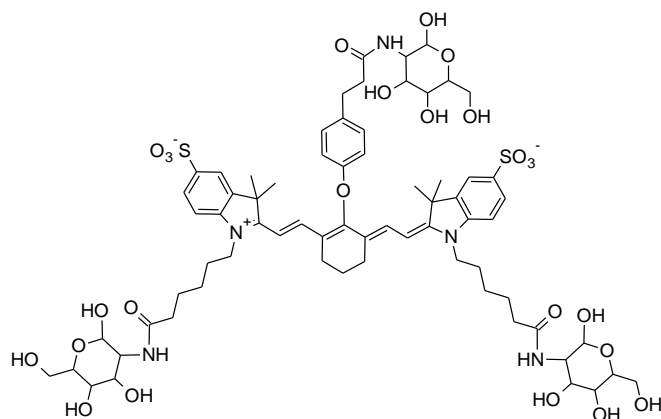


Cy7-monoGlucose C2 (37): In a 50 mL round-bottom flask, compound **29** (0.3 g, 0.287 mmol, 1 eq) was stirred with triethylamine (0.057 mL, 0.431 mmol, 1.5 eq) and 2-(2,5-Dioxopyrrolidin-1-yl)-1,1,3,3-tetramethylisouronium tetrafluoroborate (0.13 g, 0.431 mmol, 1.5 eq) in anhydrous DMSO at room temperature for 15 mins under argon. Once the ester formation was complete, a solution of glucosamine (0.082 g, 0.459 mmol, 1.6 eq) in 0.1 M sodium bicarbonate buffer pH 9.2 (1.5 mL) was added and stirred altogether overnight. After 23 hr the reaction was stopped, and the water was removed using rotary evaporator. The remaining reaction mixture in DMSO was precipitated in ethyl acetate and filtered. The crude was purified twice: first over silica column in methanol and dichloromethane. The column was prepared in 30% methanol and was run from 30% to 100% methanol. This helped in removing most of the excess glucosamine. Remaining impurities were removed using reverse phase c18 column chromatography in methanol and water, where the crude was loaded in 2% methanol and run till 100% methanol. Fractions collected were checked using HPLC and combined to get pure product. The solvent was dried under vacuum to yield a golden-green solid **37** (Cy7-monoGlucose C2, 0.25 g, yield 50%). **¹H-NMR** (600 MHz, D₂O): δ 1.06 (s, 12H), 1.83 (dt, J=17.8, 9.5 Hz, 4H), 1.98 (m, 4H), 2.27 (dd, J=16.7, 7.2 Hz, 4H), 2.48 (m, 4H), 2.82 (t, J = 6.6 Hz, 4H), 3.07-3.79 (m, 7H), 3.97 (t, 4H), 4.55 (d, J = 8.9 Hz, 1H), 5.07 (d, J = 9.2 Hz, 1H), 6.91 (d, J=7.8 Hz, 2H), 7.12 (d, J=8.1 Hz, 2H), 7.29 (d, J=8.4 Hz, 2H), 7.55 (s, 2H), 7.58-7.72 (m, 4H). **¹³C-NMR** (101 MHz, D₂O): δ 178.92, 178.64, 176.69, 175.34, 166.65, 159.47, 146.35, 144.98, 144.03, 141.53, 134.27, 129.09, 126.87, 126.23, 122.18, 117.56, 113.24, 103.26, 97.43, 93.36, 78.38, 76.29, 74.03, 73.14, 72.63, 72.41, 63.23, 63.11, 59.12, 56.53, 51.31, 50.26, 49.16, 44.97, 37.84, 37.65, 37.34, 29.49, 26.38, 24.59, 24.21, 23.20, 10.74. **LRMS (m/z):** calcd: 1204.34, found: 1204.29. **ε:** 270,000 M⁻¹ cm⁻¹. **λ_{ab}:** 770 nm, **λ_{em}:** 790 nm.

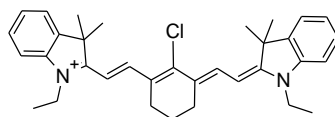


Cy7-diGlucose C2 (38): In a 50 mL round-bottom flask, compound **33** (0.2 g, 0.210 mmol, 1 eq) was stirred with 4-dimethylaminopyridine (0.064 g, 0.525 mmol, 2.5 eq) and 2-(2,5-dioxo pyrrolidine-1-yl)-1,1,3,3-tetramethylisouronium tetrafluoroborate (0.157 g, 0.525 mmol, 2.5 eq) in anhydrous DMSO at room temperature for 15 mins under argon. Once the ester formation was complete, a solution of glucosamine (0.15 g, 0.840 mmol, 4 eq) in 0.1 M sodium bicarbonate buffer pH 9.2 (3 mL) was added and stirred altogether for 4.5 hr. The reaction was stopped, and the water was removed using rotary evaporator. The remaining reaction mixture in DMSO was precipitated in ethyl acetate and filtered. The crude was purified over silica

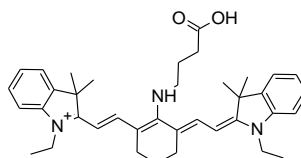
column in methanol and dichloromethane. The column was prepared in 30% methanol and was run from 30 to 100% methanol. Fractions collected were checked using HPLC and combined to get pure product. The solvent was dried under vacuum to yield a golden-green solid **38** (Cy7-diGlucose C2, 0.135 g, yield 50%). ¹H-NMR (400 MHz, D₂O): δ 1.05 (s, 12H), 1.09-1.19 (m, 4H), 1.33-1.53 (m, 8H), 1.69-1.79 (m, 2H), 2.02-2.17 (m, 4H), 2.37-2.51 (m, 4H), 3.26-3.84 (m, 11H), 4.59 (d, J = 8.4 Hz, 1H), 4.80 (d, J = 8.4 Hz, 1H), 5.02 (d, J = 3.2 Hz, 1H), 5.31 (d, J = 3.4 Hz, 1H), 5.88 (d, J=14 Hz, 2H), 6.94 (d, J = 8 Hz, 2H), 6.99 (d, J = 8.4 Hz, 2H), 7.51-7.63 (m, 4H), 7.68 (d, J=13.8 Hz, 2H). ¹³C-NMR (101 MHz, D₂O): δ 176.99, 176.64, 172.47, 162.93, 160.83, 143.71, 141.20, 139.23, 139.19, 137.49, 128.34, 126.62, 122.82, 119.59, 114.64, 110.80, 100.79, 95.00, 92.68, 90.86, 89.06, 76.09, 75.81, 73.72, 71.96, 71.49, 70.49, 70.10, 69.90, 69.60, 69.52, 69.50, 60.71, 60.60, 60.38, 60.22, 56.64, 56.57, 54.20, 53.99, 48.74, 48.71, 48.67, 43.76, 38.64, 35.72, 35.31, 26.88, 26.24, 25.37, 24.81, 23.64, 20.59. LRMS (m/z): calcd: 1301.45, found: 1300.41. ε: 270,000 M⁻¹ cm⁻¹. λ_{ab}: 775 nm, λ_{em}: 793 nm.



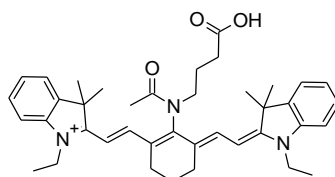
Cy7-triGlucose C2 (39): In a 50 mL round-bottom flask, compound **35** (0.25 g, 0.26 mmol, 1 eq) was stirred with triethylamine (0.142 mL, 1.04 mmol, 4 eq) and 2-(2,5-dioxo pyrrolidine-1-yl)-1,1,3,3-tetramethylisouronium tetrafluoroborate (0.312 g, 1.04 mmol, 4 eq) in anhydrous DMSO at room temperature for 15 mins under argon. Once the ester formation was complete, a solution of glucosamine (0.28 g, 1.56 mmol, 6 eq) in 0.1 M sodium bicarbonate buffer pH 9.2 (6 mL) was added and stirred altogether overnight. After 22 hr the reaction was stopped, and the water was removed using rotary evaporator. The remaining reaction mixture in DMSO was precipitated in ethyl acetate and filtered. The crude was purified over silica column in methanol and dichloromethane. The column was prepared in 30% methanol and was run from 30 to 100% methanol. Fractions collected were checked using HPLC and combined to get pure product. The solvent was dried under vacuum to yield a golden-green solid **39** (Cy7-triGlucose C2, 0.204 g, yield 54%). ¹H-NMR (400 MHz, D₂O): δ 0.90 (s, 12H), 0.96-1.14 (m, 6H), 1.20-1.42 (m, 10H), 1.44-1.61 (m, 2H), 1.93-2.07 (m, 4H), 2.12-2.31 (m, 6H), 2.61-2.48 (m, 2H), 3.09-3.74 (m, 21H), 4.42 (d, J = 8 Hz, 1H), 4.48 (d, J = 8.3 Hz, 1H), 4.87 (d, J = 3.2 Hz, 1H), 4.92 (d, J = 3.4 Hz, 1H), 5.71 (d, J = 13.3 Hz, 2H), 6.54-6.66 (m, 2H), 6.83-6.98 (m, 2H), 7.41-7.49 (m, 6H), 7.52 (d, J = 14 Hz, 2H). ε: 270,000 M⁻¹ cm⁻¹. LRMS (m/z): calcd: 1455.61, found: 1454.55. ε: 270,000 M⁻¹ cm⁻¹. λ_{ab}: 774 nm, λ_{em}: 809 nm.



Meso-chloro N-ethyl Cyanine 7 (47): A mixture of 1-ethyl-2,3,3-trimethylindolinium iodide **46** (2 g, 6.34 mmol, 2 eq), Vilsmeier-Haack reagent **26** (1.13 g, 3.17 mmol, 1 eq) and anhydrous sodium acetate (0.93 g, 9.51 mmol, 3 eq) in 20 mL of absolute ethanol was refluxed for 2.5 hr under argon. The reaction mixture was cooled to room temperature, and then concentrated under reduced pressure to yield a brownish green residue. The residue was suspended in DCM, filtered, and dried in vacuum. The crude product was purified by silica gel column chromatography in methanol and dichloromethane (10/90) to yield a golden-green solid **47** (1.28 g, yield 79.2%). $^1\text{H-NMR}$ (400 MHz, CDCl_3): δ 1.46 (t, 6H), 1.72 (s, 12H), 1.99 (m, 2H), 2.77 (t, 4H), 4.24 (q, 4H), 6.25 (d, $J=14$ Hz, 2H), 7.25(m, 4H), 7.39 (m, 4H), 8.34 (d, $J=14$ Hz, 2H). ϵ : 270,000 $\text{M}^{-1} \text{cm}^{-1}$. λ_{ab} : 770 nm, λ_{em} : 805 nm.

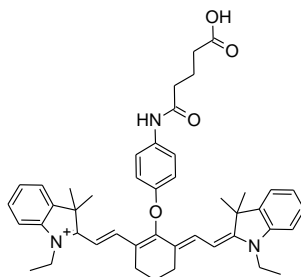


SV620C-01 (40): A mixture of compound **47** (0.8 g, 1.25 mmol, 1 eq) and 4-aminobutanoic acid **48** (0.387 g, 3.75 mmol, 3 eq) in DMSO was heated at 65 °C for 4 hr. The reaction mixture was cooled to room temperature and dissolved in DCM. It was extracted twice in water and once in brine. The organic layer was collected, and dried using sodium sulphate, filtered, and dried overnight. The crude product was purified by silica gel column chromatography in methanol and dichloromethane (10/90) to yield a golden-blue solid **40** (SV620C-01, 0.3 g, yield 42%). $^1\text{H-NMR}$ (400 MHz, DMSO): δ 1.18 (t, 6H), 1.56 (s, 12H), 1.71 (m, 2H), 1.82 (m, 2H), 2.33 (m, 2H), 3.71 (t, 2H), 3.90 (m, 4H), 5.6 (d, $J=12$ Hz, 2H), 6.98 (m, 4H), 7.23 (t, 2H), 7.35 (d, $J=7$ Hz, 2H), 7.5 (d, $J=12$ Hz, 2H). ϵ : 90,000 $\text{M}^{-1} \text{cm}^{-1}$. λ_{ab} : 620 nm, λ_{em} : 750 nm.

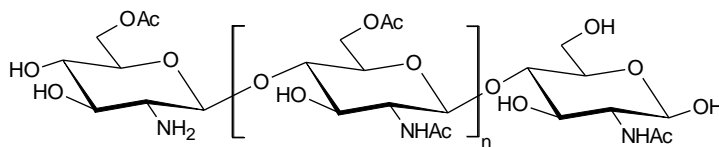


SV770C-01 (44): In a 2-necked round -bottom flask, compound **40** (0.05 g, 0.070 mmol, 1 eq) was dissolved in dichloromethane (12 mL) in an ice bath under argon atmosphere. Acetyl chloride (29.25 μL , 0.375 mmol, 5 eq) and *N,N*-diisopropylethylamine (240.5 μL , 1.875 mmol, 25 eq) were injected into the reaction flask and stirred for 15 mins. The reaction was quenched in 0.1 N HCl solution (20 mL) and then dried off over rotary evaporator. The crude product was purified by silica gel column chromatography in methanol/dichloromethane (10/90) to yield a golden-green solid **44** (SV770C-01, 0.032 g, yield 75%). $^1\text{H-NMR}$ (400 MHz, DMSO): δ 1.27 (t,

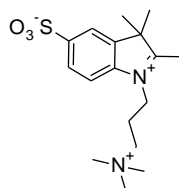
6H), 1.53 (s, 12H), 2.36 (m, 2H), 1.82 (m, 2H), 2.65 (m, 2H), 3.29 (s, 2H), 3.66 (t, 2H), 4.20 (m, 4H), 6.23 (d, $J=12$ Hz, 2H), 7.24 (m, 4H), 7.39 (t, 2H), 7.45 (d, $J=7$ Hz, 2H), 7.55 (d, $J=12$ Hz, 2H). ϵ : 270,000 $M^{-1} cm^{-1}$. λ_{ab} : 790 nm, λ_{em} : 805 nm [71].



SV770C-02 (45): A mixture of compound **47** (0.912 g, 1.42 mmol, 1 eq) and compound **28** (1.2 g, 4.2 mmol, 3 eq) in DMSO and water (1:1) was heated at 65 °C for 23 hr. The reaction mixture was cooled to room temperature and acidified with 0.1% formic acid. The reaction was extracted in dichloromethane and water, dried over sodium sulfate, and then put on rotary evaporator overnight to give solid crude. The crude product was purified by silica gel chromatography in methanol/dichloromethane (10/90) to yield a golden-green solid compound **45** (SV770C-02, 0.416 g, yield 42%). 1H -NMR (400 MHz, DMSO): δ 1.15 (s, 12H), 1.9 (m, 4H), 2.25 (m, 6H), 2.4 (t, 2H), 2.63 (m, 4H), 3.13 (s, 18H), 3.49 (m, 4H), 4.04 (s, 4H), 6.14 (d, $J=14$ Hz, 2H), 6.96 (d, $J=8$ Hz, 2H), 7.17 (d, $J=8$ Hz, 2H), 7.40 (d, $J=8$ Hz, 2H), 7.68 (s, 1H), 7.72 – 7.86 (m, $J=12.0$ Hz, 4H). ϵ : 270,000 $M^{-1} cm^{-1}$. λ_{ab} : 770 nm, λ_{em} : 805 nm.

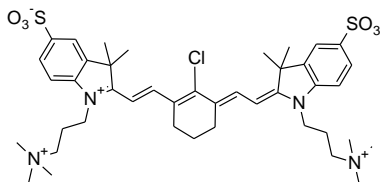


WS Chitosan (51): In a 100 mL round-bottom flask, Chitosan **50** (2.2 g, 0.0169 mmol, 1 eq) was stirred in 22 mL of methane sulfonic acid. After 1.5 hr, acetyl chloride was added to this flask, and was stirred altogether for 5 hr. The reaction was stopped by adding 50 g ice to the flask and the reaction mixture was transferred to a dialysis bag and dialysed against Milli-Q water. After 36 hours, the content of the dialysis bag was neutralised using sodium bicarbonate solution and continued to dialyse for 2 days. The dialysing medium was changed every 12 hours. After 2 days, the content of the dialysis bag was freeze-dried to give a white solid **51** (WS Chitosan, 1.45 g, yield 66.4%). 1H -NMR (600 MHz, 0.5 M DCl/D₂O): 1.58-2.0 (m, 4.46 H), 2.52 (s, 0.27 H), 3.22-3.70 (m, 8.36 H), 4.58 (m, 0.79H) [73].

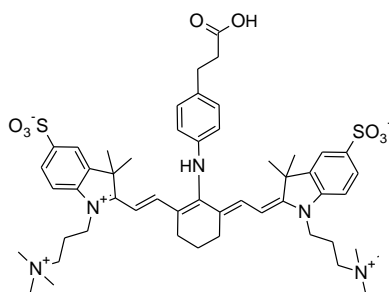


Zwitterionic indolium salt (54): A mixture of 2,3,3-trimethyl-3H-indole-5-sulfonic acid **52**

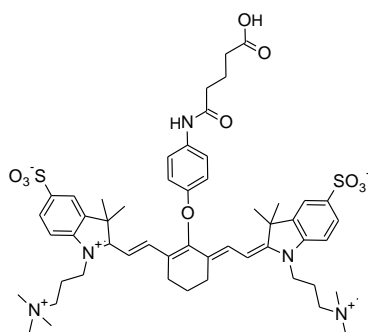
(1.20 g, 5 mmol, 1 eq) and (3-bromopropyl) trimethyl ammonium bromide **53** (1.56 g, 6.0 mmol, 1.2 eq) in 1,2-dichlorobenzene (16 mL) was heated at 130 °C for 72 hr under argon. The mixture was cooled to room temperature and the solvent was decanted. The crude product was washed with dichloromethane, dissolved in acetone, and re-precipitated into a large volume of ethyl acetate to obtain a red solid **54** (1.36 g, yield 80%), which was used in the next step without further purification [46].



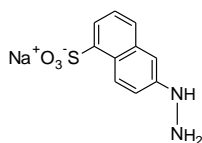
Meso-chloro zwitterionic Cyanine 7 (55): A mixture of bromide salt **54** (0.50 g, 1.48 mmol, 2 eq), Vilsmeier-Haack reagent **26** (0.27 g, 0.73 mmol, 1 eq) and anhydrous sodium acetate (0.25 g, 3.0 mmol, 4 eq) in 10 mL of absolute ethanol was refluxed for 6 hr under argon. The reaction mixture was cooled to room temperature, and then concentrated under reduced pressure to yield a brownish green residue. The crude product was washed with dichloromethane. The residue was suspended in methanol/ dichloromethane (25/75), filtered, and dried in vacuum to yield a golden-green solid **55** (0.5 g, yield 84.9%). **¹H-NMR** (400 MHz, D₂O): δ 1.72 (s, 12H), 1.88 (m, 2H), 2.18 (m, 4H), 2.74 (m, 4H), 3.08 (s, 18H), 3.49 (m, 4H), 4.18 (m, 4H) m 6.37 (d, J=15 Hz, 2H), 7.45 (d, J=6 Hz, 2H), 7.69 (d, J=6 Hz, 2H) 7.85 (s, 2H), 8.31 (d, J=15 Hz, 2H). **ε**: 270,000 M⁻¹ cm⁻¹. **λ_{ab}**: 770 nm, **λ_{em}**: 805 nm [46].



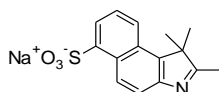
SV700Z-01 (57): A mixture of compound **55** (1 g, 1.18 mmol, 1 eq) and 3-(4-aminophenyl) propanoic acid **56** (0.78 g, 4.73 mmol, 4 eq) in DMSO was heated at 65 °C overnight. The reaction mixture was cooled to room temperature and precipitated in dichloromethane. The crude product was purified by reverse-phase C18 chromatography to yield a blue solid **57** (SV700Z-01, 0.6 g, yield 55%). **¹H-NMR** (400 MHz, D₂O): δ 1.26 (s, 12H), 1.75 (m, 2H), 2.17(m, 4H), 2.38 (m, 2H), 2.51 (m, 3H), 2.80 (m, 2H), 3.14 (s, 18H), 3.48 (m, 4H), 4.01 (s, 4H), 5.98 (d, J= 18 Hz, 2H), 7.11 (m, 6H), 7.76 (m, 4H), 7.99 (d, J=15 Hz, 2H). **ε**: 76,000 M⁻¹ cm⁻¹. **λ_{ab}**: 706 nm, **λ_{em}**: 790 nm [46].



SV770Z-01 (58): A mixture of compound **55** (0.5 g, 0.47 mmol, 1 eq) and compound **28** (0.5 g, 1.88 mmol, 4 eq) in DMSO and water (1:1) was heated at 65 °C for 2.5 hr. The reaction mixture was cooled to room temperature and precipitated slowly in ethyl acetate and absolute ethanol (1:1) with 0.1% formic acid. The precipitate was filtered and washed with excess ethanol. The crude product was purified by reverse-phase C18 chromatography to yield a golden-green solid compound **58** (SV770Z-01, 0.205 g, yield 42%). $^1\text{H-NMR}$ (400 MHz, D_2O): δ 1.15 (s, 12H), 1.9 (m, 4H), 2.25 (m, 6H), 2.4 (t, 2H), 2.63 (m, 4H), 3.13 (s, 18H), 3.49 (m, 4H), 4.04 (s, 4H), 6.14 (d, $J = 14$ Hz, 2H), 6.96 (d, $J = 8$ Hz, 2H), 7.17 (d, $J = 8$ Hz, 2H), 7.40 (d, $J = 8$ Hz, 2H), 7.68 (s, 1H), 7.72 – 7.86 (m, $J = 12.0$ Hz, 4H). ϵ : 270,000 $\text{M}^{-1} \text{cm}^{-1}$. λ_{ab} : 775 nm, λ_{em} : 805 nm.

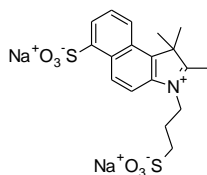


6-Hydrazinyl-1-naphthalenesulfonic acid (60): 5-amino-2-naphthalenesulfonic acid **59** (60 g, 268.8 mmol, 1 eq) was added to a 1 L jacketed flask connected to a cryostat at -5°C. Concentrated hydrochloric acid (300 mL) was added very slowly with continuous stirring. Once fully dissolved, a solution of sodium nitrate (18.55 g, 268.8 mmol, 1 eq) in 120 mL water was added very slowly using a dropping funnel over 60 mins. The reaction was run for 30 mins at 2 °C. Temperature was again brought down to -5 °C and a solution of tin (II) chloride dihydrate (182 g, 806.4 mmol, 3 eq) in concentrated hydrochloric acid (180 mL) was added slowly using a dropping funnel over 2 hr. The reaction was allowed to run at 2 °C for 1 hr. The reaction mixture was filtered and washed with excess absolute ethanol. The precipitate was dried under vacuum for 2 days to give a yellow solid **60** (75 g, yield 100 %). This was directly used for the next step.

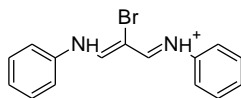


1,1,2-Trimethyl-1H-benz[e]indole-6-sulfonic acid (61): Compound **60** (75 g, 288 mmol, 1 eq) was taken in a round bottom flask with 3-methyl-2-butanone (74.5 g, 865 mmol, 3 eq) and 150 mL of acetic acid. The reaction mixture was refluxed at 130 °C for 5 hr with

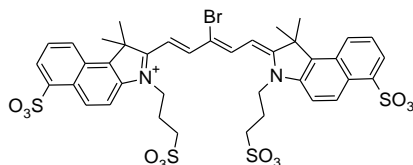
continuous stirring. The reaction was then cooled down and precipitated into ethyl acetate. The precipitate was filtered over Gooch funnel and dried under vacuum to give compound **61** (44 g, yield 50%). This was used directly for the next step without purification.



1,1,2-trimethyl-6-sulfo-3-(3-sulfopropyl)-1H-Benz[e]indolium (62): Compound **61** (1.5 g, 4.8 mmol, 1 eq) was taken in a round-bottom flask and dissolved completely in sulfolane (5 mL), to which 1,3-propanesultone (0.631 mL, 7.2 mmol, 1.5 eq) was added. Altogether they were refluxed at 130 °C for 20 hr. The reaction was then cooled down and the solvent was decanted. 5 mL of methanol was added to quench the reaction and dissolve the solid block, which was then precipitated in acetone. The precipitate was filtered over Gooch funnel and washed with acetone, ethanol, and diethyl ether. The solid was dried under vacuum to give compound **62** (1.45 g, yield 66.6%).

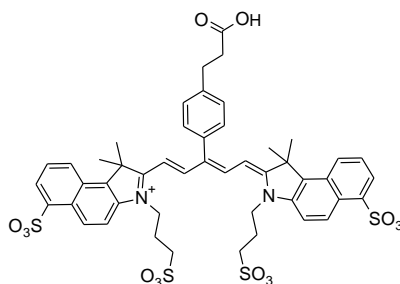


N-[(1E,2Z)-2-bromo-3-(phenylamino)prop-2-en-1-ylidene]anilinium (63): In a 250 mL vacuum Erlenmeyer flask, aniline (7.08 g, 76.02 mmol, 2 eq), was dissolved in 30 mL absolute ethanol. Separately, mucobromic acid (10 g, 38.01 mmol, 1 eq) was dissolved in 30 mL absolute ethanol and transferred to a closed dropping funnel. The solution was added dropwise to the aniline mixture with constant cooling. The vacuum flask was equipped with a silicon tube that was put in a beaker containing ethanol to control the carbon dioxide formation. At the end of the addition, the mixture was transferred to a 250 mL beaker equipped with magnetic stirrer and was heated on a water bath till its volume reduced to half. The resulting solution was cooled down and chilled in the freezer for 1 hr. The yellow crystalline precipitate was filtered and washed with cold ethanol and ether to obtain a yellow solid **63** (6.4 g, yield 45.5%). **¹H-NMR** (600 MHz, DMSO): δ 3.35 (s, 4H), 7.32 (t, $J = 7.4$ Hz, 1H), 7.50 (dd, $J = 10.7, 5.3$ Hz, 2H), 7.60 – 7.53 (m, 2H), 9.18 (s, 1H).

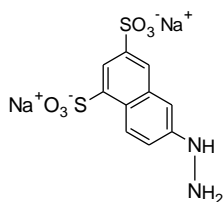


Meso-bromo tetra-sulfonate Cyanine 5.5 (64): In a 100 mL round-bottom flask, Compound **62** (1 g, 2.4 mmol, 2 eq) was stirred along with triethylamine (3.34 mL, 24 mmol, 10 eq) in absolute ethanol (10 mL) at room temperature for 30 mins till it fully dissolved.

Compound **63** (0.458 g, 1.2 mmol, 1 eq) and acetic anhydride (5 mL) was added to the flask and the reaction was stirred at 80 °C for 1 hr. The reaction was cooled and precipitated in excess acetone. The precipitate was filtered over Gooch funnel and was dried under vacuum. The crude was purified using reverse-phase C18 column chromatography to yield a blue powder **64** (0.56 g, yield 50 %). **¹H-NMR** (400 MHz, D₂O): δ 1.54 (s, 12H), 1.93-2.24 (m, 4H), 2.60-3.18 (m, 4H), 3.94-4.28 (m, 4H), 6.00 (d, J = 14.0 Hz, 2H), 7.14-8.25 (m, 10H), 8.72 (d, J = 14.0 Hz, 2H). **ε**: 240,000 M⁻¹ cm⁻¹. **λ_{ab}**: 674 nm, **λ_{em}**: 703 nm.

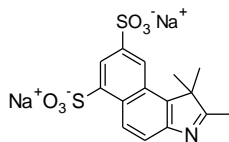


SV680A-03 (66): In a 10 mL round-bottom flask under argon atmosphere, Compound **64** (0.075 g, 0.08 mmol, 1 eq) was taken along 4-(2-carboxyethyl) benzene boronic acid **65** (0.046 g, 0.24 mmol, 3 eq) and cesium carbonate (0.052 g, 0.16 mmol, 2 eq) in absolute ethanol and water (50/50) and stirred at room temperature for 30 mins, till it was fully dissolved. Tetrakis(triphenylphosphine)palladium (0) (0.018 g, 0.016 mmol, 20% by weight) was added to the flask and the temperature was raised to 80 °C. The reaction was stirred for 4 hr and then extracted in ethyl acetate and water. The crude was purified using reverse-phase C18 column chromatography to yield a golden-blue solid **66** (SV680A-03, 0.05 g, yield 63 %). **¹H-NMR** (400 MHz, D₂O): δ 1.70 (s, 12H), 1.82-1.97 (m, 4H), 2.45 (t, 2H), 2.56-2.68 (m, 4H), 2.86 (t, 2H), 3.64-3.86 (m, 4H), 5.48 (d, J = 13.9 Hz, 2H), 6.93 (d, J = 7.0 Hz, 2H), 7.31 (d, J = 7.7 Hz, 2H), 7.42 (t, J = 7.6 Hz, 2H), 7.49 (d, J = 9.2 Hz, 1H), 7.86 (d, J = 7.0 Hz, 2H), 8.06 (d, J = 14.2 Hz, 2H), 8.22 (d, J = 7.9 Hz, 2H), 8.61 (d, J = 9.4 Hz, 2H). **ε**: 240,000 M⁻¹ cm⁻¹. **λ_{ab}**: 674 nm, **λ_{em}**: 703 nm.

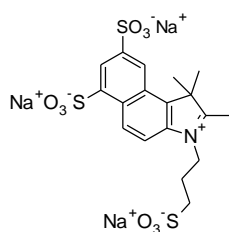


6-Hydrazinyl-1,3-naphthalenedisulfonic acid (68): 6-amino-1,3-naphthalenedisulfonic acid disodium salt **67** (31.1 g, 89.58 mmol, 1 eq) was added to a 1 L jacketed flask connected to a cryostat at -5°C. Concentrated hydrochloric acid (100 mL) was added very slowly with continuous stirring. Once fully dissolved, a solution of sodium nitrate (9.27 g, 89.58 mmol, 1 eq) in 40 mL water was added very slowly using a dropping funnel over 60 mins. The reaction was run for 30 mins at 2 °C. Temperature was again brought down to -5 °C and a solution of tin (II) chloride dihydrate (60.62 g, 268.74 mmol, 3 eq) in concentrated hydrochloric acid (60 mL)

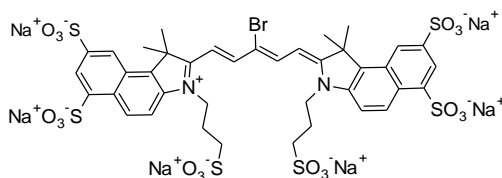
was added slowly using a dropping funnel over 2 hr. The reaction was allowed to run at 2 °C for 1 hr. The reaction mixture was filtered and washed with excess absolute ethanol. The precipitate was dried under vacuum for 2 days to give a yellow solid **68** (16 g, yield 50 %). **¹H-NMR** (400 MHz, DMSO): δ 8.72 (d, J = 9.2 Hz, 1H), 8.1 (d, J = 1.2 Hz, 1H), 7.95 (s, 1H), 7.3 (s, 1H), 7.15 (d, J = 9.2 Hz, 1H) [76].



1,1,2-Trimethyl-1H-benz[e]indole-6,8-disulfonic acid (69): Compound **68** (7 g, 19.3 mmol, 1 eq) was taken in a round bottom flask with 3-methyl-2-butanone (6.125 mL, 57 mmol, 3 eq) and 25 mL of acetic acid. The reaction mixture was refluxed at 130 °C for 5 hr with continuous stirring. The reaction was then cooled down and precipitated into ethyl acetate. The precipitate was filtered over Gooch funnel and dried under vacuum to give compound **69** (6 g, yield 75%). **¹H-NMR** (400 MHz, D₂O): δ 8.8 (d, J = 7 Hz, 1H), 8.7 (s, 1H), 8.45 (s, 1H), 7.9 (d, J = 7 Hz, 1H), 2.4 (s, 3H), 1.5 (s, 6H) [76].

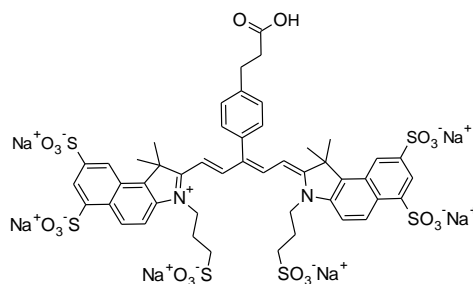


1,1,2-trimethyl-6,8-disulfo-3-(3-sulfopropyl)-1H-Benz[e]indolium (70): Compound **69** (6.5 g, 14.5 mmol, 1 eq) was taken in a round-bottom flask along with 1,3-propanesultone (2 mL, 21.8 mmol, 1.5 eq) in 1,2-dichlorobenzene (35 mL) and refluxed at 130 °C for 20 hr. The reaction was then cooled down and the solvent was decanted. The precipitate was triturated with 40 mL of ethyl acetate and filtered over Gooch funnel. The solid precipitate was further triturated with ethyl acetate (4 X 40 mL) after which it was re-dissolved in hot methanol (100 mL) and precipitated in isopropanol. The precipitate was filtered and washed with isopropanol, diethyl ether and ethyl acetate. The solid was dried under vacuum to give compound **70** (3.5 g, yield 43.4%), which was used directly for the next step without purification [76].

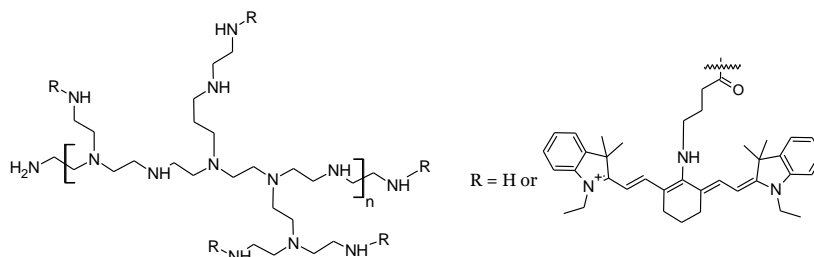


Meso-bromo hexa-sulfonate Cyanine 5.5 (71): In a 100 mL round-bottom flask, Compound **70** (3.5 g, 6.3 mmol, 2 eq) was stirred along with triethylamine (8.78 mL, 63 mmol, 10 eq) in absolute ethanol (30 mL) at room temperature for 30 mins till it fully dissolved.

Compound **63** (1.202 g, 3.15 mmol, 1 eq) and acetic anhydride (10 mL) was added to the flask and the reaction was stirred at 80 °C for 2 hr. The reaction was cooled and precipitated in excess acetone. The precipitate was filtered over Gooch funnel and was dried under vacuum. The crude was purified using reverse-phase C18 column chromatography to yield a blue powder **71** (1.72 g, yield 50 %). **¹H-NMR** (400 MHz, D₂O): δ 1.81 (s, 12H), 2.16-2.28 (m, 4H), 2.93-3 (m, 4H), 4.36 (t, 4H), 6.33 (d, J = 13.4 Hz, 2H), 7.83 (d, J = 9.4 Hz, 2H), 8.18 (dd, J = 15.2, 7.5 Hz, 4H), 8.64 (d, 2H), 8.77 (d, J = 9.8 Hz, 2H). **ε**: 240,000 M⁻¹ cm⁻¹. **λ_{ab}**: 674 nm, **λ_{em}**: 703 nm [76].

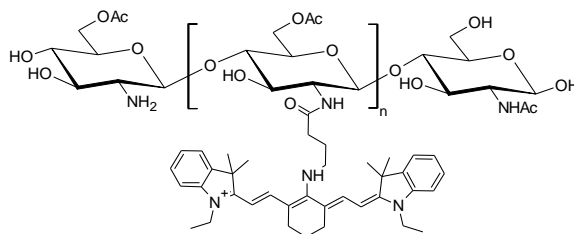


SV680A-02 (72): In a 10 mL round-bottom flask under argon atmosphere, Compound **71** (0.09 g, 0.057 mmol, 1 eq) was taken along 4-(2-carboxyethyl) benzene boronic acid **65** (0.033 g, 0.173 mmol, 3 eq) and cesium carbonate (0.037 g, 0.115 mmol, 2 eq) in absolute ethanol and water (50/50) and stirred at room temperature for 30 mins, till it was fully dissolved. Tetrakis(triphenylphosphine)palladium (0) (0.013 g, 0.0115 mmol, 20% by weight) was added to the flask and the temperature was raised to 80 °C. The reaction was stirred for 4 hr and then extracted in ethyl acetate and water. The crude was purified using reverse-phase C18 column chromatography to yield a golden-blue solid **72** (SV680A-02, 0.05 g, yield 80 %). **¹H-NMR** (400 MHz, D₂O): δ 1.95 (s, 12H), 1.99-2.07 (m, 4H), 2.52 (t, J = 7.8 Hz, 2H), 2.66-2.78 (m, J = 7.7 Hz, 4H), 2.93 (t, 2H), 3.92-4.04 (m, 4H), 5.76 (d, J = 14.1 Hz, 2H), 7.26 (d, J = 8.1 Hz, 2H), 7.47 (d, J = 7.8 Hz, 2H), 7.70 (t, J = 9.7 Hz, 2H), 8.20-8.30 (m, 4H), 8.65-8.76 (m, 4H). **ε**: 240,000 M⁻¹ cm⁻¹. **λ_{ab}**: 674 nm, **λ_{em}**: 703 nm [76].

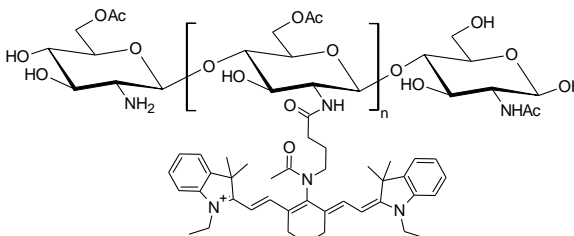


SV620C-01-PEI (73): In a 25 mL round-bottom flask, a mixture of SV620C-01 **40** (0.025 g, 0.04 mmol, 15 eq), N-hydroxy succinimide (0.02 g, 0.18 mmol, 60 eq) and 1-ethyl-3-(3-dimethylamino- propyl) carbodiimide (0.028 g, 0.18 mmol, 60 eq) was stirred in 5 mL anhydrous DMSO at room temperature under argon for 20 mins. To this reaction mixture, a solution of PEI (0.25 g, 0.003 mmol, 1 eq) in 10 mL anhydrous DMSO was added and stirred

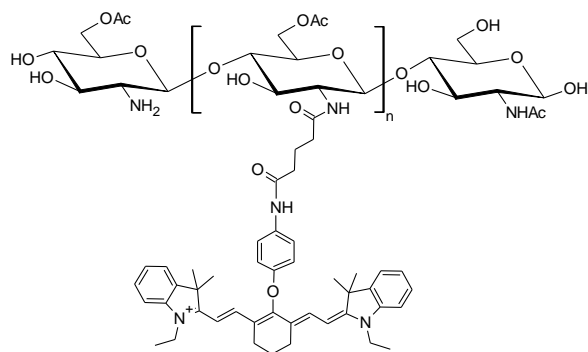
altogether for 4.5 hr at room temperature. The reaction was stopped, and the content of the flask was transferred to a dialysis bag. The reaction mix was dialysed against 1X PBS buffer (pH 7.4) for 36 hr with change of the dialysis medium every 12 hours. The resulting solution inside the dialysis bag was lyophilised to obtain a blue powder **73** (SV620C-01-PEI, 0.17 g, 70% yield). ϵ : 90,000 M⁻¹ cm⁻¹. λ_{ab} : 620 nm, λ_{em} : 750 nm.



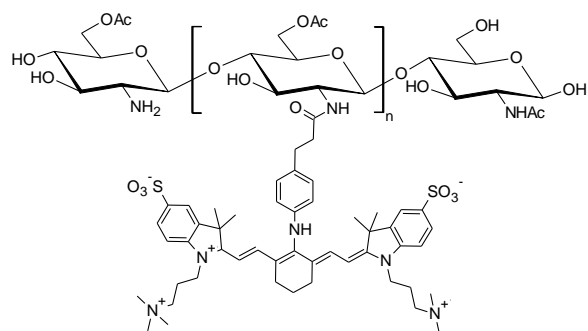
SV620C-01-WS Chitosan (74): In a 25 mL round-bottom flask, a mixture of SV620C-01 **40** (0.025 g, 0.04 mmol, 40 eq), N-hydroxy succinimide (0.02 g, 0.18 mmol, 200 eq) and 1-ethyl-3-(3-dimethylamino-propyl) carbodiimide (0.028 g, 0.18 mmol, 200 eq) was stirred in 5 mL anhydrous DMSO at room temperature under argon for 20 mins. To this reaction mixture, a solution of WS Chitosan **51** (0.1 g, 0.0009 mmol, 1 eq) in 10 mL anhydrous DMSO was added and stirred altogether for 4.5 hr at room temperature. The reaction was stopped, and the content of the flask was transferred to a dialysis bag. The reaction mix was dialysed against 1X PBS buffer (pH 7.4) for 24 hr with change of the dialysis medium every 12 hours, and later against Milli-Q water for another 12 hours. The resulting solution inside the dialysis bag was lyophilised to obtain a blue powder **74** (SV620C-01-WS Chitosan, 0.07 g, 70% yield). ϵ : 90,000 M⁻¹ cm⁻¹. λ_{ab} : 620 nm, λ_{em} : 750 nm.



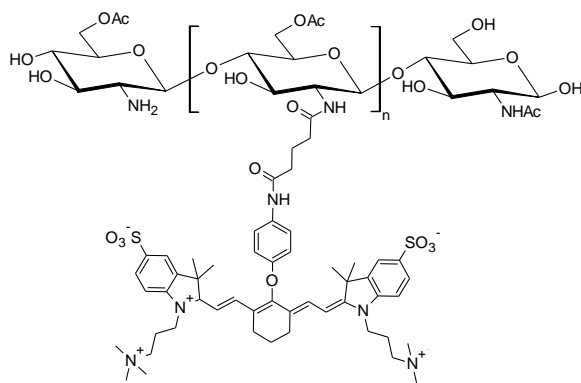
SV770C-01-WS Chitosan (75): In a 25 mL round-bottom flask, a mixture of SV770C-01 **44** (0.025 g, 0.04 mmol, 40 eq), N-hydroxysuccinimide (0.02 g, 0.18 mmol, 200 eq) and 1-ethyl-3-(3-dimethylamino-propyl)carbodiimide (0.028 g, 0.18 mmol, 200 eq) was stirred in 5 mL anhydrous DMSO at room temperature under argon for 20 mins. To this reaction mixture, a solution of WS Chitosan **51** (0.1 g, 0.0009 mmol, 1 eq) in 10 mL anhydrous DMSO was added and stirred altogether for 4.5 hr at room temperature. The reaction was stopped, and the content of the flask was transferred to a dialysis bag. The reaction mix was dialysed against 1X PBS buffer (pH 7.4) for 24 hours with change of the dialysis medium every 12 hours, and later against Milli-Q water for another 12 hours. The resulting solution inside the dialysis bag was lyophilised to obtain a blue powder **75** (SV770C-01-WS Chitosan, 0.07 g, 70% yield). ϵ : 270,000 M⁻¹ cm⁻¹. λ_{ab} : 790 nm, λ_{em} : 805 nm.



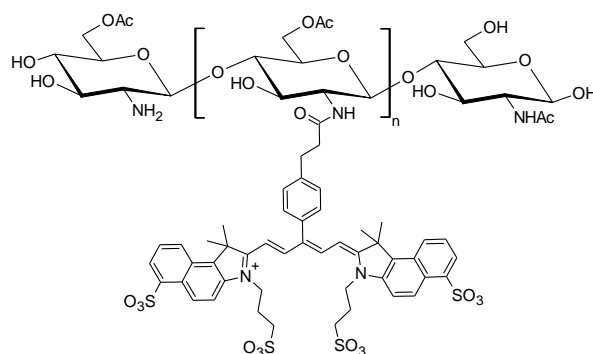
SV770C-02-WS Chitosan (76): In a 25 mL round-bottom flask, a mixture of SV770C-02 **45** (0.056 g, 0.04 mmol, 40 eq), N-hydroxysuccinimide (0.02 g, 0.18 mmol, 200 eq) and 1-ethyl-3-(3-dimethylamino-propyl)carbodiimide (0.028 g, 0.18 mmol, 200 eq) was stirred in 5 mL anhydrous DMSO at room temperature under argon for 20 mins. To this reaction mixture, a solution of WS Chitosan **51** (0.1 g, 0.0009 mmol, 1 eq) in 10 mL anhydrous DMSO was added and stirred altogether for 4.5 hr at room temperature. The reaction was stopped, and the content of the flask was transferred to a dialysis bag. The reaction mix was dialysed against 1X PBS buffer (pH 7.4) for 24 hours with change of the dialysis medium every 12 hours, and later against Milli-Q water for another 12 hours. The resulting solution inside the dialysis bag was lyophilised to obtain a blue powder **76** (SV770C-02-WS Chitosan, 0.07 g, 70% yield). ϵ : 270,000 M⁻¹ cm⁻¹. λ_{ab} : 770 nm, λ_{em} : 805 nm.



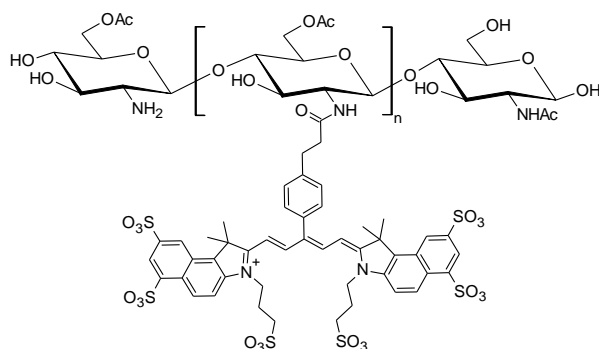
SV700Z-01-WS Chitosan (77): In a 25 mL round-bottom flask, a mixture of SV700Z-01 **57** (0.033 g, 0.036 mmol, 40 eq), N-hydroxysuccinimide (0.02 g, 0.18 mmol, 200 eq) and 1-ethyl-3-(3-dimethylamino-propyl)carbodiimide (0.028 g, 0.18 mmol, 200 eq) was stirred in 5 mL anhydrous DMSO at room temperature under argon for 20 mins. To this reaction mixture, a solution of WS Chitosan **51** (0.1 g, 0.0009 mmol, 1 eq) in 10 mL anhydrous DMSO was added and stirred altogether for 4.5 hr at room temperature. The reaction was stopped, and the content of the flask was transferred to a dialysis bag. The reaction mix was dialysed against 1X PBS buffer (pH 7.4) for 36 hours with change of the dialysis medium every 12 hours. The resulting solution inside the dialysis bag was lyophilised to obtain a blue powder **77** (SV700Z-01-WS Chitosan, 0.07 g, 70% yield). ϵ : 76,000 M⁻¹ cm⁻¹. λ_{ab} : 706 nm, λ_{em} : 790 nm.



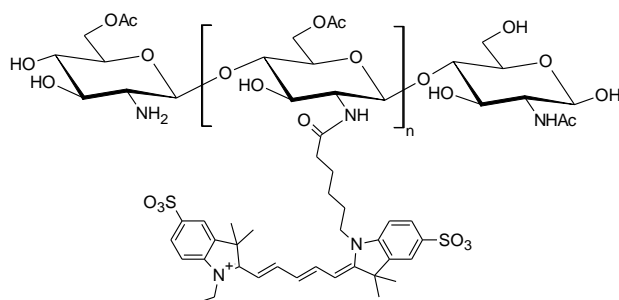
SV770z-01-WS Chitosan (78): In a 25 mL round-bottom flask, a mixture of SV770Z-01 **58** (0.056 g, 0.04 mmol, 40 eq), N-hydroxysuccinimide (0.02 g, 0.18 mmol, 200 eq) and 1-ethyl-3-(3-dimethylamino-propyl)carbodiimide (0.028 g, 0.18 mmol, 200 eq) was stirred in 5 mL anhydrous DMSO at room temperature under argon for 20 mins. To this reaction mixture, a solution of WS Chitosan **51** (0.1 g, 0.0009 mmol, 1 eq) in 10 mL anhydrous DMSO was added and stirred altogether for 4.5 hr at room temperature. The reaction was stopped, and the content of the flask was transferred to a dialysis bag. The reaction mix was dialysed against 1X PBS buffer (pH 7.4) for 36 hours with change of the dialysis medium every 12 hours. The resulting solution inside the dialysis bag was lyophilised to obtain a green powder **78** (SV770Z-01-WS Chitosan, 0.07 g, 70% yield). ϵ : 270,000 M⁻¹ cm⁻¹. λ_{ab} : 775 nm, λ_{em} : 805 nm.



SV680A-03-WS Chitosan (79): In a 25 mL round-bottom flask, a mixture of SV680A-03 **66** (0.048 g, 0.04 mmol, 40 eq), N-hydroxysuccinimide (0.02 g, 0.18 mmol, 200 eq) and 1-ethyl-3-(3-dimethylamino-propyl) carbodiimide (0.028 g, 0.18 mmol, 200 eq) was stirred in 5 mL anhydrous DMSO at room temperature under argon for 20 mins. To this reaction mixture, a solution of WS Chitosan **51** (0.1 g, 0.0009 mmol, 1 eq) in 10 mL anhydrous DMSO was added and stirred altogether for 4.5 hr at room temperature. The reaction was stopped, and the content of the flask was transferred to a dialysis bag. The reaction mix was dialysed against 1X PBS buffer (pH 7.4) for 36 hours with change of the dialysis medium every 12 hours. The resulting solution inside the dialysis bag was lyophilised to obtain a blue powder **79** (SV680A-03-WS Chitosan, 0.07 g, 70% yield). ϵ : 240,000 M⁻¹ cm⁻¹. λ_{ab} : 674 nm, λ_{em} : 703 nm.



SV680A-02-WS Chitosan (80): In a 25 mL round-bottom flask, a mixture of SV680A-02 **72** (0.042 g, 0.036 mmol, 40 eq), N-hydroxysuccinimide (0.02 g, 0.18 mmol, 200 eq) and 1-ethyl-3-(3-dimethylamino-propyl)carbodiimide (0.028 g, 0.18 mmol, 200 eq) was stirred in 5 mL anhydrous DMSO at room temperature under argon for 20 mins. To this reaction mixture, a solution of WS Chitosan **51** (0.1 g, 0.0009 mmol, 1 eq) in 10 mL anhydrous DMSO was added and stirred altogether for 4.5 hr at room temperature. The reaction was stopped, and the content of the flask was transferred to a dialysis bag. The reaction mix was dialysed against 1X PBS buffer (pH 7.4) for 36 hours with change of the dialysis medium every 12 hours. The resulting solution inside the dialysis bag was lyophilised to obtain a blue powder **80** (SV680A-02-WS Chitosan, 0.07 g, 70% yield). ϵ : 240,000 M⁻¹ cm⁻¹. λ_{ab} : 674 nm, λ_{em} : 703 nm.



SV645A-01-WS Chitosan (81): In a 25 mL round-bottom flask, a mixture of SV645A-01 **18** (0.025 g, 0.036 mmol, 40 eq), N-hydroxysuccinimide (0.02 g, 0.18 mmol, 200 eq) and 1-ethyl-3-(3-dimethylamino-propyl)carbodiimide (0.028 g, 0.18 mmol, 200 eq) was stirred in 5 mL anhydrous DMSO at room temperature under argon for 20 mins. To this reaction mixture, a solution of WS Chitosan **51** (0.1 g, 0.0009 mmol, 1 eq) in 10 mL anhydrous DMSO was added and stirred altogether for 4.5 hr at room temperature. The reaction was stopped, and the content of the flask was transferred to a dialysis bag. The reaction mix was dialysed against 1X PBS buffer (pH 7.4) for 36 hours with change of the dialysis medium every 12 hours. The resulting solution inside the dialysis bag was lyophilised to obtain a blue powder **81** (SV645A-01-WS Chitosan, 0.07 g, 70% yield). ϵ : 240,000 M⁻¹ cm⁻¹. λ_{ab} : 648 nm, λ_{em} : 667 nm.

8. Curriculum Vitae and Publications

Name: Srishti Vajpayee

Date of birth: 29 June 1996

Place of birth: Faridabad, India

Nationality: Indian

E-mail id: srishti.vajpayee@gmail.com

Languages known: English (bilingual proficiency), Hindi (bilingual proficiency), Italian (A2) and German (A1)

Education

- 2019 – 2022 Ph.D. within H2020 Marie Curie Ph.D. fellowship for ETN
RenalToolBox
Cyanagen S.R.L., Italy and University of Heidelberg, Germany
- 2017 – 2019 Master of Science in Biomedical Sciences with specialisation
from Radboud Institute for Molecular Life Sciences
(RIMLS)
Radboud University, Nijmegen, The Netherlands
- 2014 – 2017 Bachelor of Science (Honours) in Biomedical Science
University of Delhi, New Delhi, India

Work Experience

- September 2019 – Ph.D. within H2020 Marie Curie Ph.D. fellowship for ETN
October 2022 *Topic: Development of dyes/tracers for analysis of renal
functions*
- October 2018 – Research internship at Institute of Pharmaceutical Sciences,
August 2019 Albert-Ludwigs-University of Freiburg, Germany
Topic: Fungal enzyme-catalysed phenol coupling reactions
- February 2018 – Research internship at Synthetic Organic Chemistry lab
June 2018 (IMM), Radboud University, The Netherlands
Topic: Synthesis of a new group of cholesterol-lowering

compounds

- February 2018 – Literature thesis at Radboud University, The Netherlands
March 2018 *Topic: Life of a drug: From industry to market to trash can*
- September 2015 – Group research project under Delhi University Innovation
October 2016 Project (DUIP) fellowship by University of Delhi, India
Topic: Design, synthesis, and biological evaluation of oxindole-based isooxazolines towards the analogue synthesis of marine natural product Flustraminol-B
- June 2015 – July 2015 Research project under ELITE fellowship at Acharya Narendra Dev College, India
Topic: Search for a novel protein in bacteria through analysing its proteogenomic data using Genosuite

Publications

1. Mohammed, Y, **Vajpayee, S**, Picascia, T, Gretz, N, Perciaccante, R: An overview of non-invasive methods for transcutaneous measurements of glomerular filtration. *J Exp Nephrol*, 2: 7-14, 2021.
<https://doi.org/10.46439/nephrology.2.008>
2. Rodriguez-Niño, A, Pastene, DO, Hettler, SA, Qiu, J, Albrecht, T, **Vajpayee, S**, Perciaccante, R, Gretz, N, Bakker, SJL, Krämer, BK, Yard, BA, van den Born, J: Influence of carnosine and carnosinase-1 on diabetes-induced afferent arteriole vasodilation: implications for glomerular hemodynamics. *Am J Physiol Renal Physiol*, 323: F69-F80, 2022.
<https://doi.org/10.1152/ajprenal.00232.2021>

Patent

1. Perciaccante, R, Jansen, TP, **Vajpayee, S**, Picascia, T, Gretz, N: Fluorescent water-soluble polycationic chitosan polymers as markers for biological 3D imaging. Italian Patent Application No. 102022000022113. 2022.

9. Acknowledgements

I would like to express my sincere gratitude to my supervisors, Prof. Dr Norbert Gretz and Dr Rossana Perciaccante, for providing me with this great opportunity and trusting me with the project. I would like to especially thank Rossana, for introducing me to the field of dye chemistry and giving me the independence to have fun with it. A special thanks to EU'S Horizon 2020 research and innovation programme under the Marie Skłodowska-Curie project 'RenalToolBox' (grant agreement number 813839), which provided me a great experience with an industry-academia mix Ph.D. and allowed me to collaborate with researchers all over the world.

I am grateful to Dr Paul Jansen for his supervision in lab, and with my thesis and patent writing. I would also like to thank Dr Erminia Dell'Avo, who has been by my side since my first day in Bologna and has unceasingly helped and supported me with not only the project administration but also with my everyday life in Italy. I am also thankful to all my colleagues, especially Giacomo Rodeghiero, Nicholas Sesu, Lorenzo Biagini, Fabio Bernardini, Nicola Dall'Omo, Marina Vettraino, Dario Foglietta, Chiara Cevenini and Alessandro Romaniello for making the past three years less stressful and more fun.

I wish to show my appreciation for all the valuable collaborations I had with the other ESRs within the RenalToolBox consortium: Tiziana Picascia, João Faria, Yinuo Xie, Mohammed Yusuf, James Littlewood and Alejandra Hernández-Pichardo.

Finally, I would like to thank, with a heart full of love and gratitude, my friends and family: my parents, for believing in me and providing me with every kind of comfort that helped me fulfil my dream; my brother, Arnav, who will always be my number one; Gaetano, for making me feel at home in Bologna, and for hyping my every little success; my best friend Aparna, for her constant support and encouragement; Himani and Aashi, for their long-distance love and friendship; Mike and Will for always being there to celebrate every occasion; and Rachel, Ylfa and Karolina for the endless girls night. Life as an expat in Italy wouldn't have been the same without my Bolognese family.